Spring 2022

MODELING AND ASSESSING THE SUSTAINABILITY OF DISTRIBUTED SOLAR PHOTOVOLTAICS ADOPTION

Mingcheng Ren
University of New Hampshire, Durham

MODELING AND ASSESSING THE SUSTAINABILITY OF DISTRIBUTED SOLAR PHOTOVOLTAICS ADOPTION

BY

MINGCHENG REN

B.S., Tianjin Normal University, 2013

M.S., East China Normal University, 2016

DISSERTATION

Submitted to the University of New Hampshire

in Partial Fulfillment of

the Requirements for the Degree of

Doctor of Philosophy

in

Earth and Environmental Sciences

December 2021

This dissertation was examined and approved in partial fulfillment of the requirements for the degree of Doctor of Philosophy in Earth and Environmental Sciences by:

Dissertation Committee Chair, Dr. Weiwei Mo, Associate Professor of Civil and Environmental Engineering, University of New Hampshire

Dr. Kevin Gardner, Professor of Civil and Environmental Engineering, University of Louisville

Dr. Clayton Mitchell, Lecturer of Natural Resources and the Environment, University of New Hampshire

Dr. Cameron Wake, Research Professor of Earth Systems Research Center, University of New Hampshire

Dr. Sharon Klein, Associate Professor of the School of Economics, University of Maine

On October 8th, 2021

Approval signatures are on file with the University of New Hampshire Graduate School.

ACKNOWLEDGEMENTS

I would like to express my greatest appreciation and respect to my Advisory Committee members, Dr. Weiwei Mo, Dr. Kevin Gardner, Dr. Clayton Mitchell, Dr. Cameron Wake, and Dr. Sharon Klein. I appreciate their valuable guidance and help for my doctoral research. My deepest appreciation goes to my advisor, Dr. Weiwei Mo for her kind support and mentoring along the way. It is my great honor and blessing to work with her in the past five years.

I would also like to thank Dr. Marek Petrik, Dr. Catherine Ashcraft, Dr. Matteo Muratori from the National Renewable Energy Laboratory, Lynne Cooper, the Connors Writing Center, the Research Computing Center, the Center for Excellence and Innovation in Teaching and Learning, the Office of International Students & Scholars, and the Graduate School at the University of New Hampshire for the heartful support and encouragement. My research work cannot be achieved without the help and support from my friends and colleagues Dr. Cuihong Song, Dr. Masoumeh Khalkhali, Taler Bixler, Dr. Alexandra Evans, Roozbeh Ghasemi, Danyi Feng, Nan Yang, Huishan Li, Yufan Yan, Yongji Zhou as well as many other friends who have helped me in many ways during this journey. I am also very thankful for the funding support for my research from the National Science Foundation under a CBET award (#1706143) and a CRISP Type I Award (#1638334).

I would also like to acknowledge my family members my father Guoqiang Ren, my mother Nenghui Wang, my grandfather Shulin Wang, and my grandmother Yangai Yi for always supporting next to me. My special gratitude goes to my Lord Jesus Christ for his unconditional love and bringing peace, joy, kindness, and power to my life when I doubt and discourage myself.

DEDICATION

To

Guoqiang Ren

Nenghui Wang

Shulin Wang

And

Yangai Yi

TABLE OF CONTENTS

LIST OF TABLES

LIST OF FIGURES

ABSTRACT

MODELING AND ASSESSING THE SUSTAINABILITY OF DISTRIBUTED SOLAR PHOTOVOLTAICS ADOPTION

By

Mingcheng Ren

University of New Hampshire

Participation of distributed solar photovoltaic (PV) generation in the organized electricity wholesale market is expected to increase under the Federal Energy Regulatory Commission Order 2222 announced in 2020. Our understanding about the technical, economic, and environmental tradeoffs and co-benefits of solar PV adoption on both building and regional scales remains limited, especially considering the complexity of varied distributed solar PV-battery system designs and operation strategies as well as the dynamic interactions of these distributed generations with the centralized grid. This dissertation therefore aims to investigate the grid load reduction, life cycle cost, and life cycle environmental (e.g., carbon, water, and energy footprints) performances of typical distributed PV systems considering their dynamic interactions with the centralized grid. This dissertation intends to examine the possible scenarios in which future adoption of PV systems can facilitate economic saving, reduce environmental footprints, relieve centralized grid stress, and supplement differential electricity demands of residential energy users on both building and city scales. To this end, a modeling framework was developed consisting of a stochastic residential electricity demand model, a system dynamics model of solar energy generation, energy balance, storage, and selling, and life cycle economic and environmental assessment model. The stochastic residential electricity demand simulation considered five typical types of household occupants and eight types of households. The generated solar energy, grid supply, and residential demand were

balanced for each residential building using energy balance model. This model was further scaled up to a city level using Boston, MA as a testbed. On the building level, we found a clear tradeoff between the life cycle cost and environmental savings when sizing the PV systems differently. Moreover, installing a solar PV-battery system but without an effective control strategy can result in sub-optimized peak-load reduction, economic, and environmental outcomes. Installing solar PV-battery systems with proper controls can achieve the highest on-peak load reductions and economic benefits under the time-of-use utility rate design. However, they do not necessarily provide the highest environmental benefits, indicating a potential technical, environmental, and economic tradeoff. Our regional analysis found a large penetration of solar PV systems may result in a steeper ramp-up of the grid load during winter days, but it may provide load-shedding benefits during summer days. Large buildings may perform the best technically and environmentally when adopting solar PV systems, but they may have higher life cycle costs.

1. CHAPTER 1: INTRODUCTION

The US solar photovoltaic (PV) electricity generation has increased substantially in recent years. Up from less than 0.1% in 1990, around 2.3% of U.S. electricity generation was provided from solar energy in 2020, accounting for around 11.6% of the total renewable energy generation (EIA, 2021b). By the end of 2020, around 41.7 billion kWh of electricity was generated through small-scale solar PV systems with the estimated generating capacity of 27,724 MW (EIA, 2021b). Moreover, solar PV systems present benefits in terms of supplementing the increasing energy demands (Aghaei and Alizadeh, 2013; Strbac, 2008), providing affordable energy, alleviating the depletion of conventional energy sources (Bazmi and Zahedi, 2011; Klass, 1998), and fulfilling the goal for sustainable and resilient development (Dincer, 2000). There is also strong incentive from the federal and state governments to support the PV adoption (FERC, 2020; The White House, 2021). These benefits all call for understanding, developing, and implementing distributed renewable energy systems such as solar PV systems (Larsen and Drews, 2019; Lopes et al., 2007; Singh, 2013; Turconi et al., 2013). On the other hand, considering the increasing recognition of the centralized and decentralized energy systems' interactions (Liu et al., 2019, 2017), the side-effects induced by the increase of these new energy technologies like solar PV systems and their potential techno-economic and environmental impacts are increasingly being recognized and debated (Alam et al., 2013; Hosenuzzaman et al., 2015; Solangi et al., 2014; Tsoutsos et al., 2005).

Specifically, although solar PV technologies are widely acknowledged as a renewable and environmentally friendly power source during their operations, increasing concerns have been raised to assess the whole life cycle economic and environmental costs behind these technologies, such as economic and environmental costs in the manufacture, transportation, and end-of-life life

stages (Alsema, 2012; Bilich et al., 2017; García-Valverde et al., 2009; Kannan et al., 2006; Sherwani et al., 2010a; Solangi et al., 2014; Wu et al., 2017a). Additionally, some studies indicate that the large penetration of residential solar PV systems might result in a steeper ramp-up after the sun begins to set and use rises (Alam et al., 2014; Sukumar et al., 2018), making it more difficult for the grid operators to accommodate (Eltawil and Zhao, 2010). Moreover, it is important to understand that different energy service suppliers and end-users have different preferences, concerns and motivations behind the fundamental social, technical, economic, and environmental outcomes of the distributed PV technology. Therefore, identifying and assessing the performances and trade-offs between the technical, economic, and environmental outcomes of these energy systems in the assessments show the importance to the guidance of planning, optimization, and implementation of the energy systems to achieve their overall sustainability. However, the complexity and difficulty of the assessments could be aggravated by the diverse energy stakeholders and end-users involved in the time- and demand-dependent decision-making of energy management (e.g., renewable energy subsidies, time-of-use utility rates, battery storage dispatch control). Lastly, the potential technical (e.g., grid load reduction and peak load reduction), economic (e.g., the decrease of utility bills of PV hosts and changes of the wholesale electricity prices), environmental (e.g., changes of energy and water footprints), and societal impacts (e.g., social energy injustice of electricity rate) due to the scheme shifts of centralized and decentralized energy supplies caused by the solar penetration into the regional energy infrastructure network is heated yet less comprehensively studied and/or assessed (Eftekharnejad et al., 2012; Quezada et al., 2006; Tonkoski et al., 2012). Moreover, the increase implementation of solar PV systems and concerns of the above impacts have led to a critical shift in energy

planning/management as well as urban energy service's decision-making (Lopes et al., 2007; Zhang et al., 2013).

Nonetheless, our understanding of comprehensive PV assessment remains limited mainly from the following four perspectives. First, many previous studies focused on a single type of performance, including either technical, economic, or environmental performance. The comprehension and tradeoffs of multiple indicators were not considered. Second, there is a lack of life cycle consideration in the studies investigating various technical, economic, and environmental outcomes of PV adoptions. Third, the dynamic characteristics of energy systems were usually not considered. Due to the dynamic characteristics of renewable energy sources (e.g., intermittent solar radiation) and energy consumptions as well as other real-time behaviors in the energy system (e.g., marginal energy management), it is important to apply "dynamics" in the relevant assessment. More importantly, research into the grid-PV interaction requires us to understand the dynamic complexity of centralized and distributed systems, which energy exchange may be constantly taking place, tightly coupled, nonlinear, artificially determined, and time-sensitive. These requires the application of an innovative, comprehensive, holistic, systematic, more importantly, dynamic methodology to overcome the static life cycle assessment. Fourth, the technical, economic, and environmental interrelations and feedbacks between distributed PVs and centralized grids (wholesale electricity markets) were often not considered.

To fill the above knowledge gaps, this dissertation aims to answer the following major questions.

- How to comprehensively assess the technical, economic, and environmental performances of residential solar PV-battery systems (Chapter 2) and their regional adoptions (Chapter 4) while considering the dynamic and life-cycle characteristics?
- Are there economically and environmentally co-optimized PV-battery system designs that benefit the balance of the economic and environmental tradeoffs? (Chapter 2)
- How do external utility factors (e.g., utility time-varying pricing design and grid mix for power generation) affect the economic and environmental outcomes of PV-battery systems? (Chapter 3)
- Can typical dynamic PV-battery system operational strategies further benefit the balance of tradeoffs between technical, economic, and environmental performances? (Chapter 3)
- How will increasing PV adoption influence the grid performance, PV hosts' energy reliance, life cycle cost, and life cycle environmental impacts of the PV systems? (Chapter 4)
- What is the optimal PV adoption rate that maximizes regional load reduction, cost saving, and environmental benefits? (Chapter 4)

2. CHAPTER 2: DYNAMIC LIFE CYCLE ECONOMIC AND ENVIRONMENTAL ASSESSMENT OF RESIDENTIAL SOLAR PHOTOVOLTAIC SYSTEMS[1]

2.1. Introduction

Over the last decade, solar PV energy generation in the US has increased substantially, primarily driven by cost reduction (Verlinden et al., 2013) as well as concerns related to greenhouse gas and air pollutant emissions (Azzopardi and Mutale, 2010). Around 92.6 TWh of solar PV energy was generated across the US in 2018, representing 2.2% of the nation's total electricity generation and 12.5% of the total renewable energy generation (EIA, 2019a, 2019b). Specifically, around 32% of this energy was generated by small-scale distributed solar PV systems that are commonly found on residential and commercial rooftops (EIA, 2019b), while the remaining was generated at utility scale facilities. Cost reduction has been one of the major drivers for the increased adoption of distributed solar PV systems. It has been estimated that a 63% drop in the residential PV manufacturing and installation cost has taken place since 2010, with an average cost of $2.70 per Watt DC in 2018 (Fu et al., 2018). The cost of solar PV systems is often positively related to the system capacity or size (Fu et al., 2018). Larger systems are likely to have higher upfront costs, and hence impose a greater financial burden on individual households (Nelson et al., 2006). Yet such systems may create a higher environmental benefit when the generated solar energy can be fully utilized by the household or sold to the grid (Kaundinya et al., 2009). Therefore, it is imperative to understand the economic and environmental tradeoffs of the distributed solar PV systems to inform their co-optimization.

[1] This chapter has been published as a journal article in Science of the Total Environment. Please use the following citation for work related to this chapter: Ren M, Mitchell C R, Mo W. Dynamic life cycle economic and environmental assessment of residential solar photovoltaic systems[J]. Science of the Total Environment, 2020, 722: 137932.

The economic performance of solar PV systems is often assessed through life cycle cost assessment (LCCA), which accounts for all costs and savings that incur during the life span of the PV systems (Rebitzer et al., 2004), utilizing indicators such as levelized cost of electricity (LCOE) (e.g., Allouhi et al., 2019, 2016; Burns and Kang, 2012; Jones et al., 2018; Kazem et al., 2017; Lai and McCulloch, 2017; Zhang et al., 2016), investment payback time (IPBT) (e.g., Berwal et al., 2017; Chandel et al., 2014; Lee et al., 2018; Poullikkas, 2013), and life cycle cost (e.g., Adriana et al., 2012; Akinyele and Rayudu, 2016a, 2016b; Bortolini et al., 2014; De Souza et al., 2017; Gürtürk, 2019; Uddin et al., 2017). Meanwhile, their environmental performances are often examined through life cycle assessment (LCA), which is a methodological framework that assesses environmental impacts attributable to the entire life cycle of a product (Rebitzer et al., 2004). The common types of environmental impacts that have been studied via previous solar PV LCAs include carbon footprint (e.g., Akinyele et al., 2017; Akinyele and Rayudu, 2016a, 2016b, Allouhi et al., 2019, 2016; Jones et al., 2018; Rawat et al., 2018; Xu et al., 2018) and cumulative energy demand (CED) (e.g., Gerbinet et al., 2014; M. Raugei, 2015; Peng et al., 2013; Rawat et al., 2018; Tsang et al., 2016; Wu et al., 2017). Not many studies have evaluated solar PV systems from both economic and environmental perspectives to allow understandings of their tradeoffs. Indeed, tradeoffs in solar PV systems' economic and environmental performances exist when comparing different types of PV system designs for a particular application (Allouhi et al., 2019, 2016; Jones et al., 2018) and integrating solar PVs into grids with different energy mixes (Bernal-Agustín and Dufo-López, 2006). However, such tradeoffs have not been fully investigated for different solar PV and battery sizing scenarios under both the grid-connected (GC) and standalone (SA) contexts.

Furthermore, many of the previous solar PV LCCAs and LCAs have limited consideration of the dynamic diurnal or seasonal patterns of solar power generation and demand (Adriana et al., 2012; Chandel et al., 2014; De Souza et al., 2017; Rawat et al., 2018). Such dynamic patterns, however, are important in informing management actions as well as regulatory incentives, including battery dispatch strategies, time-of-use rates, net metering, and energy and water conservation practices. Studies utilizing static or averaged solar energy generation or demand data were limited in their transferability to different spatial and temporal conditions. Of the studies that did include dynamic solar power generation and/or demand patterns, Kazem et al. (2017) estimated the generation potential of a grid-connected 1-MW power plant in Adam, Oman in offsetting peak load using local hourly solar radiation, humidity, temperature, and wind speed data (Kazem et al., 2017). Lee et al. (2018) used hourly solar radiation and building energy consumption data to estimate the economic potential of grid-connected rooftop PV systems for each building in Seoul, South Korea (Lee et al., 2018a). Uddin et al. (2017) examined the influence of battery degradation on the technical and economic performances of solar PV systems, using a residential mid-sized family house in the UK as a case study. While these studies provided important insights into the influence of dynamic solar generation and demand patterns on the PV systems' economic performances, the environmental performances of solar PV systems were excluded. Very few studies have included the dynamic solar energy generation and consumption patterns in assessing the life cycle environmental outcomes of the solar PVs. Akinyele et al. (2016a, 2016b) combined a process-based load demand model with LCCA and LCA to evaluate the technical, economic, and environmental (i.e., carbon emissions) performances of SA PV systems in off-grid communities in Nigeria. They found the proposed PV systems could meet as much as 99.56% of the demand, while performing better both economically and environmentally than conventional diesel power

plants. Jones et al. (2018) developed a spreadsheet model to simulate hourly electricity flows into and from a non-domestic building in UK under three system configurations: no solar PV installed, solar PV alone, and solar PV combined with battery storage. The model was then combined with LCA and discounted cash-flow analysis to assess the carbon emissions and the net present values associated the three system configurations. Neither of these studies, however, investigated the influence of panel and battery sizing on PV systems' performances. Additionally, HOMER (Hybrid Optimization of Multiple Energy Resources) is a popular tool that can be used to assess both the technical-economic and environmental performances of solar PV systems. However, the environmental impacts assessed through HOMER are limited to the use phase of the solar PV systems.

Building upon these previous modeling efforts, this study seeks to develop a comprehensive and generalizable modeling framework to capture the dynamic life cycle economic and environmental performances of solar PV systems. A system dynamics model (SDM) of distributed residential solar PV systems was developed and combined with LCA and LCCA to evaluate the environmental and economic tradeoffs of GC and SA solar PV systems under different panel and battery sizing scenarios. The SDM framework was selected based upon its capability to be adapted to various spatial and temporal conditions as well as to visualize the detailed system processes. The modeling framework was demonstrated using a prototype house in Boston, MA of the United States. This study aims to test the following two hypotheses: 1) environmental and economic tradeoffs exist when optimizing the panel and battery sizes for the SA solar PV system, but not for the GC system; and 2) there are optimal panel and battery sizes that can simultaneously optimize the percent demand met and the life cycle cost of SA solar PV systems.

2.4. **Methodology**

The modeling framework developed in this study combines LCA and LCCA with SDM. SDM is a computational approach applying linked differential equations to simulate the behavior of complex systems over a certain time period. It has been recognized as a cogent tool to study interactions among system components by capturing system feedback loops and delays (Forrester, 1997; Sterman, 2000). Life cycle phases considered in this study include manufacturing, transportation, and use phases. The end-of-life phase was neglected because of the low total amount, concentration and value of reclaimable material in collecting and recycling solar cells (Spanos et al., 2015). The manufacturing and transportation phases of the solar PV systems were assessed based upon unit costs and emission rates associated with individual solar PV components through conventional LCCA and LCA. The use phase was modelled through SDM. Particularly, SDM was used to dynamically simulate the solar energy generation, demand, and storage processes during the use phase of solar PV systems. The modeling framework enables assessment of the net present value (NPV), CED, carbon footprint, and water footprint of solar PV systems over their life span. Figure 2-1 illustrates the modeling framework developed in this study.

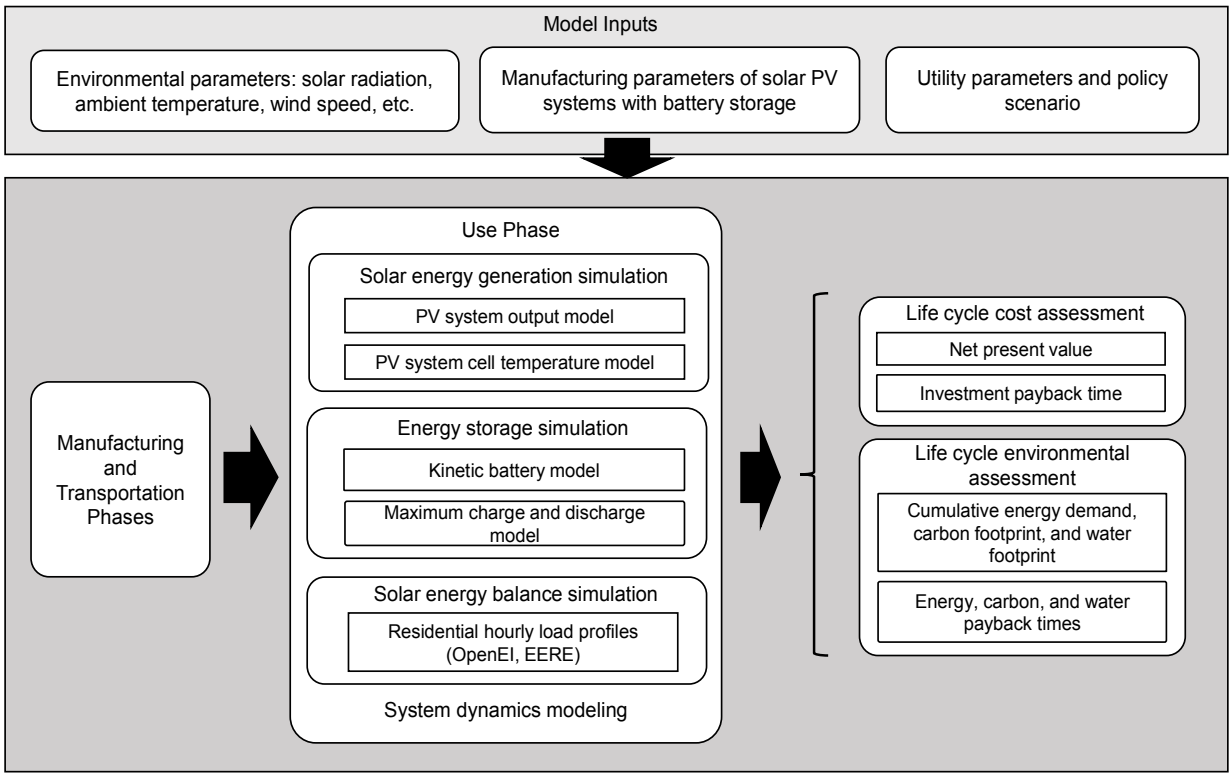

Figure 2-1. Modeling framework of dynamic life cycle assessment of solar PV systems

2.4.4. System Description

This study focuses on polycrystalline silicon (poly-Si) solar PV systems based upon their popularity and economic competitiveness (Fthenakis and Kim, 2011; Sharma et al., 2015). The system investigated in this study consists of solar panels (composing PV array) (poly-Si), balance of system (BOS), and energy storage (if any) (Parida et al., 2011). BOS includes inverters, electrical wiring, mountings, and meters. We assumed that the size of the solar panels was not constrained by the roof size. Two system settings were examined: GC and SA systems (Figure 2-2). GC system uses the grid as a supplement to the solar energy generated onsite and allows users to sell surplus solar energy to the grid (Elhodeiby et al., 2011). SA system refers to an off-grid solar PV system that does not allow selling of surplus energy (Abu-jasser, 2010).

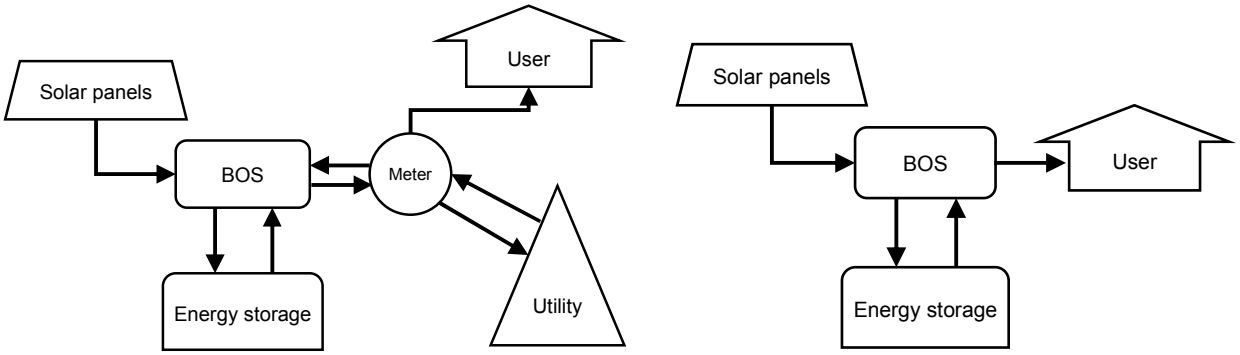

Figure 2-2. Sketch of the designs of the grid-connected (GC; left) and standalone (SA; right) solar PV systems that were investigated in this study

Boston, MA was selected as a testbed in our study because of its high electricity price (EIA, 2017), strong in-place solar incentive programs (Eid et al., 2014; Heeter et al., 2014), and its active pursue of renewable energy (Burns and Kang, 2012). Currently, around 10.7% of the state's electricity comes from solar energy (EIA, 2019c). The solar energy capacity for power generation is projected to grow to 1,603 MW over the next 5 years (SEIA, 2019a). Boston has an average solar energy potential of around 4.48 kWh/m^2/day (DOE, 2021), with July being the highest (5.86 kWh/m^2/day) and December being the lowest (1.60 kWh/m^2/day) (NREL, 2015). Boston has a continental climate with warm summers and cold and snowy winters (Kottek et al., 2006). The annual average ambient temperature of Boston is around 10.5 °C, with the lowest temperature of -21.14 °C in January and the highest of 36.02 °C in July (NREL, 2015). The annual average wind speed in Boston is around 0.89 m/s, with the lowest wind speed of 0.01 m/s in July and the highest of 2.45 m/s in February (NREL, 2015).

A prototype low-rise multifamily house with five housing units based upon the US Department of Energy's House Simulation Protocol was used for model application (Wilson et al., 2014). An hourly energy demand profile specific to the multifamily house in Boston, MA was obtained from

the Open Energy Information database (NREL, 2014) and each data point was then divided into equal halves to achieve 30-minute simulation. Typical baseline SA and GC PV systems with 40 panels (1.63 m^2/panel) and 40 batteries (1.02 kWh_c/battery) in each system was simulated on a 65 m^2 rooftop in the model. The 40-panel PV system's capacity was assumed to be sufficient enough to cover the peak load of demand in the selected house with the consideration of future electrification applications like electric vehicles. The 40-battery storage was calculated to cover the average daily demand of the house based on the energy demand profile.

2.2.2. System dynamics modeling of the solar PV system

The system dynamics model was developed using the Vensim DSS® software. Vensim DSS® is a powerful simulation tool for developing, analyzing, and visualizing dynamic feedback models (Ventana Systems, 2015). It has wide applications in management (Sterman, 2000) and environmental studies (Ford and Ford, 1999) to support decision-making. This model includes three main components: solar energy generation, storage, and balance simulations (Figure 2-3). Details of each component are provided in the following sub-sections. The simulation ran over one year with a thirty-minute time step, which is typical among previously renewable energy system simulation efforts (Connolly et al., 2010).

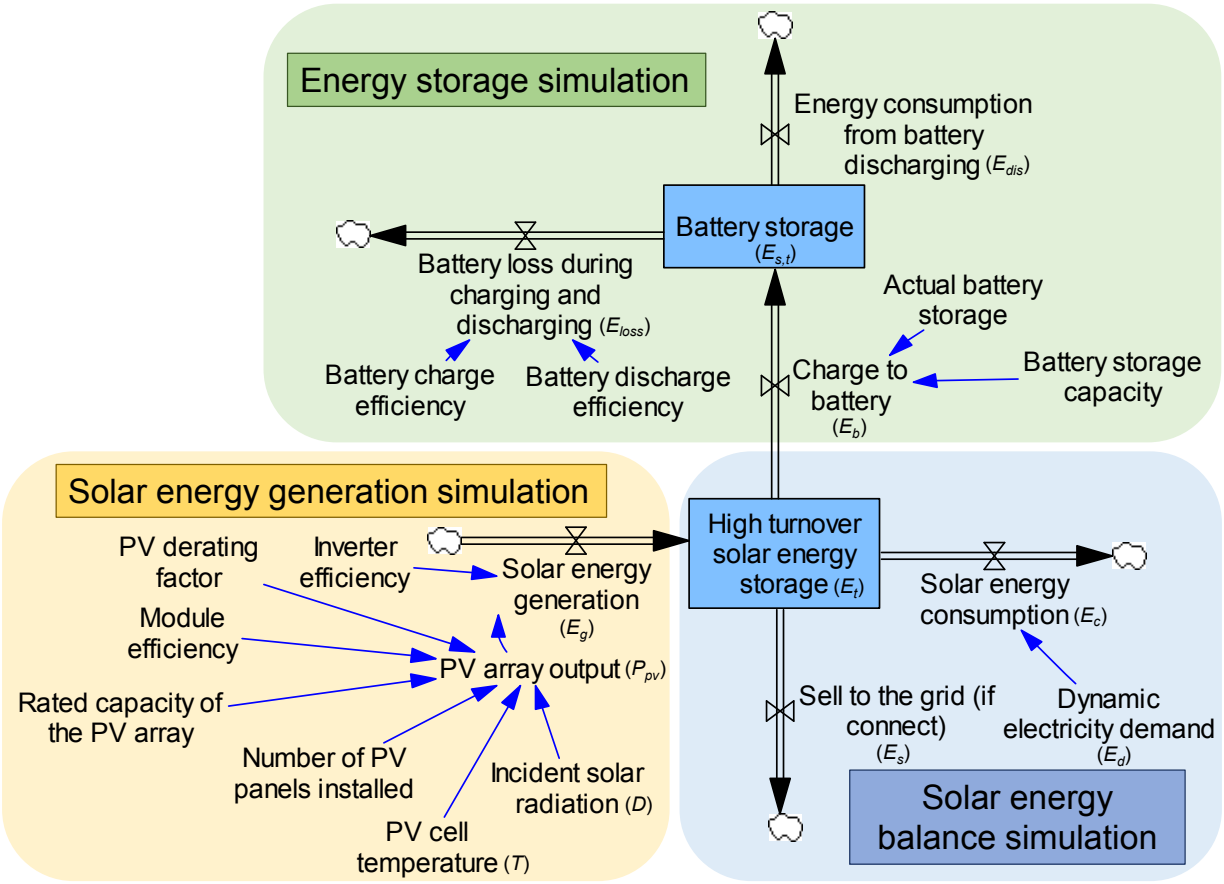

Figure 2-3. A simplified structure of the system dynamics model of the solar PV systems

2.2.2.1. Solar energy generation simulation

The output of PV array (P_{pv}, kW) was simulated based upon Equation 2-1. Specifically, the 30-minute solar radiation profile for the City of Boston was obtained from the National Solar Radiation Database (NREL, 2015) and used to calculate the incident solar radiation (D, kW/m^2) at each time step. The average residential panel size (S) and the PV module efficiency (β) indicate the rated capacity of a PV panel, which were assumed to be 1.63 m^2 and 15% (NREL, 2017). The number of PV panels installed (n) was simulated. A PV derating factor (f_{pv}) of 95% was used (HOMER, 2017). An hourly degradation rate (f_d) of the PV system was calculated based upon the annual degradation rate of 0.5% obtained from Köntges et al. (2016). The temperature coefficient

of power (α) indicates the influence of the PV cell temperature on the system efficiency, which was assumed to be -0.48 %/°C (HOMER, 2018). The incident radiation at standard test conditions (D_{STC}) and the PV cell temperature under standard test conditions (T_{STC}) were assumed to be 1 kW/m^2 and 25 °C respectively (HOMER, 2017).

$$P_{pv,t} = S\beta n f_{pv} \left(\frac{D_t}{D_{STC}}\right) [1 + \alpha(T_t - T_{STC})] \, (1 - f_d)^t \qquad \text{Equation 2-1}$$

Where $P_{pv,t}$ represents the actual output of the PV array in the current time step, kW; t is a time step index, which goes from 0, 0.5, up to 8759.5; S is the average residential panel size, 1.63 m^2 (length: 65 inches, width: 39 inches); β is the PV module efficiency, 15%; n is the number of PV panels installed; f_{pv} is the PV derating factor, 95%; D_t is the incident solar radiation on the PV array in the current time step, kW/m^2 (NREL, 2015); D_{STC} is the incident radiation at standard test conditions, 1 kW/m^2; α is the temperature coefficient of power, -0.48 %/°C; T_t stands for the PV cell temperature in the current time step, °C; T_{STC} is the PV cell temperature under standard test conditions, 25 °C; f_d is the hourly degradation rate of the PV system, 0.000057%.

The PV cell temperature (T, °C) was further calculated using Equation 2-2 (Duffie and Beckman, 1991; HOMER, 2018). Ambient temperatures in Boston at 30-min intervals (T_a, °C) were obtained from the National Solar Radiation Database (NREL, 2015). In addition, the Sandia Module Temperature Model (SNL, 2018) (Section A3 of APPENDIX A) and Faiman Module Temperature Model (Faiman, 2008) (Section A3 of APPENDIX A) were used to validate results obtained from Equation 2-2.

$$T = \begin{cases} \dfrac{T_a + \left(T_{pv,NOCT} - T_{a,NOCT}\right)\left(\dfrac{D}{G_{T,NOCT}}\right)\left[1 - \dfrac{\eta_{mp,STC}(1 - \alpha T_{STC})}{\tau\alpha_b}\right]}{1 + \left(T_{pv,NOCT} - T_{a,NOCT}\right)\left(\dfrac{D}{G_{T,NOCT}}\right)\left(\dfrac{\alpha\eta_{mp,STC}}{\tau\alpha_b}\right)}, & D > 0 \\ T_a, & D = 0 \end{cases}$$

Equation 2-2

Where T represents the PV cell temperature in the current time step, °C; T_a is the ambient temperature in the current time step, °C; $T_{pv,NOCT}$ is the nominal operating cell temperature, 46.5 °C (HOMER, 2017); $T_{a,NOCT}$ is the ambient temperature at which the NOCT is defined, 20 °C (García and Balenzategui, 2004; Koehl et al., 2011); D is the solar radiation striking the PV array in the current time step, kW/m^2 (NREL, 2015); $G_{T,NOCT}$ is the solar radiation at which the NOCT is defined, 0.8 kW/m^2 (García and Balenzategui, 2004; Koehl et al., 2011); $\eta_{mp,STC}$ is the maximum power point efficiency under standard test conditions, 13% (HOMER, 2017); α is the temperature coefficient of power, -0.48 %/°C (NREL, 2017); T_{STC} is the cell temperature under standard test conditions, 25 °C (Devices—Part, 1AD; Muñoz-García et al., 2012); τ is the solar transmittance of any cover over the PV array, 90% (Duffie and Beckman, 1991); α_b is the solar absorptance of the PV array, 90% (Duffie and Beckman, 1991).

2.2.2.2. Energy storage simulation

Battery energy storage system was simulated based upon Equation 2-3. Generic Li-Ion battery was modelled with information obtained from (HOMER, 2017). The amount of energy available in the battery system ($E_{s,t}$, kWh) was modeled as a stock, which is a time integral of differences between the rate of solar power charged to the battery (E_b, kW), the rate of battery discharges for end uses (E_{dis}, kW), and the rate of battery loss during charging and discharging (E_{loss}, kW). The initial battery storage ($E_{s,\,t_0}$) was assumed to be zero. The rate of charging (E_b) is determined by the PV

array output (P_{pv}), the user's energy demand, as well as the vacant capacity of the battery system at a given time step. The rate of discharging (E_{dis}) is determined by the battery storage and the user demand. The rate of battery loss (E_{loss}) is determined by the battery charge and discharge efficiency. Furthermore, both E_b and E_{dis} are constrained by the maximum rates which were calculated using the Kinetic Battery Model (HOMER, 2017; Manwell and McGowan, 1993) with consideration of the battery storage and charge current limitations. Details about the calculation of the maximum charging and discharging rates are provided in the Section A3 of APPENDIX A.

$$E_{s,t} = \int_{t_0}^{t} (E_b - E_{dis} - E_{loss})\, dt + E_{s,\,t_0} \qquad \text{Equation 2-3}$$

Where E_b is the charge to the battery, kW; E_{dis} is the discharge of electricity energy from the battery, kW; E_{loss} is the battery loss during charging and discharging, kW; $E_{s,t}$ and $E_{s,\,t_0}$ are the energy storage in battery at time *t* and t_0, kWh.

The useful battery lifespan (T_b, year) was calculated based on the total lifetime throughput of the battery system and the annual actual charge-discharge throughput (Equation 2-4). The lifetime throughput of one battery was assumed to be 2,430 kWh (HOMER, 2018), and total throughput was assumed to be linearly related to the number of batteries in the system. The actual annual charge-discharge throughput of the battery storage (C_a) was calculated as a time integral of the charging rate (Spanos et al., 2015).

$$T_b = \frac{C_l m}{C_a} \qquad \text{Equation 2-4}$$

Where T_b represents the actual useful lifespan of the battery storage, year; C_l is the lifetime throughput of one battery, 2,430 kWh; m is the number of batteries installed in the battery system; C_a is the actual annual charge-discharge throughput of the battery storage, kWh/year.

2.2.2.3. Solar energy balance simulation

The dynamic energy balance between solar energy generation, battery storage, consumption, and selling to the grid was simulated based upon Equation 2-5. A fictitious high turnover stock was simulated to allocate the generated solar energy (E_g) to the three outflows, E_c, E_b, and E_s (Equation 2-6).

$$E_t = \int_{t_0}^{t} \left(E_g - E_c - E_b - E_s\right) dt + E_{t_0} \qquad \text{Equation 2-5}$$

$$E_g\ (\text{inflow}) = E_c + E_b + E_s\ (\text{outflow}) \qquad \text{Equation 2-6}$$

Where E_t and E_{t_0} are the solar energy storage at time t and t_0, kWh; E_g is the solar energy generation by the PV system, kW; E_c is the solar energy consumption to meet the demand, kW; E_b is the solar energy for charging the battery storage, kW; E_s is the solar energy that feeds into the grid, kW.

The decision-making process for the solar energy generated to be allocated to the three outflows is illustrated in Figure 2-4. Whenever solar energy is available, it is first used to meet the household energy demand. The surplus solar energy is used to charge the battery if it is present and has not reached the maximum capacity. After the battery is fully charged, the excess solar energy is sold to the grid through net metering.

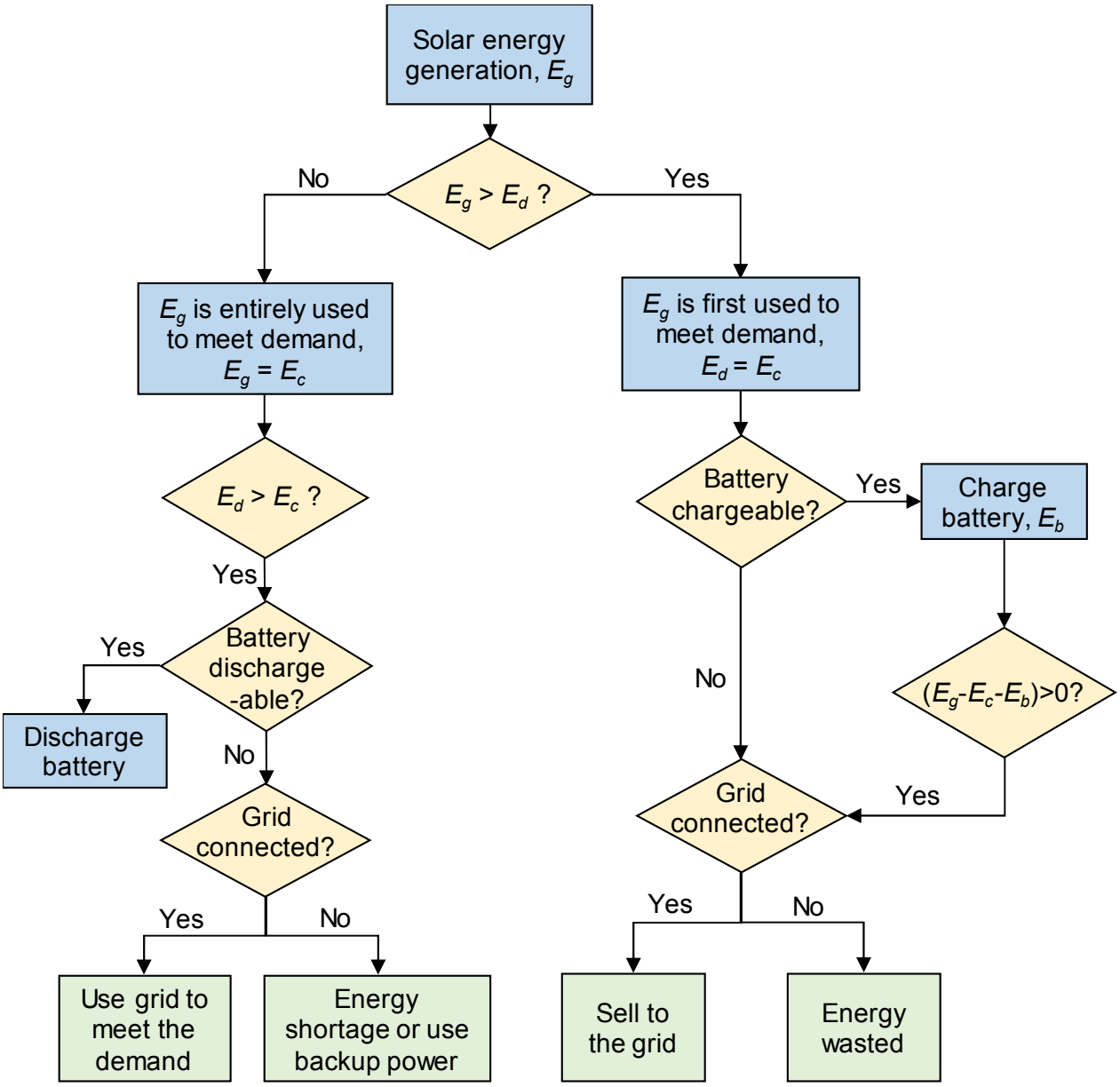

Figure 2-4. Solar energy balance simulation decision flow (E_g is the solar energy generation by the PV system, kW; E_c is the solar energy consumption to meet the demand, kW; E_b is the solar energy for charging the battery storage, kW; and, E_d is the electricity demand in current time step, kW.)

2.2.3. Life cycle cost assessment

The life cycle cost of installing solar PV systems was determined by the capital cost of the PV systems, savings from solar energy generation, tax credit and rebate, cost of labor and the annual operation and maintenance (O&M) cost (Equation 2-7). A 20-year life cycle cost was calculated

based upon the initial net cost and annual net cost (i.e., annual O&M cost subtracts annual savings from solar energy generation) accumulated to 20 years. All future costs were discounted to the year of 2018 applying a typical discount rate of 5% (Jeong et al., 2019; Leckner and Zmeureanu, 2011; Shea et al., 2020). The capital cost of the PV system includes costs related to battery, panels and racking, inverters, permission, and installation. The cost of battery storage was assumed to be \$209 per kWh of storage capacity (kWh_c) (Curry, 2017). Panels and racking were assumed to cost \$1 per Watt of generation capacity (McFarland, 2014; Reichelstein and Yorston, 2013). Inverters were assumed to be \$300 per piece (HOMER, 2018). Permission and installation cost including meters were assumed to be \$450 (NREL, 2017). Savings from solar energy generation were calculated as a product of the cumulative amount of solar energy that is consumed and/or sold to the grid and the electricity retail price. The electricity rate was assumed to be \$0.16/kWh, which is the average flat rate in New England area from 2016 to 2017 (NREL, 2017). A tax credit of 30% (Burns and Kang, 2012; IRS, 2019) of the capital cost was applied. In addition, a rebate of \$0.25 per Watt of installed capacity was applied to all solar systems (NHMA, 2015). The cost of labor is a tiered function of the system capacity, which was obtained from (HomeAdvisor, 2019) (Figure A-1 in the Section A3 of APPENDIX A). The cost of O&M includes the annual replacement cost of battery storage during the system life cycle. The interconnection costs (e.g. application fees) of GC system were neglected (Eversource, 2018). Investment Payback Time (IPBT) of the PV systems was calculated using a cash flow method using Equation 2-8.

$$Life\ cycle\ cost = C_c - R + \sum_{n=1}^{N} \frac{C_{o,n}}{(1+i)^n} - \sum_{n=1}^{N} \frac{S_n}{(1+i)^n} \quad \text{Equation 2-7}$$

$$\text{IPBT} = T_y + \frac{-v}{p} \quad \text{Equation 2-8}$$

Where C_c is the capital cost of the PV systems, \$; R is the tax credit and rebate, \$; N is the life span of the solar PV systems, 20 years; $C_{o,n}$ is the O&M cost in the year n, \$; i is the discount rate, 5%; S_n is the saving from solar energy generation in the year n, \$; T_y is the number of years after the initial investment at which the last negative value of cumulative cash flow occurs, year; p is the net cash flow within the year when the first positive value of cumulative cash flow occurs, \$/year; v is the cumulative cash flow up to the year at which the last negative value of cumulative cash flow occurs, \$.

2.2.4. Life cycle environmental assessment

Three types of environmental impacts were simulated: CED, carbon footprint, and water footprint. The system boundary includes manufacturing, transportation, installation, and use phases. The environmental costs related to labor and administration during the use phase were neglected. However, the replacement of batteries was included. Due to various disposal behavior of the PV users as well as no regulation on the residential level for separating batteries from PV systems and disposing the systems, the battery disposal is not included (Grinenko, 2018). SimaPro 8.3 was used for characterization of the environmental impacts. Particularly, the cumulative energy demand V1.09 method was used for estimating CED. The IPCC 2013 GWP 20a was used for estimating carbon footprint. No significant difference was found in model output applying the IPCC 2013 GWP 20a or 100a. The Berger et al 2014 (Water Scarcity) method was used for estimating water footprint (Boulay et al., 2018). Environmental savings from solar energy generation during the use phase were calculated as a product of the cumulative amount of solar energy that is consumed and/or sold to the grid and the environmental impacts units. Equation 2-9 is the governing equation of the solar PV systems' life cycle environmental performance. Energy, carbon, and water payback

time were calculated using Equation 2-10. Table 2-1 presents the unit costs and environmental impacts obtained from SimaPro 8.3.

$$I = I_{t_0} + I_s - \int_{t_0}^{t} (P_{pv}\, f_{unit})\, dt \qquad \text{Equation 2-9}$$

Where I and I_{t_0} are the cumulative environmental costs at time t and t_0; I_s is the environmental costs of the PV system (from cradle to gate without the solar generation savings); P_{pv} is the actual output of the PV array in the current time step, kW; f_{unit} is the environmental impacts unit, environmental impacts/kWh, Table 2-1.

$$\text{PBT} = \frac{E_p + E_t}{E_g - E_m} \qquad \text{Equation 2-10}$$

Where PBT represents the environmental payback time, which can be either energy, carbon, or water payback time, year; E_p is the environmental cost to produce and manufacture the solar PV system; E_t is the environmental cost to transport materials used during the life cycle; E_g is the average annual environmental savings from electricity generation by the installed solar PV system; E_m is the average annual environmental cost of O&M including the battery replacement.

Table 2-1. CED, carbon footprint, water footprint and cost unit of solar PV systems

Solar PV systems	SimaPro entry	CED unit	Carbon footprint unit	Water footprint unit	Cost unit
PV panel	Photovoltaic panel, multi-Si wafer {GLO}| market for | Alloc Def, S	3480 MJ/m^2	202 kg CO_2 eq/m^2	4360 L/m^2	\$1/W
Battery	Battery, Li-ion, rechargeable, prismatic {GLO}| market for | Alloc Def, S	96.5 MJ/kg	7.52 kg CO_2 eq/kg	101 L/kg	\$209/kWh$_c$
Inverter	Inverter, 2.5kW {GLO}| market for | Alloc Def, S	2400 MJ/piece	243 kg CO_2 eq/ piece	1910 L/piece	\$300/piece
Meter and wiring	Not considered				\$450
Replaced grid electricity	Electricity, at grid, US/US, kWh	10.9 MJ/kWh	0.878 kg CO_2 eq/kWh	44.1 L/kWh	\$0.16/kWh

2.2.5. Sensitivity analysis

A sensitivity analysis was conducted to analyze the influence of discount rate and the local electricity grid mix on the environmental and economic outcomes of the typical GC and SA PV systems with 40 panels and 40-batteries. Each of these factors were varied by ± 10, 30, 50, 70, 90, and 100% to assess its influence on the NPV, CED, carbon footprint, and water footprint. A sensitivity index (S) was calculated for each input change using Equation 2-11 (Song et al., 2019a).

$$S = \frac{\frac{O_i - O_b}{O_b}}{\frac{I_i - I_b}{I_b}} \quad \text{Equation 2-11}$$

Where O_i is the output value after the input was changed; O_b is the base output value; I_i is the altered input value; and I_b is the original input value. Inputs were considered "highly sensitive" if $|S| > 1.00$.

2.3. Results and Discussion

2.3.1. Solar energy utilization and demand met by SA and GC PV systems

For the prototype house with 40 PV panels and 40 batteries, 42.6% of the solar energy generation is directly consumed and 44.4% is stored for later consumption. Around 13.0% of the solar energy will either be wasted in a SA system or sold to the grid in a GC system. Solar energy generated, stored, and sold/wasted all present strong seasonal trends (Figure 2-5). Solar energy generation peaks between May and July, when the monthly average energy demand of the prototype house is the lowest. Hence, a larger amount of solar energy can be sold or stored during these months. Furthermore, grid demand is the highest during summer months nationally (EIA, 2011). Utilities often use natural gas (71.5% in the New England region), hydro and nuclear generation to meet

the additional demand (ISO-NE, 2018a). Installation of a GC PV system can hence alleviate local energy stress and replace fuels that have higher carbon emission factors. Nevertheless, the opposite seasonal patterns of solar energy demand and generation will not be ideal for households looking to install SA PV systems. More solar energy is likely to be wasted and a larger battery capacity might be required to reduce waste. However, this will come with a higher initial investment and replacement cost.

Figure 2-6 presents the percent demand met through solar energy for the prototype house when the panel and battery numbers changed. Either the number of panels or the number of batteries could be a limiting factor for further increase in percent demand met. The shaded numbers present where the PV array size serves as a primary limiting factor, while the rest presents where the battery size serves as a primary limiting factor. The borderline between the two sections represents the approximate optimized battery size to achieve the highest possible percentage of demand met with a given array size. Achieving 100% demand met requires large numbers of both panels (>200 units) and batteries (>160 units), which often accompanies a high cost. However, the size of 40 panels (1.63 m^2/panel, 65.2 m^2 in total) already occupies the entire available roof size of the prototype house (65 m^2). Urban PV hosts are likely be more restricted by the land or space available for further increasing demand met compared to rural or suburban PV hosts. An integration of multiple decentralized energy supplies, such as PV and diesel generator, or PV and geothermal energy might be desirable to improve demand met.

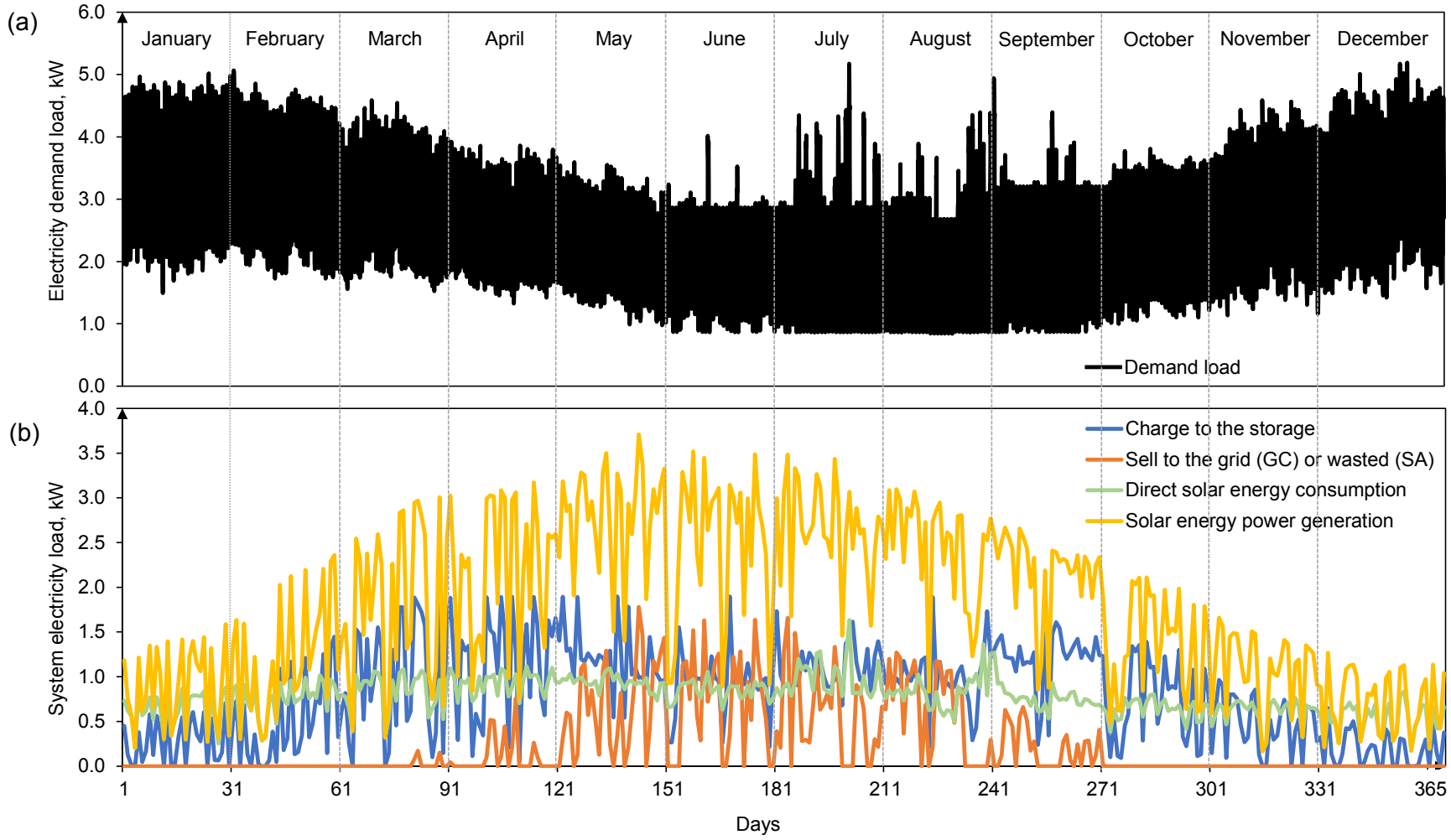

Figure 2-5. (a) Annual electricity demand load profile of the selected house; (b) Dynamic generated solar energy allocation of typical PV system from the model simulation

Number of Panels	Number of Batteries									
	0	1	5	10	15	20	40	80	160	320
1	1.6%	1.6%	1.6%	1.6%	1.6%	1.6%	1.6%	1.6%	1.6%	1.6%
5	8.1%	8.1%	8.1%	8.1%	8.1%	8.1%	8.1%	8.1%	8.1%	8.1%
10	15.8%	16.1%	16.1%	16.1%	16.1%	16.1%	16.1%	16.1%	16.1%	16.1%
15	21.2%	22.0%	23.5%	23.7%	23.7%	23.7%	23.7%	23.7%	23.7%	23.7%
20	24.9%	26.0%	29.0%	30.8%	31.0%	31.0%	30.9%	30.9%	30.9%	30.9%
25	27.6%	28.9%	32.7%	36.1%	37.7%	38.0%	38.0%	38.0%	38.0%	38.0%
30	29.7%	31.1%	35.4%	39.7%	42.8%	44.4%	44.9%	44.9%	44.9%	44.9%
35	31.2%	32.8%	37.7%	42.4%	46.4%	49.3%	51.4%	51.7%	51.7%	51.7%
40	32.5%	34.1%	39.4%	44.7%	49.1%	52.9%	56.2%	57.1%	57.6%	58.3%
60	35.8%	37.5%	43.6%	50.5%	56.6%	61.6%	68.4%	69.8%	70.2%	70.9%
80	37.8%	39.5%	45.9%	53.4%	60.4%	66.6%	75.4%	77.8%	78.8%	79.5%
100	39.1%	40.9%	47.4%	55.2%	62.7%	69.3%	80.7%	83.6%	84.4%	85.2%
150	41.0%	42.8%	49.6%	57.7%	65.7%	72.9%	87.2%	92.2%	93.3%	94.1%
200	42.0%	43.8%	50.7%	59.2%	67.3%	74.5%	89.9%	96.2%	98.4%	99.2%
300	43.2%	45.1%	52.0%	60.5%	69.1%	76.5%	92.5%	98.7%	99.9%	99.9%

Figure 2-6. Percentage of demand met via solar PV systems

2.3.2. Life cycle cost assessment

The life cycle cost of the baseline SA system is -$754.9 in 2018 value with 18.5 years of IPBT, while the baseline GC system presents a lower life cycle cost of -$1,739.4 with 16.8 years of IPBT. Our IPBTs found in this study are within the IPBT range of 2.8-40.8 years reported by previous residential solar PV studies (Muhammad-Sukki et al., 2014; Yang et al., 2015). Allowing selling of the surplus energy created about $984.5 of additional savings over 20 years of life span. In our

simulation, to further increase 1% of the percent demand met from baseline system would result in an additional $409.0 through the increase of array size or $626.5 through the increase of battery size. Both are higher than the amount of economic savings that can be achieved through the 1% demand met increase ($31.3).

Figure 2-7 presents the cost breakdowns of the baseline SA and GC PV systems. Primary costs for solar PV systems come from panels and racking (31% of total cost), battery storage (27% of total cost), replacement of battery (23% of total cost), and labor for installation (16% of total cost). Without system rebate and tax credit, both systems are not able to be paid back within its life time.

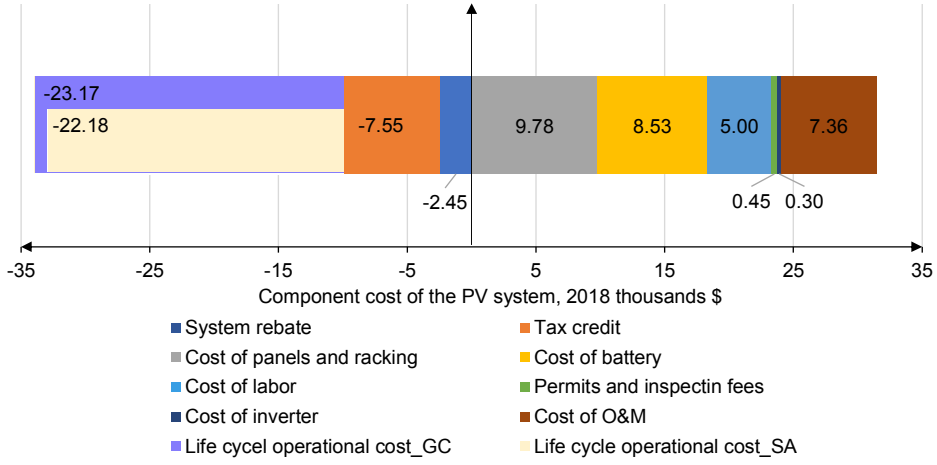

Figure 2-7. Cost breakdown of baseline 40-panel 40-battery SA and GC PV systems

Figure 2-8 presents the life cycle cost under different array sizes for the prototype house. Results show that when demand met is not a concern, life cycle economic savings are achievable under a range of panel and battery sizes for both GC and SA systems. No battery installation is preferred for SA systems with relatively small panel sizes (<25 panels). This indicates the saving from power generation cannot offset the battery cost within this range of panel sizes. With further increase in array size, the optimum battery size increases. The maximum life cycle economic saving can be

achieved with 20 panels with no battery in this prototype house. This optimum configuration could meet ~25% of total demand with NPV of -$4,616.7. Compared with the baseline SA system, this optimized SA system increases the life cycle economic savings by 511.6%, yet decreases the demand met by 55.7%. Additional analyses were conducted to investigate the tradeoffs between percent demand met and life cycle cost. The Pareto-optimal frontier between percent demand met and life cycle cost was provided in Figure 2-9 (additional analyses related to tradeoffs between cost and demand met were provided in the Section A4 of the APPENDIX A). We found the optimal panel size ranges from 60 to 80 with 20~40 batteries, which can meet 66.6~68.4% of the demand with life cycle costs of -$887.5~ -$3011.7.

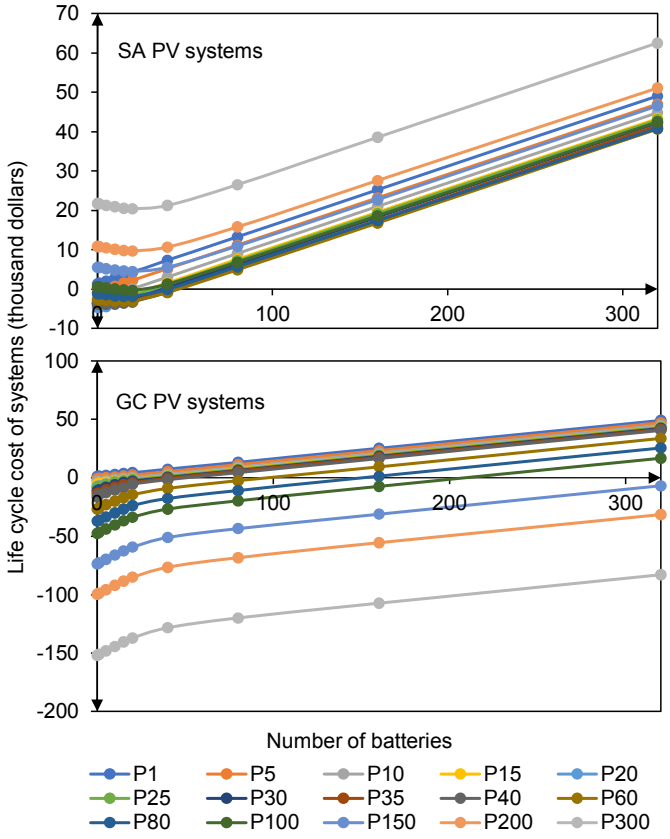

Figure 2-8. Life cycle cost (2018$) of SA and GC PV systems under different array sizes

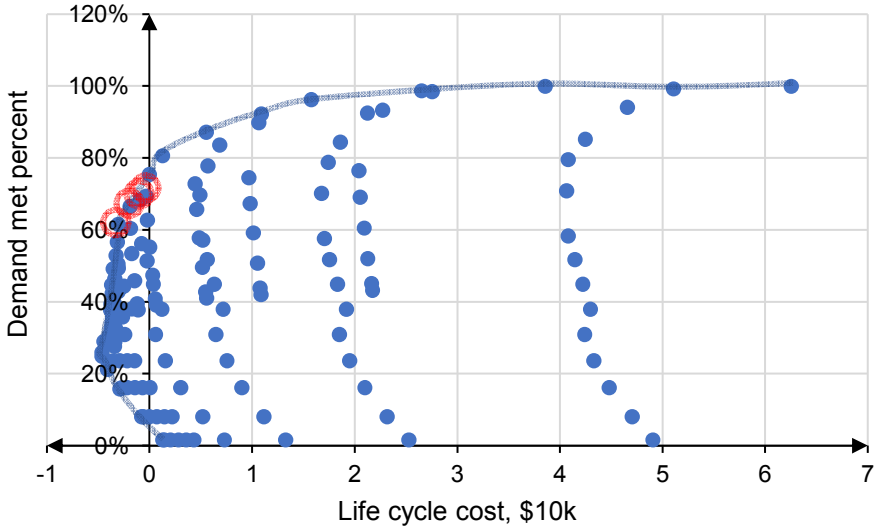

Figure 2-9. The Pareto-optimal front of demand met percent and life cycle cost of SA PV systems (dots with red circles represent the preferred solutions for both objectives.)

For GC systems, with a given array size, the life cycle cost increases with the increase of battery size. When there is no limit on when and how much excess solar energy can be sold to the grid, batteries do not provide extra benefit to the GC system owners. However, when policy constraints such as limitations/caps of grid sell are in place, tradeoffs would present as whether or not to install batteries for excess energy storage. For example, Pennsylvania Public Utility Commission attempted to cap the amount of surplus grid sell from PV systems to no more than 200% of residential customers' annual consumption over the 60 months before they installed PV systems (Legere, 2016; Parrish, 2016). Under such a policy, the prototype house with the baseline system would have a maximum grid sell of 39,080 kWh annually. With the decrease of the selling cap, this could result in a larger optimal battery storage capacity. Potential future charges on distribution and transmission services, overage tariffs, and a lower retail rate of solar energy can also influence the optimal sizing of the panels and batteries of the GC PV systems. In these conditions, storing the surplus solar energy for later household uses will result in a higher economic benefit than

selling it directly back to the grid. Hence, having certain battery storage capacities might become appealing even for GC PV system owners. Different policies could alter the economic cost and benefit of GC systems through the change of economic gain from selling to the grid variously. Therefore, the optimal array size for maximum economic saving is determined by specific policy. For example, the cap of grid sell restricts the optimum array size.

2.3.3. Life cycle environmental assessment

Both baseline GC and SA PV systems can result in reduced CED, carbon footprint, and water footprint compared to the grid when installed in the prototype house. The GC system has higher life cycle environmental benefits in terms of all three measures than the SA system (-2.1 TJ, -177.0 Mg CO_2 eq, and -9.4 ML of water for the SA system and -2.3 TJ, -187.0 Mg CO_2 eq, and -9.9 ML of water for the GC system). This shows that allowing selling of the excess energy rather than wasting it can slightly increase the environmental benefits by 5.3~9.5% over 20 years of life span. The energy, carbon, and water payback times are 2.15, 1.62, and 0.65 years for the baseline SA system, and 2.05, 1.54, and 0.62 years for the baseline GC system. Previously reported energy, carbon, and water payback times are 0.8-4.7 years (Gerbinet et al., 2014; Grant and Hicks, 2020; Perez et al., 2012), 0.4-7.8 years (Grant and Hicks, 2020), and 0.06-1.08 years (Fthenakis and Kim, 2010a; Meldrum et al., 2013) respectively for the solar PV systems. Our results are within the ranges of these previously reported environmental payback times. Figure 2-10 presents the life cycle environmental performances of SA and GC systems under different array sizes. Compared with life cycle enconomic savings, life cycle environmental savings are achievable under a wider range of panel and battery sizes for both types of systems.

For SA systems, the optimized CED and carbon footprint outcomes was achieved when the panel size is in the range of 150-200 and the battery size is in the range of 80-320, while the optimized water footprint outcome was achieved when the panel size is in the range of 150-300 and the battery size is in the range of 80-320 when installed in the prototype house (-3.02~ -2.85 TJ, -262.2~ -254.0 Mg CO_2 eq, and -15.4~ 14.7 ML of water). These optimized configurations increase the life cycle environmental savings of the baseline SA system up to 64.6%, but decreases the life cycle economic saving largely up to 6,868.4%. The environmentally optimal SA system array size can be up to 14 times larger than the economically optimal array size. This large preferred size is potentially a result of the relatively low environmental emissions/impacts during the panel and battery manufacturing phase compared with the potential environmental benefits resulted from preventing the use of the grid during the use phase, although a large amount of solar energy will be wasted under the optimized size (up to 69.3% of total solar energy generation wasted). This shows that an environmental and economic tradeoff exists for SA systems. However, with further reductions in the capital costs of the PV and battery systems, such tradeoffs may be minimized, especially for regions with relatively high retail electricity price. Potential future policies such as carbon pricing (Tierney, 2019) and increased water pricing of the thermal power supply (EPA, 2019; USC, 1986) may also help promoting adoption of larger sized solar PV and battery systems as well as minimizing the environmental and economic tradeoffs.

For GC systems, environmental benefits are the highest when no battery is installed, and the benefits increase with the increase of panel size. However, the increase of array size is restricted by the amount of rooftop area or land availablibility. When the panel size is restricted to the rooftop area, the lowest life cycle environmental costs in CED, carbon footprint, and water footprint are -

2.5 TJ, -209.2 Mg CO_2 eq, and -10.9 ML respectively. This optimized configuration increases the environmental and economic savings by 8.7~11.9% and 843.7% respectively compared with the baseline GC system over 20 years. No outstanding economic and environmental tradeoffs were found for the GC system under the modelled conditions.

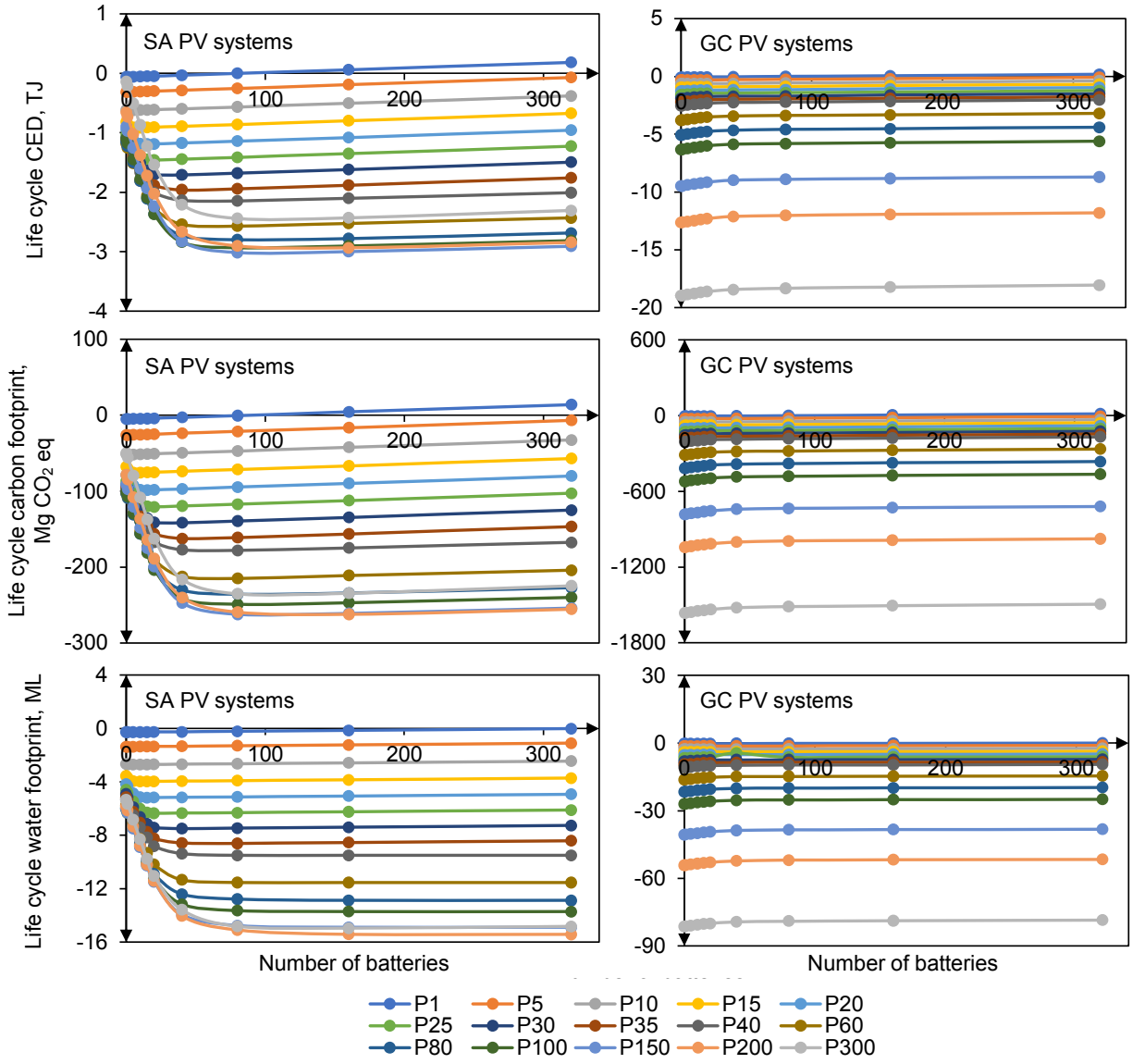

Figure 2-10. Life cycle environmental costs of SA and GC PV systems under different array sizes

2.3.4. Sensitivity analysis

Figure 2-11 shows the changes of the life cycle cost in response to decreases or increases of the discount rate as well as the changes of the life cycle environmental outcomes in response to the changes in the grid energy, carbon, and water intensities. Life cycle cost of the baseline PV system is highly sensitive to the changes of the discount rate under the investigated range. Increasing discount rate is associated with lower life cycle economic savings from installing solar panels. The discount rate of 5.6% (12% increase from the default value) and 6.3% (26% increase from the default value) are the tipping points where a SA and GC baseline system starts to lose money, respectively. Life cycle environmental outcomes of the solar PV system change linearly with the change of the grid energy, carbon, and water intensities. Carbon footprint has the highest sensitivity to the changes in the grid, followed by water footprint, and the CED is the least sensitive to the grid changes. Additionally, the GC system is slightly more sensitive to changes in the grid than the SA system from an environmental perspective.

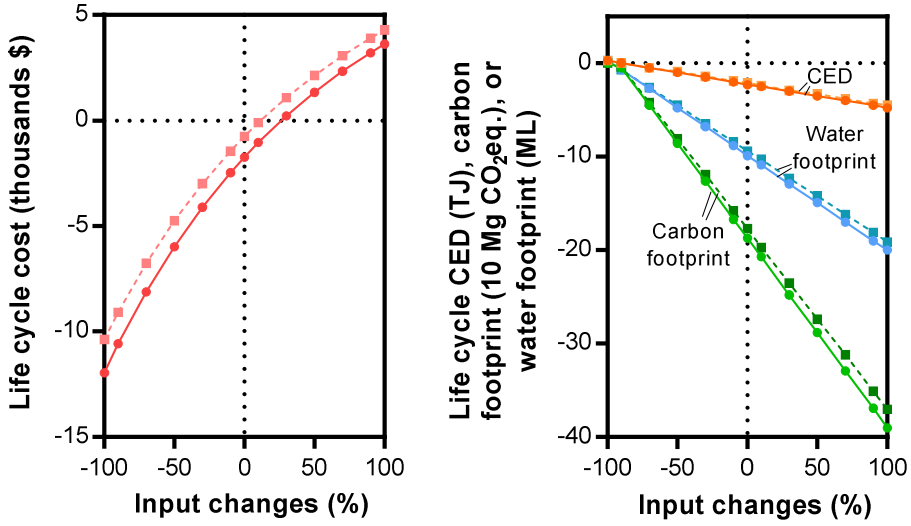

Figure 2-11. Life cycle costs and environmental impacts of the baseline SA (dashed lines) and GC (solid lines) PV system under changes in discount rate (left figure) and the unit environmental impact of the grid (right figure)

2.4. Conclusion

A dynamic life cycle economic and environmental assessment that combines system dynamics modeling with the conventional LCA and LCCA was conducted for residential solar PV systems. Two PV system designs were investigated: the GC and the SA systems. A prototype house located in Boston, MA was used as a testbed for the modeling framework developed in this study. When installed with 40 PV panels (roughly the size of the entire roof) and 40 batteries, the prototype house will directly use 42.6% of the solar energy generated, store 44.4% of the energy for later consumption, and sell or waste round 13.0% of the solar energy depending on whether it is a GC or a SA system. Solar energy generated, stored, and sold/wasted all present strong seasonal trends. The prototype house has the lowest monthly demand during summer, while the solar energy generation is the highest during the period. Hence, a larger amount of solar energy can be sold or stored during these months. Hence, a larger amount of solar energy can be sold or stored during these months. Achieving 100% demand met requires large numbers of both panels (>200 units) and batteries (>160 units) for the prototype house, which can be unrealistic for households with land or roof area availabilities. The 40-panel 40-battery SA system has a life cycle cost saving of $754.9 in 2018 value with 18.5 years of IPBT and a life cycle reduction of 2.1 TJ of CED, 177.0 Mg CO_2 eq, and 9.4 ML of water. The corresponding GC system presents a slightly higher life cycle cost saving of $1,739.4 with 16.8 years of IPBT and a slightly higher life cycle environmental benefit (reduction of 2.3 TJ CED, 187.0 Mg CO_2 eq, and 9.9 ML of water). This study also found the tradeoffs between demand met and life cycle cost in the SA systems can be best balanced when the panel size is between 60 and 80 units and the battery size is between 20 and 40 units, which can meet 66.6–68.4% of the demand with a life cycle cost between -$3011.7 and -$887.5.

When examining the influence of panel and battery sizes on the outcome, we found life cycle economic savings are achievable under a range of panel and battery sizes for both GC and SA systems when demand met is not a concern. For the SA systems, the maximum life cycle economic saving can be achieved with 20 panels with no battery in the prototype house, which increases the life cycle economic savings of the baseline system by 511.6%, yet decreases the demand met by 55.7%. However, the optimized environmental performance is achieved with significantly larger panel (up to 300 units) and battery (up to 320 units) sizes. These optimized configurations increase the life cycle environmental savings of the baseline SA system up to 64.6%, but decreases the life cycle economic saving largely up to 6,868.4%. There is a clear environmental and economic tradeoff when selecting the size of the SA systems. For GC systems, when there is no limit on when and how much excess solar energy can be sold to the grid, batteries do not provide extra benefit to the GC system owners. Hence, both the economic and environmental benefits are the highest when no battery is installed, and the benefits increase with the increase of panel size. However, when policy constraints such as limitations/caps of grid sell are in place, tradeoffs would present as whether or not to install batteries for excess energy storage. The modeling framework that is developed in this study can be further generalized for future investigations in varied PV system designs under different policy scenarios in different spatial and temporal contexts.

3. CHAPTER 3: MANAGING RESIDENTIAL SOLAR PHOTOVOLTAIC-BATTERY SYSTEMS FOR GRID AND LIFE CYCLE ECONOMIC AND ENVIRONMENTAL CO-BENEFITS UNDER TIME-OF-USE RATE DESIGN[2]

3.1. Introduction

Managing the daily and hourly fluctuations in electricity demand has been a long-standing problem within the power utility sector (Gelazanskas and Gamage, 2014; Oconnell et al., 2014; Uddin et al., 2018). To meet the peak demand, excess generation with fast response capabilities have to be installed, and more expensive fuels, such as natural gas, are normally used (ISO-NE, 2018b). These peaking resources require substantial capital and operational investment (Uddin et al., 2018), yet they are only used during the limited on-peak windows (IRENA, 2019). Residential solar photovoltaic (PV) systems have traditionally been viewed as a potential means to reduce peak load (H. Huang et al., 2017). Over the last decade, installations of residential PV systems have boomed, and these systems currently contribute to around 0.77% of the total generation in the US (EIA, 2019d, 2020a). However, recent studies indicate that the large penetration of residential solar PV systems might result in a steeper ramp-up after the sun begins to set and use rises (Alam et al., 2014; Sukumar et al., 2018), making it more difficult for the grid operators to accommodate (Eltawil and Zhao, 2010). One potential solution to this steep ramp could be expanding storage at the residential scale (Sukumar et al., 2018). Less than 5% of the residential and commercial PV systems in the US have energy storage capacities currently (SEIA, 2020a, 2020b). Even among this small number of storage installations, only about 15% are managed for load control (Nottrott et al., 2012; O'Shaughnessy et al., 2018).

[2] This chapter has been published as a journal article in Resources, Conservation and Recycling. Please use the following citation for work related to this chapter: Ren M, Mitchell C R, Mo W. Managing residential solar photovoltaic-battery systems for grid and life cycle economic and environmental co-benefits under time-of-use rate design[J]. Resources, Conservation and Recycling, 2021, 169: 105527.

To help alleviate peak load pressure, utilities in the US have started to explore or implement residential time-of-use (TOU) pricing rates (Newsham and Bowker, 2010). TOU pricing refers to a rate structure that establishes a higher electricity use/sell price during the on-peak and/or mid-peak hours, and a lower price during off-peak hours (Dufo-López and Bernal-Agustín, 2015; Haider et al., 2016). Implementation of TOU rates can promote residential battery installations by encouraging increased selling/utilization of solar energy during the on-peak hours (Zhang and Tang, 2019). The design and operation strategy for these systems can influence the economic, environmental, as well as the peak load reduction benefits. For instance, management strategies that target peak load reduction might also speed up battery degradation and hence increase replacement or maintenance costs (Martins et al., 2018). Our understanding regarding how to design and manage solar PV-battery systems for economic, environmental, and grid co-benefits remains limited. Such an understanding is especially important given the Federal Energy Regulatory Commission's recent Order 2222, which will result in promoting the participation of aggregated distributed energy resources in the organized electricity wholesale markets (FERC, 2020).

Many previous studies only focused on the technical performances of the solar PV-battery systems under TOU rate designs, which were often measured in terms of the ramp rate of the PV output (Sukumar et al., 2018), solar energy consumption (Alramlawi et al., 2018; Khoury et al., 2016), grid use and sell (Alramlawi et al., 2018; Khoury et al., 2016), and peak load reduction (H. Huang et al., 2017; Schibuola et al., 2017; Uddin et al., 2018). Particularly, peak load reduction was found to be up to 50% at a household scale when the PV-battery systems were managed according to the

TOU rate designs (H. Huang et al., 2017; Schibuola et al., 2017; Uddin et al., 2018). Additional studies have investigated both the peak load reduction and economic performances of solar PV-battery systems under TOU rate, comparing different battery control strategies (Khalilpour and Vassallo, 2016; Martins et al., 2018; Zhang and Tang, 2019), demand load profiles (Linssen et al., 2017), battery types (Parra and Patel, 2016), and battery storage capacities (van der Stelt et al., 2018; Zhang et al., 2017). Some of these studies found the installation of solar PV-battery systems can provide synergistic benefits of both peak load reductions and economic benefits for users (Khalilpour and Vassallo, 2016; Linssen et al., 2017; van der Stelt et al., 2018; Zhang et al., 2017; Zhang and Tang, 2019), while others highlighted tradeoffs between peak load reductions and economic savings, especially when the batteries' initial and replacement costs were considered (Martins et al., 2018; Parra and Patel, 2016). Not many studies have investigated the environmental performances of solar PV-battery systems under the TOU rate design. Hiremath et al. (2015) and Sun et al. (2019) investigated the cumulative energy demand or carbon footprint of various solar PV-battery system designs (e.g., different battery types and storage capacities) considering grid mix changes during on- and off-peak hours. None of these studies, however, considered the influence of battery management strategies on the environmental outcomes. Fares and Webber (2017) and Litjens et al. (2018) further investigated tradeoffs between the peak load reduction and the life cycle environmental impacts of residential solar PV-battery systems. While both studies consistently reported reduced peak load when battery is added to a solar PV system, no consensus was found on whether or not the battery additions can reduce carbon emissions. Only three studies further considered solar PV-battery systems' economic performance in addition to their peak load reduction and environmental performances under the TOU rate design (Mariaud et al., 2017; Nojavan et al., 2017; Yang and Xia, 2017). Nojavan et al. (2017) and Yang and Xia (2017) found

peak load reduction, economic, and carbon benefits can be achieved simultaneously through optimized battery control strategies. However, Mariaud et al. (2017) found installation of a PV-battery system can provide peak load reduction and carbon benefits, but it might increase the overall cost. This discrepancy is potentially a result of the different incentive designs and PV-battery technology costs considered. None of these studies, however, took account of the carbon emissions associated with battery manufacturing and replacement.

To address this knowledge gap, this study integrated system dynamics modeling (SDM) with life cycle cost and environmental assessment to investigate the preferred design and operation strategies of PV-battery systems under TOU rate design. The modeling framework was applied to a 5-unit prototype house in the Boston-Logan area, Massachusetts of the United States as a testbed. The Boston area was selected because of its strong in-place solar incentive programs (MassCEC, 2020), and its active pursue of renewable energy and storage (Mass.gov, 2020a). Five performance measures were used to evaluate different PV-battery system design and management scenarios: peak load reduction, life cycle cost (LCC), fossil fuel depletion, carbon footprint, and water footprint. This study aims to evaluate and understand the tradeoffs among the peak load reduction, economic, and environmental performances of different solar PV-battery system design and management scenarios under TOU rates in support of future pertinent policy and incentive designs.

3.2. Methodology

3.2.1. System and scenario descriptions

The grid-connected polycrystalline silicon (poly-Si) PV panel and Li-Ion battery system was selected in this study given their popularity and cost competitiveness (Sharma et al., 2015). Figure

3-1 presents a schematic of the setup of the studied system. The PV-battery system was applied to a prototype low-rise multifamily house based on the US Department of Energy's House Simulation Protocol (Wilson et al., 2014). The hourly load profiles of this prototype house was collected from the Open Energy Information database for the Boston Logan area, MA for our simulation (NREL, 2014). The grid fuel mix was collected from ISO New England Inc. (ISO-NE), an independent and non-profit Regional Transmission Organization (RTO) serving the New England area (ISO-NE, 2018b).

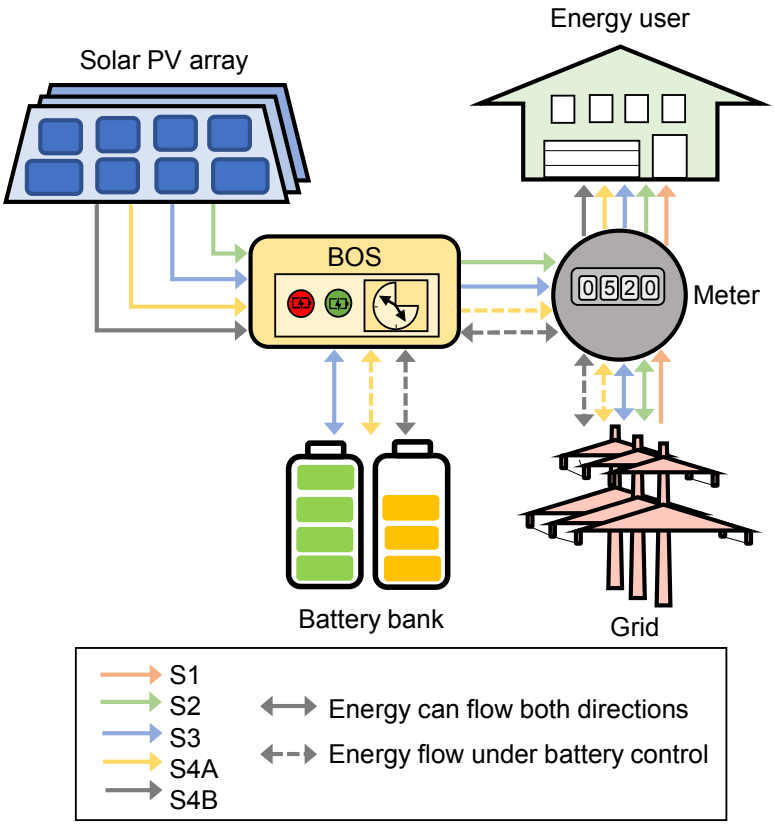

Figure 3-1. Schematic of the GC solar PV-battery system

The TOU rate structure adopted in this study came from a pilot study conducted by the Liberty Utilities in 2018 (Tebbetts, 2018), which includes an off-peak, mid-peak, and on-peak rate (Figure 3-2). For comparison purpose, a flat rate structure was also investigated, which utilizes a constant

rate of 16 cents/kWh calculated as the average electricity rate in New England area from 2016 to 2017 (NREL, 2017). For simplicity, solar feed-in-tariffs were assumed to be the same as electricity retail prices under both TOU and flat rate structures.

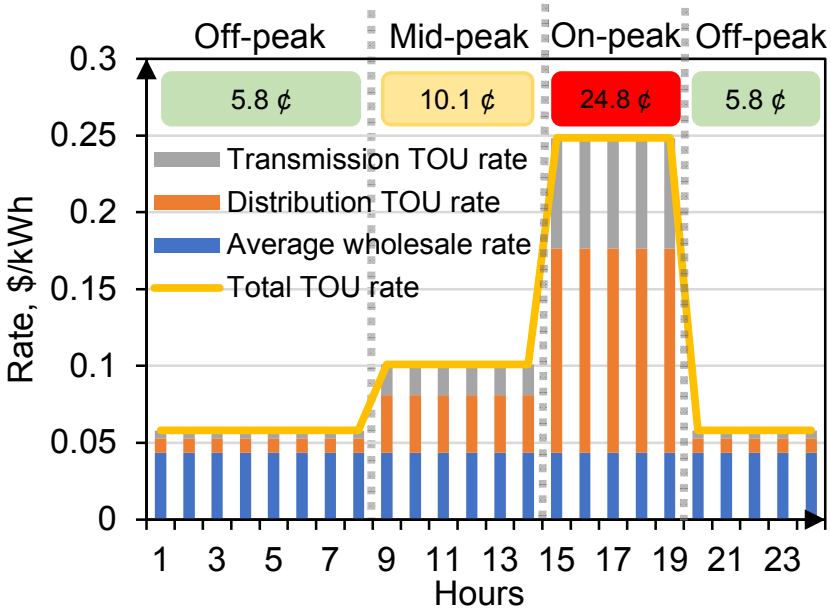

Figure 3-2. The TOU rate design that is utilized in this study

Five solar PV-battery design and management scenarios were investigated (Figure 3-1). Scenario 1 (**S1**) describes a baseline condition where no PV or battery was installed. The household relies entirely on the grid. Scenario 2 (**S2**) represents a condition where only PV panels were installed. The panel size was assumed to be 12.2 kW, which was designed to meet the peak load of the prototype house. The same panel size was also utilized in the following scenarios. Scenario 3 (**S3**) is when both PV and batteries were installed but the battery system was not managed according to the TOU rate structure. Only solar energy can charge the battery. Scenario 4A (**S4A**) is when both PV and batteries were installed and managed according to the TOU rate structure. Only solar energy can charge the battery. Scenario 4B (**S4B**) is similar to S4A except that both solar energy and the grid were allowed to charge the batteries. These scenarios are reflective of the typical

residential PV system designs and/or operation strategies with consideration of potential user benefits and the developing policy initiatives in the energy industry. The rules of system control under each scenario were further discussed in Section 3.2.2.1.

3.2.2. Description of the modeling framework

Load reduction, economic, and environmental performances were assessed in this study by integrating SDM, life cycle cost assessment (LCCA), and life cycle assessment (LCA). SDM is a computational method applying a set of linked differential equations to simulate the behavior of complex systems over a certain time period and studying the interactions among system components through capturing system feedback loops and delays (Forrester, 1997; Sterman, 2000). LCCA adopts a net present value (NPV) method to account for all economic costs and savings that incur during the life span of a PV-battery system (Durairaj et al., 2002). LCA assesses the supply chain environmental impacts attributable to the entire life cycle of a PV-battery system (Rebitzer et al., 2004). In this study, the SDM was used to simulate the dynamic behavior of energy generation, storage, and grid sell on a thirty-minute step over a typical year (Peng et al., 2017; Reddi et al., 2013; Ren et al., 2020). Outcomes from the SDM were used to inform the off-, mid-, and on-peak load reductions, costs/savings, fossil fuel depletion, carbon footprint, and water footprint calculations over the 20-year use life of the solar PV-battery systems. The conventional LCCA and LCA methods were applied to the manufacturing, transportation, maintenance (i.e., battery replacement) phases of the solar PV-battery systems.

3.2.2.1. System dynamics modeling of the solar PV-battery system

The SDM was developed in Vensim DSS® software given its wide application (Ford and Ford, 1999). This section was intended to provide a brief overview of the SDM, while a more detailed model description can be found in Ren et al. (2020).

Solar energy generation was calculated following a method that was used in the HOMER software, adjusted to consider the cooling effect provided by wind (Section A3 in APPENDIX A) (Ren et al., 2020). The amount of generation depends on three key time-varying input variables: incident solar radiation, ambient temperature, and wind speed. All three variables were obtained from the National Solar Radiation Database (NREL, 2015). Battery storage was simulated based upon battery charge, discharge, and energy loss at each time step. The initial battery storage was assumed to be zero. The charging and discharging rates depend on the total charging/discharging need and the existing battery storage at each time step, as well as the total battery storage capacity. These rates were constrained by the maximum charging and discharging rates calculated based upon the percent vacancy of the battery capacity at each time step (Equation. A4-8 in Section A3 of APPENDIX A) (Energy, 2017). Energy loss during charging and discharging was calculated based upon the system round-trip efficiency, which was assumed to be 80% (around 10.6% of the charging and discharging rates was lost) (Dufo-López and Bernal-Agustín, 2015). In addition, battery replacement over the system lifespan was estimated through the ratio of the actual battery system throughput to the rated battery system throughput (HOMER, 2017).

The SDM contains an energy balance sub-model which controls the allocation of the generated solar energy to house consumption, battery charge, and grid sell as well as the timing and amount

of battery charge and discharge. Grid sell was assumed to be unconstrainted considering the current Massachusetts Net Metering policy (Mass.gov, 2020b). Table 3-1 presents the rules of system control under the five scenarios.

Table 3-1. Prioritization of generated solar energy distribution

<table>
<tr><th>Peak time</th><th>S1</th><th>S2</th><th>S3</th><th>S4A</th><th>S4B</th></tr>
<tr><td>off-peak</td><td rowspan="3">No solar energy is generated.</td><td rowspan="3">Solar energy generated is prioritized for meeting household demand before grid sell.</td><td rowspan="3">Solar energy prioritization goes from meeting household demand, battery charging to grid sell. Battery storage is discharged whenever household demand cannot be met by the solar energy before the grid kicks in.</td><td rowspan="2">Solar energy prioritization goes from battery charging, meeting household demand to grid sell. Battery is not discharged during this period.</td><td>Solar energy prioritization goes from battery charging, meeting household demand to grid sell. Grid charge only kicks in if the battery is not fully charged by the solar energy 30 mins before the off-peak period ends. Thirty minutes were assumed to be sufficient to fully charge the battery system. Battery is not discharged during this period.</td></tr>
<tr><td>mid-peak</td><td>Solar energy generated during this period is prioritized for meeting household demand and then grid sell. The battery system remains fully charged and inactive.</td></tr>
<tr><td>on-peak</td><td colspan="2">Battery is fully discharged for grid sell and then remains inactive. Solar energy generated is prioritized for meeting household demand before grid sell.</td></tr>
</table>

Load reductions (kWh) during different time periods were calculated using Equation 3-1.

$$R_{load} = \int_{t_0}^{t} \left(E_{solar} + E_{sell,PV} + E_{discharge,g}\right) dt \qquad \text{Equation 1}$$

Where, R_{load} represents the load reduction of the grid, kWh; E_{solar} is the household demand met by solar energy, kW; $E_{sell,PV}$ is the direct grid sell from the PV system, kW; $E_{discharge,g}$ is the grid sell from the battery storage, kW.

3.2.3. Life cycle cost assessment

The LCC of installing a solar PV-battery system was calculated as the NPV of the capital cost, operation and maintenance (O&M) cost, tax credit and rebate using Equation 3-2. The capital cost of the system includes the costs of panels and racking ($1/Watt of generation capacity) (McFarland, 2014), batteries ($209/kWh of storage capacity) (Curry, 2017), inverters ($300/inverter unit) (HOMER, 2018), permission ($450/system) (NREL, 2017), and labor (calculated based upon a tiered pricing; Figure A-1 in Section A3) (HomeAdvisor, 2019). All future costs were discounted to the year of 2020 applying a discount rate of 5% (Ren et al., 2020).

$$C = C_c - C_r + \sum_{n=0}^{n=L}\left[\frac{C_{o,n} + r_{off}\int_{t_{off}}\left(E_{u,t} - E_{s,t} - E_{d,t}\right)dt + r_{mid}\int_{t_{mid}}\left(E_{u,t} - E_{s,t} - E_{d,t}\right)dt + r_{on}\int_{t_{on}}\left(E_{u,t} - E_{s,t} - E_{d,t}\right)dt}{(1+d)^n}\right]$$

Equation 3-2

Where, C represents the LCC of a PV-battery system, $; C_c is the capital cost of the system, $; C_r is the tax credit (30% of the capital cost) (IRS, 2019), and rebate ($0.25/Watt of installed PV capacity) (NHMA, 2015); L is the life span of the solar PV system, 20 years; $C_{o,n}$ is the battery replacement cost in one year, $; r_{off}, r_{mid}, and r_{on} are the off-peak, mid-peak, and on-peak rates respectively, $/kWh; t_{off}, t_{mid}, and t_{on} are the duration of off-peak, mid-peak, and on-peak time in a year respectively, hours; $E_{u,t}$ is the actual grid use, kW; $E_{s,t}$ is the direct grid sell from the PV system, kW; $E_{d,t}$ is the grid sell from the battery storage, kW; d is the discount rate, 5%; n is the year index; $E_{u,t}$, $E_{s,t}$, and $E_{d,t}$ were obtained from the SDM model.

3.2.4. Life cycle assessment

Environmental impacts considering life cycle stages of manufacturing, transportation, and operation were assessed using Equation 3-3. The global average manufacturing impacts of the solar PV-battery system components obtained from the EcoInvent 3.0 were utilized in this study. The operation phase considers the environmental impacts related to the grid use and the replacement of batteries over the life cycle. The savings from solar energy consumption and grid sell were also considered in the operation phase. The disposal phase of the PV-battery system is not considered following (Bernardes et al., 2004; Grinenko, 2018). SimaPro 8.3 was used for charactering the environmental impacts. Specifically, the ReCiPe Midpoint (H) 1.12, Europe Recipe H was used for estimating the climate change, fossil fuel depletion, and water depletion impacts associated with each PV-battery system components. The SimaPro entries, unit costs, and environmental impacts of the PV-battery system components are provided in Table B-1 of the APPENDIX B.

$$I = I_m + I_t + \left[I_r + f_{off}\int_{t_{off}}\left(E_{u,t} - E_{s,t} - E_{d,t}\right)dt + f_{mid}\int_{t_{mid}}\left(E_{u,t} - E_{s,t} - E_{d,t}\right)dt + f_{on}\int_{t_{on}}\left(E_{u,t} - E_{s,t} - E_{d,t}\right)dt\right]L \quad \text{Equation 3-3}$$

Where, I represents the life cycle environmental impacts of a PV-battery system, kg CO_2 eq., kg oil eq., or L; I_m is the environmental impacts associated with system manufacturing, kg CO_2 eq., kg oil eq., or L; I_t is the environmental impacts associated with system transportation, kg CO_2 eq., kg oil eq., or L; I_r is the annual environmental impacts of the replacement of batteries, kg CO_2 eq., kg oil eq., or L; f_{off}, f_{mid}, and f_{on} are the unit environmental impacts during off-, mid-, and on-peak periods respectively, kg CO_2 eq./kWh, kg oil eq./kWh, or L/kWh; t_{off}, t_{mid}, and t_{on} are the duration of off-peak, mid-peak, and on-peak time in a year respectively, hours; $E_{u,t}$ is the actual

grid use, kW; $E_{s,t}$ is the direct grid sell from the PV system, kW; $E_{d,t}$ is the grid sell from the battery storage, kW; L is the life span of the PV system, 20 years.

f_{off}, f_{mid}, and f_{on} were calculated based upon the 2017 New England grid fuel mix profile (Figure 3-3a) obtained from the Independent System Operator-New England (ISO-NE) database (ISO-NE, 2018b). Particularly, f_{off} was calculated based on the utility fuel mix profile of the off-peak period during 2017. f_{mid} was calculated based on the additional load in GW provided by different fuel types during the mid-peak period as compared to the off-peak period (Figure 3-3b). f_{on} was calculated based on the additional load in GW provided by different fuel types during the on-peak period as compared to the mid-peak period. As such, our calculations reflect the "actual" fuel mix that is replaced as a result of the installation of solar PV-battery systems. Figure 3-3c presents the unit environmental impacts associated with carbon emissions, water consumption, and fossil fuel depletion during the off-, mid-, and on-peak periods. Unit environmental impacts associated with each fuel type are provided in Table B-2 of the APPENDIX B.

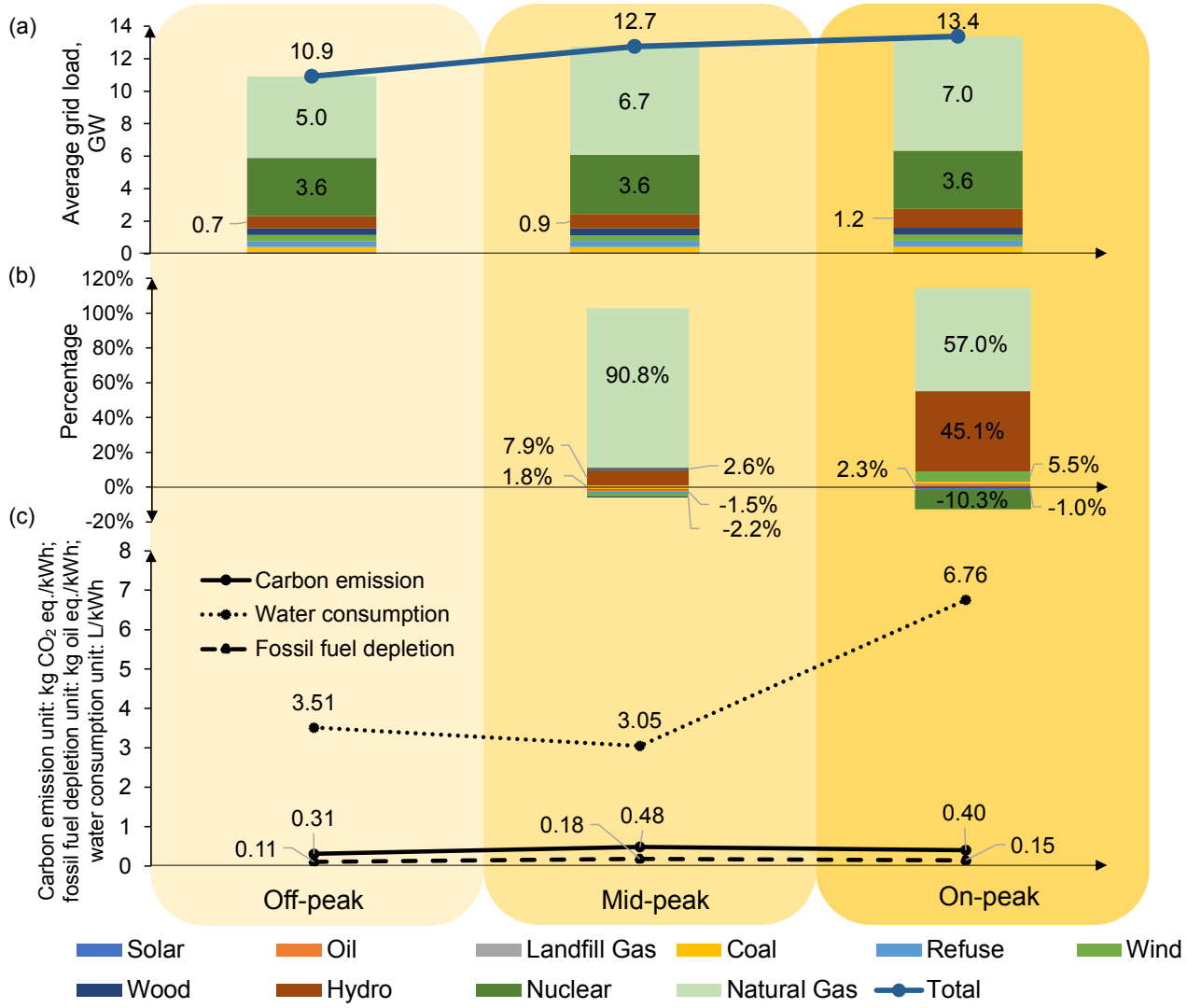

Figure 3-3. (a) Average annual grid load during the off-, mid-, and on-peak periods obtained from the Independent System Operator-New England (ISO-NE); (b) percentages of grid fuel mix that were used for calculating carbon emission, water consumption, and fossil fuel depletion factors during the mid- and on-peak periods; and, (c) estimated unit carbon emission, water consumption, and fossil fuel depletion per kWh of electricity consumption during the off-, mid-, and on-peak periods

3.2.5. Sensitivity analysis

A sensitivity analysis was performed to investigate the influence of TOU rate structure, discount rate, on-peak grid fuel mix, and duration of on-peak period on the economic and environmental performances of a typical PV-battery system with 50 panels and 50 batteries installed on the prototype house. Particularly, the model's sensitivity to changes in the on-peak grid fuel mix was

investigated by changing the hydropower and natural gas contributions in the grid during the on-peak hours, given their significance. We investigated scenarios where the increase in the percentage of on-peak hydropower grid contribution was associated with a corresponding decrease in the natural gas contribution, and vice versa. Hence, the total on-peak grid demand remained the same under these scenarios. We also assumed the change of on-peak period duration is associated with equal changes in both off- and mid-peak durations (Table B-3 of APPENDIX B). For instance, a 2.5-hour increase in the on-peak period is associated with a 1.25-hour decrease in the mid-peak period immediately preceding the on-peak period, plus a 1.25-hour decrease in the off-peak period that immediately follows. Each of the selected input variables were varied by ± 50%. A sensitivity index (D) was calculated for each input change using Equation 3-4 (Ren et al., 2020; Song et al., 2019b).

$$D = \frac{\frac{d_i - d_b}{d_b}}{\frac{I_i - I_b}{I_b}} \quad \text{Equation 3-4}$$

Where d_i is the output value after the input was changed; d_b is the base output value; I_i is the altered input value; and I_b is the original input value. Inputs were considered "highly sensitive" if $|D| > 1.00$.

3.3. Results and Discussion

3.3.1. Solar and grid energy utilization and peak load reduction

Figure 3-4 presents the daily solar energy generation and utilization, battery charge, and grid sell/use patterns of the prototype building with 50 panels and 50 batteries during a typical winter (left) and a typical summer (right) day. The building's peak electricity usage periods (6-8 AM and

PM) only slightly overlaps with the on-peak period (2-7 PM) designated by the TOU rate structure, indicating a potential need of energy storage systems. Overall, the studied building uses 1.75 times more energy on the winter day as compared to the summer day, which can be attributed to the higher heating demand in winter.

Installing a 50-panel PV system in the prototype building (Scenario S2) can provide load reductions both during mid-peak and on-peak hours (Figures 3-4a and 3-4b). The on-peak load reduction is much higher on a typical summer day mainly due to the seasonal changes in solar energy generation. Adding an "uncontrolled" 51-kW battery system (Scenario S3), however, may decrease the peak load reduction benefits (Figures 3-4c and 3-4d). The total load reductions during the mid- and on-peak periods are around 91.8% and 49.9% of those associated with Scenario S2 in winter and summer, respectively. This is because the large amount of solar energy generated during the mid- or on-peak hours, especially in summer, may be stored and used during the off-peak hours as compared to Scenario S2. While Scenario S3 has limited peak load reduction benefits in a grid-connected setting, it might appeal in a standalone system that is not grid-connected. When the on-peak load reduction is considered alone, Scenario S3 can potentially provide increased load reduction during winter but decreased load reduction during summer, indicating the importance of seasonal variations of solar energy generation patterns. When the battery system is controlled for peak load reduction (Scenario S4A), the total mid- and on-peak load reductions are 87.9% and 94.4% of those associated with Scenario S2 in winter and summer, respectively; and the on-peak load reductions are 2.7 and 1.6 times of those associated with Scenario S2 in winter and summer, respectively (Figures 3-4e and 3-4f). This shows battery control can effectively increase on-peak load reduction, but its charging and discharging losses might slightly reduce the total mid-and on-

peak load reduction benefit. When the grid is allowed to charge batteries (Scenario S4B), peak load reduction benefit is the highest (Figures 3-4g and 3-4h). The total mid- and on-peak load reductions are 2.6 and 2.0 times of those associated with Scenario S2 in winter and summer respectively, while the on-peak load reductions are 10.0 and 3.0 times of those associated with Scenario S2 in winter and summer respectively.

Figure 3-5 further presents annual load reductions under the simulated scenarios. Scenario S4B provides the highest peak load reduction benefit considering either on-peak hours alone or on-peak and mid-peak hours combined, 5.2 and 3.3 times of the lowest counterparts. However, around 80.7% of the on-peak load reduction is provided by the grid energy from off-peak hours rather than solar energy generated. Scenario S2 has the lowest on-peak load reduction, while Scenario S3 has the lowest load reduction when mid- and on-peak hours are combined.

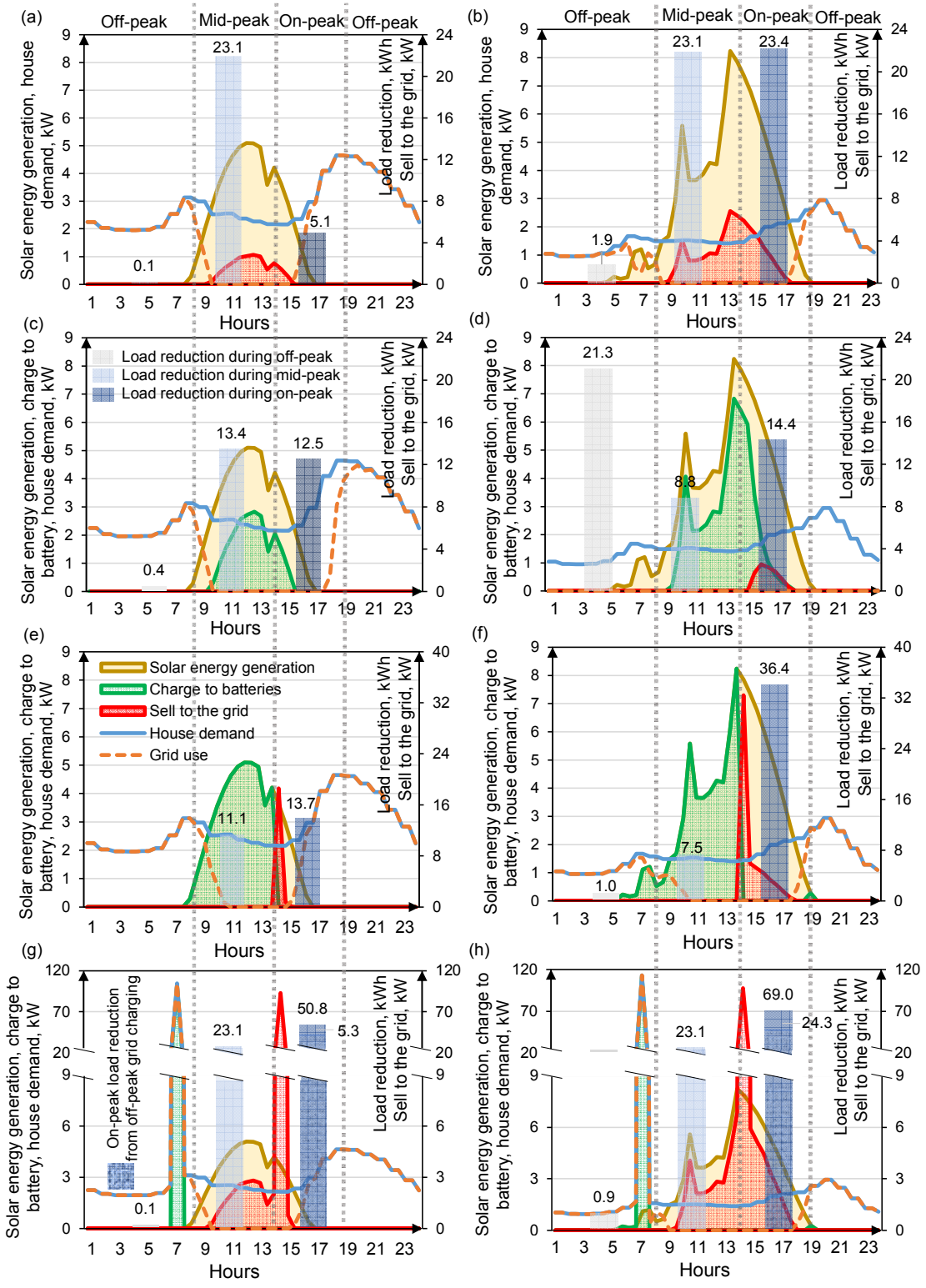

Figure 3-4. Solar energy and grid electricity utilization of the typical solar PV-battery system in Scenarios S2 (a and b), S3 (c and d), S4A (e and f), and S4B (g and h) on a typical winter day and a typical summer day. Figures on the left-hand side (a, c, e, g) correspond to a typical winter day and figures on the right-hand side (b, d, f, h) correspond to a typical summer day.

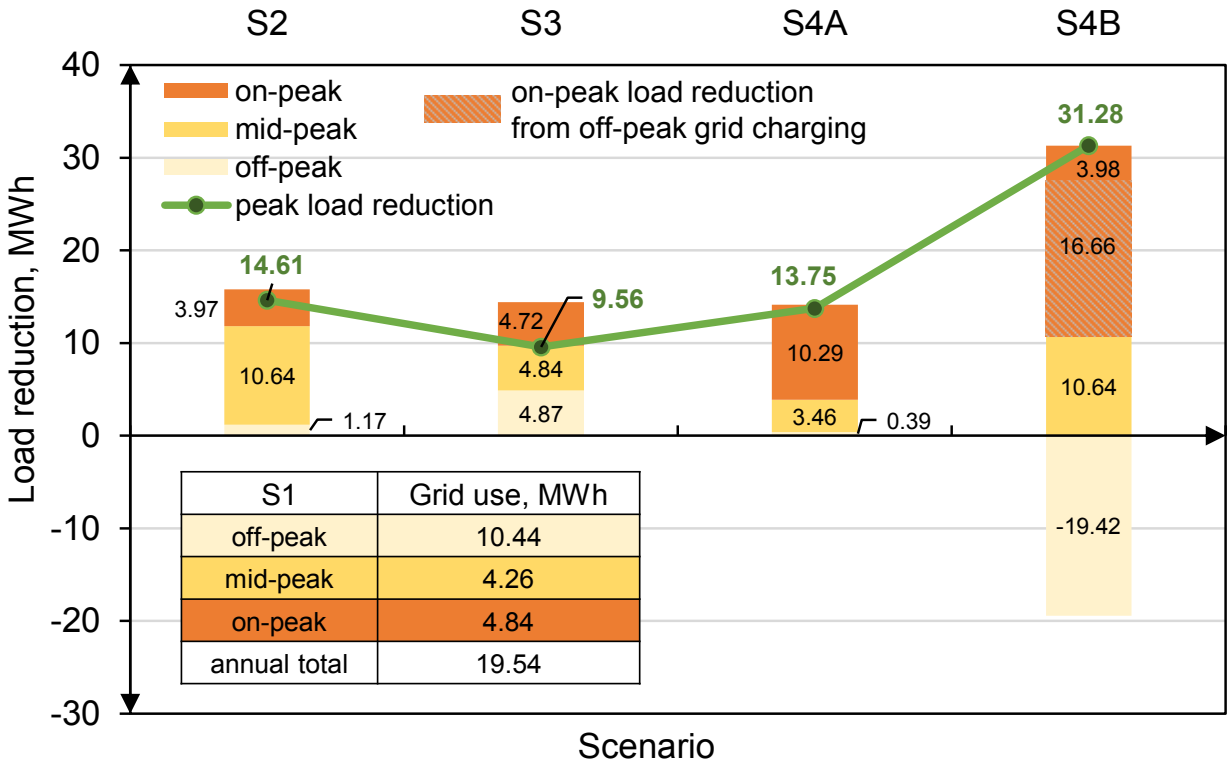

Figure 3-5. Annual total load reductions in the simulated scenarios (the green line plot shows the sum of load reductions from mid- and on-peak hours.)

3.3.2. Life cycle cost assessment

Figure 3-6 presents the LCCs of the simulated scenarios considering different battery sizes. Under the TOU rate design, Scenario S4B consistently presents the lowest LCC regardless of battery size, by taking advantage of the price difference between off- and on-peak hours. It is also the only scenario that is able to achieve net cost saving when the battery size is sufficiently large. However, this might be subject to policies including caps on residential charge from and resell to the grid. The ranking of the other scenarios change based on battery size. When the battery size is relatively small (5-20 batteries), Scenarios S2 and S4A present similarly low LCC, followed by Scenario S3, while Scenario S1 presents significantly higher LCC compared with the remaining scenarios. When the battery size is relatively large (80-160 batteries), Scenario S2 has the second lowest LCC,

followed by Scenarios S4A and S1, while Scenario S3 has the highest LCC. This indicates the importance of matching battery sizing and control strategies to achieve the lowest LCC. Compared with the current flat rate structure, the TOU rate design results in an economic benefit for the prototype house. Under the flat rate design, Scenario S2 always presents the lowest LCC regardless of battery size, indicating a potential lack of economic incentive to install battery storage systems.

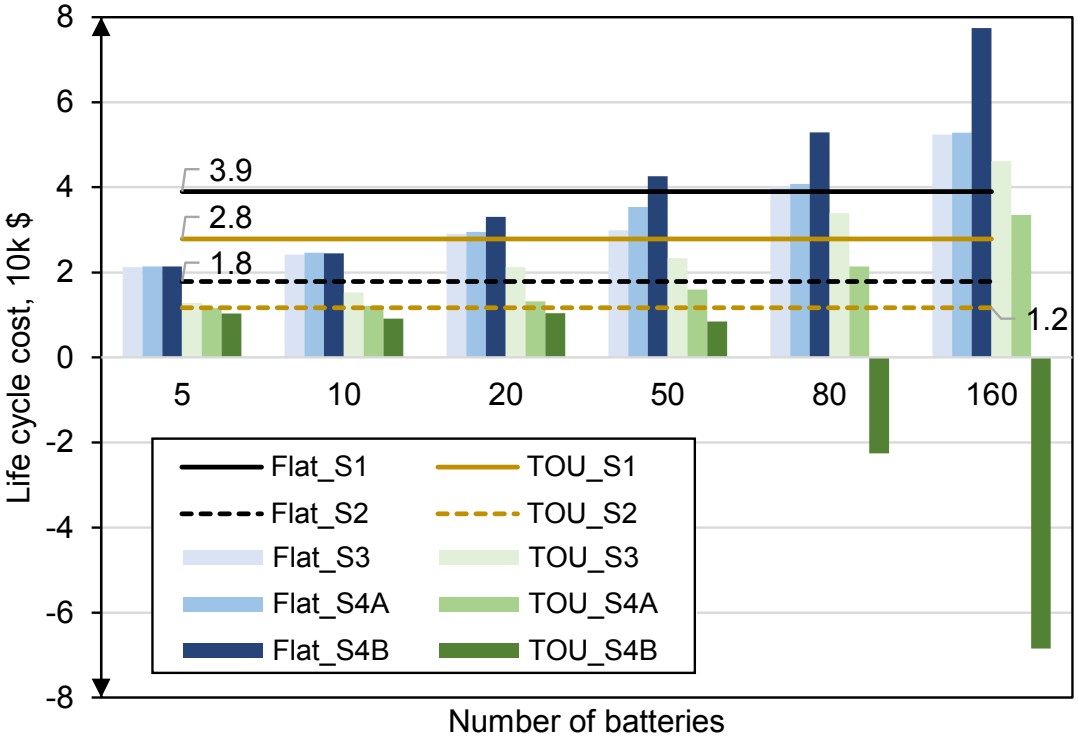

Figure 3-6. LCCs (discount rate: 5%) of the solar PV-battery systems under TOU and flat rate designs considering different management (Scenarios S1-S4B) and battery sizing scenarios

3.3.3. Life cycle environmental assessment

Figure 3-7 presents the life cycle climate change, water depletion, and fossil fuel depletion effects under varied battery sizing and control strategies for the prototype house. The life cycle climate change, water depletion, and fossil fuel depletion effects of the typical 50-panel PV system (no battery) in this study are 61.9 g CO_2 eq., 2.54 L, and 0.0165 kg Oil eq. (0.69 MJ based on 1 kg Oil eq. = 41.9 MJ (UJ, 2016)) per kWh of solar energy generated, respectively, all of which are within

the previously reported range of 50-800 g CO_2 eq./kWh, 0.73-7.2 L/kWh, 0.22-1.04 MJ/kWh for roof-mounted solar PV electricity generation, respectively (Fthenakis and Kim, 2010b; Kim et al., 2014; Stamford and Azapagic, 2018; Stolz, 2017; Stoppato, 2008). Scenario S4B generally performs the best environmentally regardless of battery sizes, while Scenario S1 performs the worst. Scenario S4A presents the second highest life cycle climate change and fossil fuel depletion effects following Scenario S1, although it provides a relatively large on-peak load reduction. This is because Scenario S4A shifted load reductions from mid-peak to on-peak period, while the on-peak period has lower carbon and fossil fuel intensities compared to mid-peak hours, due to a higher contribution from hydropower. This indicates the importance of the daily grid mix patterns in determining the environmental performance of battery control strategies that maximize on-peak load reductions. Scenario S4A also presents an optimal battery sizing at 50, which aligns with the default battery size calculated based on maximum daily electricity use. This indicates the engineering rule-of-thumb used in this study is effective in achieving the minimized household climate change, water depletion, and fossil fuel depletion effects. On the other hand, the installation of solar PV-battery systems (Scenarios 3 and S4A) does not present a significant benefit in terms of water depletion as compared to the climate change and fossil fuel depletion impacts, expect for Scenario S4B at relatively larger battery sizes. This is because of the high initial water demand associated with PV and battery productions.

Overall, our results show that while installing a solar PV system clearly provides environmental benefits, adding a battery storage does not necessary provide additional carbon, water, or energy benefits. The solar PV-battery system also does not provide essential water benefits except when a large battery capacity is installed and the battery system is allowed to charge from and resell to

the grid in Scenario S4B. When peak load reduction, economic, and environmental impacts are considered together, Scenario S2 presents relatively good economic and environmental performances, although its on-peak load reduction is limited. Scenario S4B presents excellent peak load reduction, economic, and water benefits, but its carbon and energy benefits are relatively limited as compared to Scenario S2. However, this result may differ for regions with a more fossil fuel dependent grid. Scenario S4A has relatively good on-peak load reduction and economic performances, but it does not provide effective carbon emission and fossil fuel use reductions as compared to Scenario S2. Installing a solar PV system without an effective control strategy, such as in Scenario S3 might lead to sub-optimized peak load reduction, economic, and environmental outcomes.

3.3.4. Sensitivity analysis

Figure 3-8 presents the percent changes of LCC of a typical 50-panel 50-battery solar PV-battery system in response to changes of the discount rate, TOU rates during off, mid, and on-peak periods, and the duration of the on-peak period. The LCC outcomes of Scenario S4B are highly sensitive to changes in on- and off-peak electricity rates as well as the discount rate. This can be explained by the scenario's high dependence on the difference between the electricity rates between on- and off-peak hours. Scenario S4B is also highly sensitive to changes in the discount rate. In contrast, Scenario S4A is only sensitive to the on-peak rate. This is because the economic saving in this scenario largely relies on the on-peak grid sell. All the remaining scenarios are not sensitive to ±50% change of the five input variables. Particularly, Scenario S3 presents the lowest sensitivity. This is because of the limited solar energy use during the mid- and on-peak hours under this scenario.

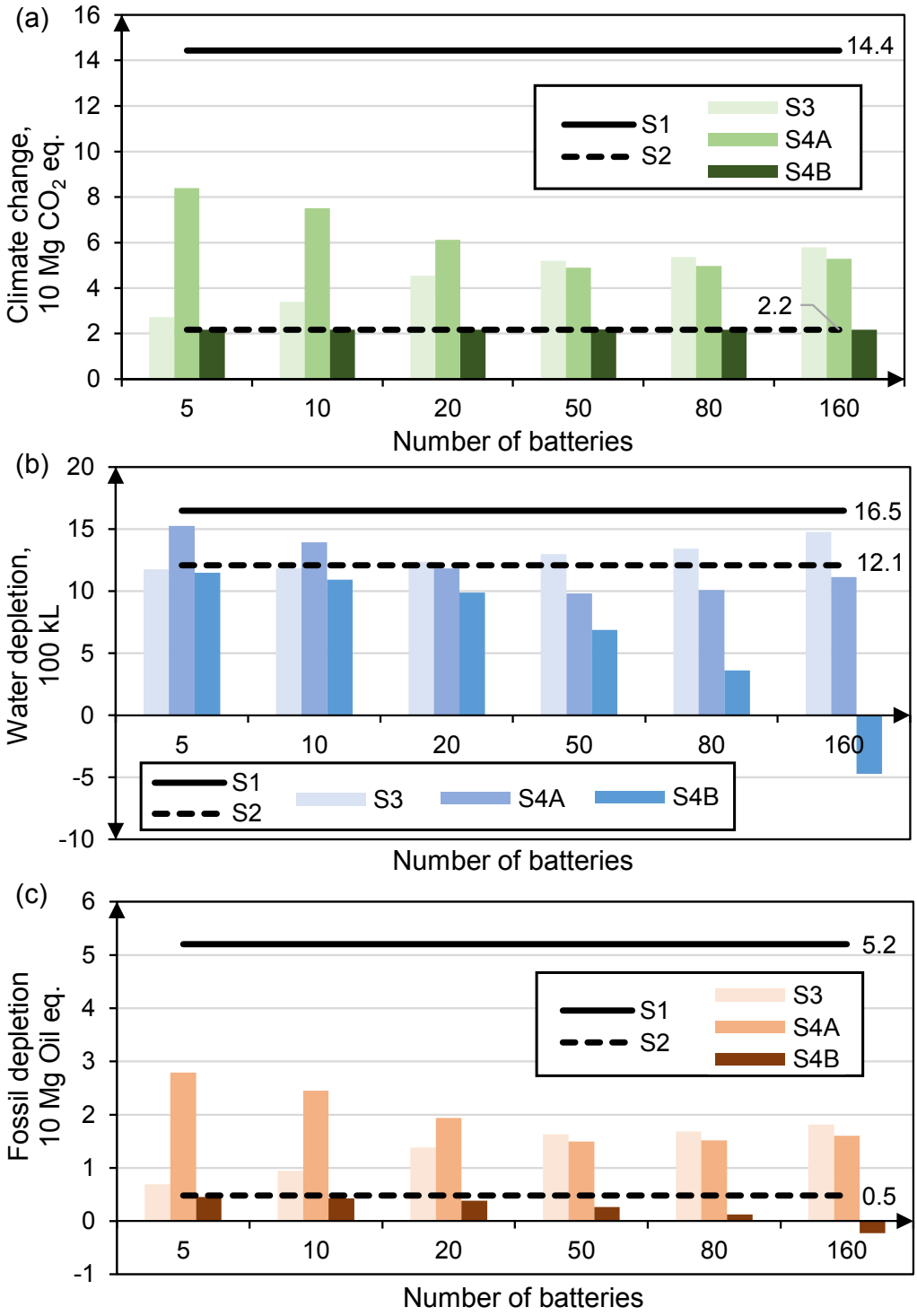

Figure 3-7. Life cycle (a) climate change, (b) water depletion, (c) fossil fuel depletion of the solar PV-battery systems under different management (Scenarios S1-S4B) and battery sizing scenarios

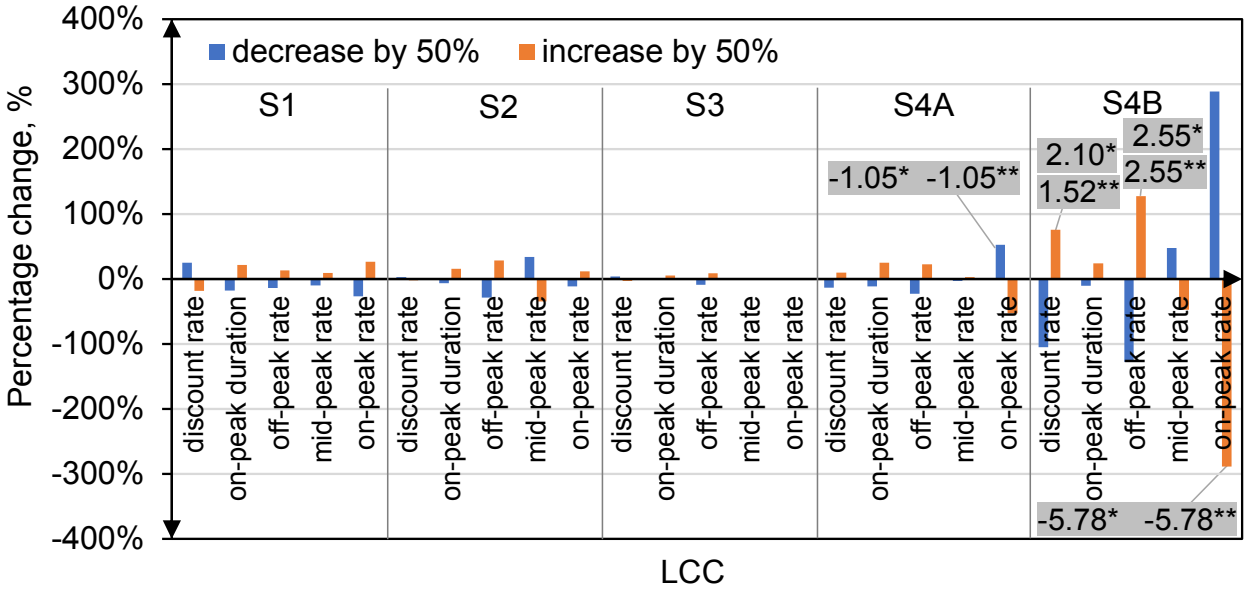

Figure 3-8. The percent change of LCC of the 50-panel 50-battery solar PV-battery system in response to decrease or increase of the selected variables by 50%. Shaded numbers indicate where the absolute values of the sensitivity index *D* are equal to or larger than 1. One asterisk and two asterisks represent the sensitivity index values that are associated with 50% decrease and increase of the tested variables, respectively.

Figure 3-9 presents the percent changes of life cycle climate change, water depletion, and fossil fuel depletion of the typical 50-panel 50-battery solar PV-battery system in response to changes in the on-peak grid fuel mix and the on-peak duration. Our results show all three environmental outcomes of Scenario S4B are highly sensitive to changes in the on-peak grid mix, as the battery system maximizes on-peak uses/sale of solar energy and shifts on-peak demand to the off-peak period. This highlights the importance of on-peak grid mix in influencing the environmental outcomes of battery management strategies that target solar energy sales during the on-peak hours. On the other hand, the on-peak duration can significantly influence the life cycle fossil fuel depletion of Scenarios S4B, as a result of changes in the amount of solar energy that will be available for sale or direct use during the on-peak hours. Scenario S3 was found to be the least

sensitive to either tested variables, mainly due to a combined effect of its high baseline environmental impacts as well as the limited solar energy use or sale during the on-peak hours.

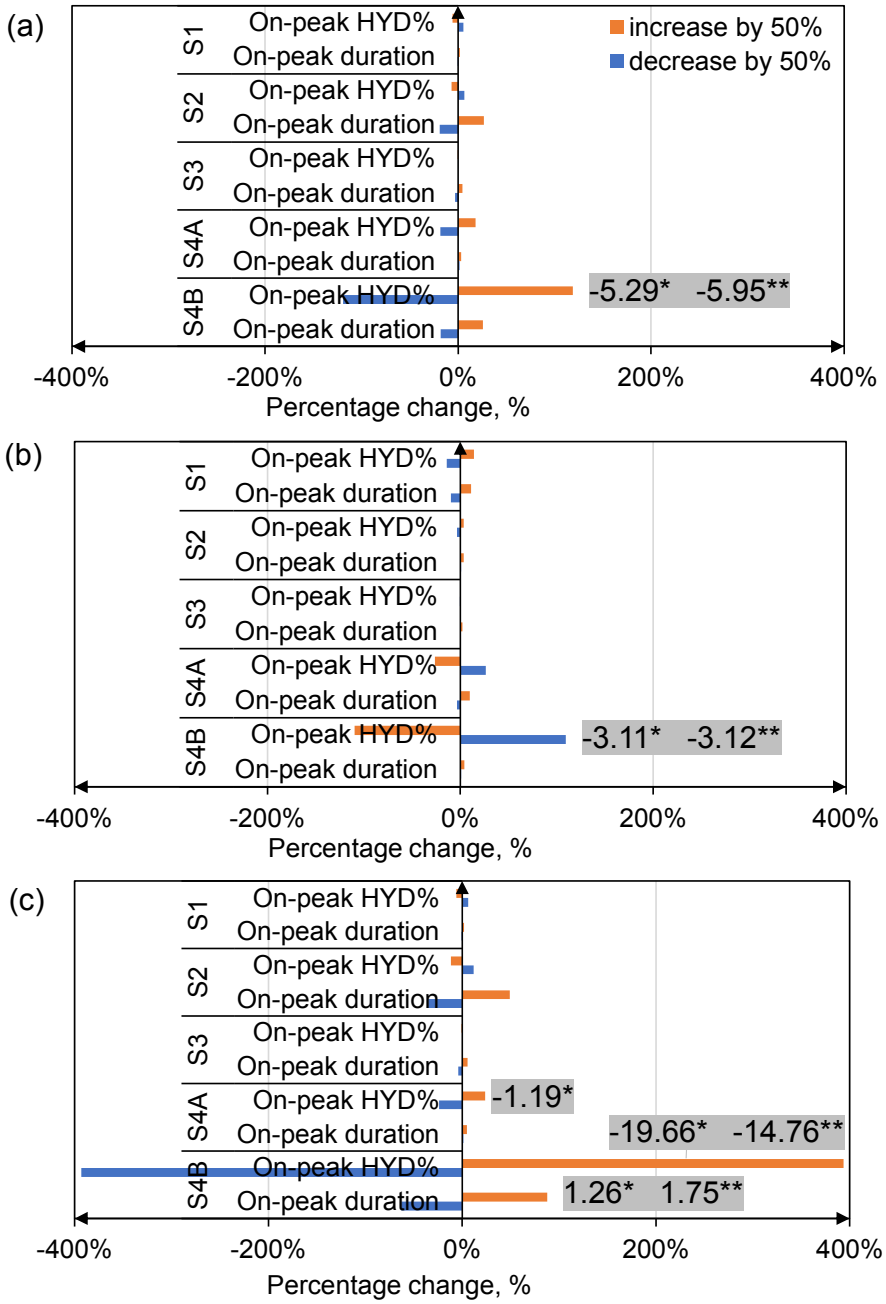

Figure 3-9. Life cycle (a) climate change, (b) water depletion, and (c) fossil fuel depletion of the PV-battery systems in response to decrease or increase of the selected variables by 50%. Shaded numbers indicate where the absolute values of the sensitivity index *D* are equal to or larger than 1. One asterisk and two asterisks represent the sensitivity index values that are associated with 50% decrease and increase of the tested variables, respectively.

3.4. Conclusion

SDM, LCCA, and LCA were integrated to investigate the design and operation of solar PV-battery systems that can achieve grid, environmental, and economic co-benefits under TOU rate design, using a 5-unit prototype house in the Boston-Logan, MA area as a case study. Five scenarios (S1-S4B) were investigated, each with different solar PV-battery system design and/or management strategy. We found scenarios that maximize the selling/use of solar energy during the on-peak hours through battery installation and control (Scenarios S4A and S4B) can achieve the highest on-peak load reductions and economic benefits under the TOU rate design. However, they do not necessary provide the highest environmental benefits, as on-peak hours in the New England grid have lower carbon emission and fossil fuel depletion factors as compared with the mid-peak hours. This indicates a potential tradeoff between the need of on-peak load reduction, economic saving, and environmental protection. From an environmental perspective, our finding demonstrates the necessity of better battery control or TOU designs that can effectively incentivize solar energy uses when the grid carbon intensity is the highest. While S4A is shown to be effective in reducing on-peak load in the grid, its overall load reduction from both mid- and on-peak hours is slightly less than Scenario S2 where PV panels are installed without battery. This is partly due to the energy loss resulted from battery charging and discharging. Overall, Scenario S4B presents relatively good performances from peak load reduction, economic, and environmental perspectives. However, its benefits might be limited by policies that cap grid charge and discharge from the battery systems. Out of the remaining scenarios, installing a PV system alone (Scenario S2) presents relatively strong economic and environmental performances, but its on-peak load reduction is limited. Installing a battery system without an effective control strategy (Scenario S3) results in relatively weak peak-load reduction, economic, and environmental outcomes. This

highlights the importance of effective battery control in the implementation of solar PV-battery systems. Future studies may further include emerging technologies such as the vehicle-to-home systems as well as the interactions between distributed solar PV-battery systems and the centralized grid to allow for a more holistic and dynamic optimization of the solar PV-battery system design and operation.

4. CHAPTER 4: DYNAMIC SIMULATION OF REGIONAL RESIDENTIAL PHOTOVOLTAICS ADOPTION AND ASSESSMENT OF ITS TECHNICAL, ECONOMIC, AND ENVIRONMENTAL IMPACTS[3]

4.1. Introduction

The residential solar photovoltaic (PV) system adoption has increased significantly in the US (EIA, 2021a), primarily due to reduced cost (K. Branker et al., 2011), environmental benefits (Sherwani et al., 2010b), and strong policy incentives (e.g., Federal Energy Regulatory Commission Order 2222) (FERC, 2020; Li and Yi, 2014). The benefit of solar PV systems was further manifested during recent extreme climate events (e.g., 2021 U.S. Northwest heatwave and 2021 Texas winter storm), which resulted in high local/regional electricity prices (EIA, 2021b; Zamuda et al., 2019). In both events, solar PVs have been recognized as an effective energy supply for increased resiliency and for offsetting the potential effects of excessive high prices for energy users (Brown et al., 2016; Chesser et al., 2018). On the other hand, increased PV penetration could also significantly alter the peak demand pattern of the electric grid, causing a steeper ramp-up which may be more difficult to management (Cheng et al., 2015). Furthermore, the regional cost saving of PV adoption may dissipate due to the increasing PV penetration and decreasing grid sell prices, which could reduce individual PV hosts' cost benefit (SEIA, 2012). Therefore, it is significant to investigate the technical, economic, and environmental tradeoffs to inform PV planning and management decisions.

[3] This chapter is a journal article under preparation. Please use the following citation for work related to this chapter: Ren M, Ghasemi R, Khalkhali M, Mo W. Dynamic simulation of regional residential photovoltaics adoption and assessment of its technical, economic, and environmental impacts[J]. 2021, in prep.

Previous technical assessments of residential PV systems have focused on assessing PV generation potential (Gagnon et al., 2016; Hofierka and Kaňuk, 2009; Lazzeroni et al., 2015; Robinson et al., 2013; Villavicencio Gastelu et al., 2018), investigating grid load fluctuations under PV adoptions (Cheng et al., 2015; Eftekharnejad et al., 2013; Thomson and Infield, 2007; Watson et al., 2016; Westacott and Candelise, 2016), optimizing individual systems for grid load peak reduction (Alam et al., 2016; Wang et al., 2020), and comparing varied system operational strategies to mitigate PV adoption's load effect on grid (Aleem et al., 2020; Mukwekwe et al., 2017; Systems, 2019). These studies highlighted that increasing PV implementation would lead to load fluctuations of the electric grid. The economic impact of increasing PV adoption has also been investigated in terms of estimating the economic potential of PV adoption (Agnew et al., 2019; Lee et al., 2018b), comparing utility revenue loss and cost reduction under varied PV adoptions (Brown and O'Sullivan, 2019; Satchwell et al., 2015), estimating additional costs to improve distribution power quality due to load ramp-up caused by increasing PV adoption (McHenry et al., 2016), and quantifying electricity rate change under increasing PV adoption (Brown and O'Sullivan, 2019; Satchwell et al., 2015). However, these studies often utilize annual and monthly average price data (Agnew et al., 2019; Cai et al., 2013; Satchwell et al., 2015), and did not consider the feedback loop between the distributed PV adoption and wholesale electricity price. Only Cai et al., (2013) considered the feedback between PV adoption and electricity rates and investigated the retail electricity rate change under varied residential PV adoption scenarios. The environmental impact of increasing PV adoption has also been assessed for the purposes of estimating and comparing the environmental impact (e.g., carbon emission) of PV adoptions in different historic and future years (Antonanzas and Quinn, 2021), investigating the sensitive variables that influence the environmental impact of PV adoptions (Blanc et al., 2008), and examining the environmental

impact of PV implementations using different system configurations or at varied locations (Lamnatou et al., 2016; Nikolakakis and Fthenakis, 2013; Tsoutsos et al., 2005). Life cycle analysis (LCA) is a popular method which considers the environmental impact of PV adoption in all life cycle stages (e.g., manufacturing, transportation, operation, and disposal) in previous studies (Rebitzer et al., 2004). However, these previous LCA studies remain static. Average annual data (e.g., solar radiation) was used and dynamic interactions between PV generation, grid, and demand were not considered to facilitate individual PVs and grid performance assessments. Moreover, all studies above solely considered a single aspect to investigate the impact of PV adoption.

Some studies investigated the technical, economic, and environmental performances and their tradeoffs of different PV adoptions (Bellocchi et al., 2019; Deltenre et al., 2020; Imam et al., 2020; Jenniches and Worrell, 2019; Thoy and Go, 2021). These studies either assessed the technical and economic feasibility with environmental savings (e.g., avoided carbon emission) of varied types of PV system adoptions (Deltenre et al., 2020; Edalati et al., 2016; Imam et al., 2020; Jenniches and Worrell, 2019; Korsavi et al., 2018; Li et al., 2018; Thoy and Go, 2021), compared the technical, economic, and environmental performances of PV adoption with other types of power generation (e.g., diesel generation) (Jurasz et al., 2020) or in different locations (Arcos-Vargas et al., 2018; Edalati et al., 2016; Li et al., 2018), or reviewed major factors (e.g., PV efficiency and energy policies) that influence PVs' technical, economic, and environmental performances (Hosenuzzaman et al., 2015). Korsavi et al. (2018) and Edalati et al. (2016) found the PV adoption in Iran was not economically beneficial even the PV adoption could achieve ideal carbon reduction. Li et al. (2018) also implied a potential economic and environmental tradeoff that the net present

value of PV adoption and cost of electricity increased with the PV adoption increased, whereas the carbon emission decreased due to the increasing PV generation. Yet Arcos-Vargas et al. (2018) identified co-benefited economic and environmental outcomes of residential PV adoption. However, the environmental assessments in these studies usually focus on the operational phase (e.g., avoided operational carbon emission) instead of the life cycle perspective. Moreover, previous studies ignored the demand side simulation (only generation simulation) or only utilized reported demand data.

The dynamic simulation of residential demand is imperative due to its capability and flexibility to capture the time-varying interactions between the demand, power grid, renewable energy generation, and storage (McAvoy et al., 2021; Muratori et al., 2013; Shimoda et al., 2020). There are two ways to simulate the temporal changes of energy demand, one is top-down models and the other is bottom-up models (Swan and Ugursal, 2009). The top-down method refers to the models that apply historic regional demand data and scale down the energy consumption to a housing unit based upon macroeconomic or climate indicators (e.g., family gross income, unemployment conditions, energy price, and ambient temperature) (Dergiades and Tsoulfidis, 2008; Swan and Ugursal, 2009). The bottom-up methods utilize physical engineering models or statistical models to simulate the energy consumption of individual households and then scale up to regional or national levels (Arghira et al., 2012; Muratori et al., 2013; Swan and Ugursal, 2009). The top-down models usually require high quality and sufficient quantity of observed data input, while the bottom-up models present relatively high computational cost. Thomson and Infield (2007) applied measured load data coupled with stochastic simulation using house information (e.g., perimeter footprint, house type) to simulate regional demand profile to investigate the technical impact of

PV adoption on electric networks. However, their approach still relies on a large amount of historical reported data and lacks transferability and applicability to other study areas to better inform future PV planning. The literature review of these two popular approaches for dynamic residential demand modeling was further provided in the Section C1 of the Supporting Information (SI).

In order to address the knowledge gaps, this study developed an integrative modeling framework to investigate the dynamic life cycle technical, economic, and environmental outcomes of PV adoptions, considering the influence of PV adoptions on electricity price. This modeling framework was later applied to residential buildings in the metro area of Boston, Massachusetts of the United States as a case study. Specifically, PV generation, residential demand, energy balancing, and regional adoption models were developed. Performance measures in terms of load reduction, off-, mid-, on-peak load reductions, life cycle cost (LCC), life cycle CED, carbon emission, and water consumption were used to evaluate different levels of PV adoptions. This study intends to answer the following research questions: 1. How will increasing PV adoption influence the grid performance, PV hosts' energy reliance, life cycle cost, and life cycle environmental impacts of the PV systems? 2. What is the optimal PV adoption rate that maximizes regional load reduction, cost saving, and environmental benefits?

4.2. Methodology

Figure 4-1 illustrates the schematic of the modeling framework developed in this study. An integrated system dynamics modeling (SDM), life cycle assessment (LCA), and life cycle cost assessment (LCCA) framework was developed to investigate the technical, economic, and

environmental outcomes and tradeoffs of PV adoptions. Indicators including load reduction, life cycle cost (LCC), carbon footprint, CED, and water footprint were assessed under varied PV adoption rates. SDM is a computational modeling approach capturing system feedback loops and delays. In this study, we first applied Vensim DSS software to simulate the dynamic interactions of solar energy generation, residential demand, and the grid using thirty-minute time step over a typical year on a building level. This building-level model was then converted into a Python model for regional PV adoption simulation. LCA and LCCA assess the environmental and economic impacts of PV adoption in all life cycle stages including manufacturing, transportation, operation, maintenance stages. The twenty-year assessment was extrapolated from the one-year model in alignment with typical residential PV systems' lifespan. LCCA utilizes a net present value (NPV) method to discount the 20-year future costs to 2021.

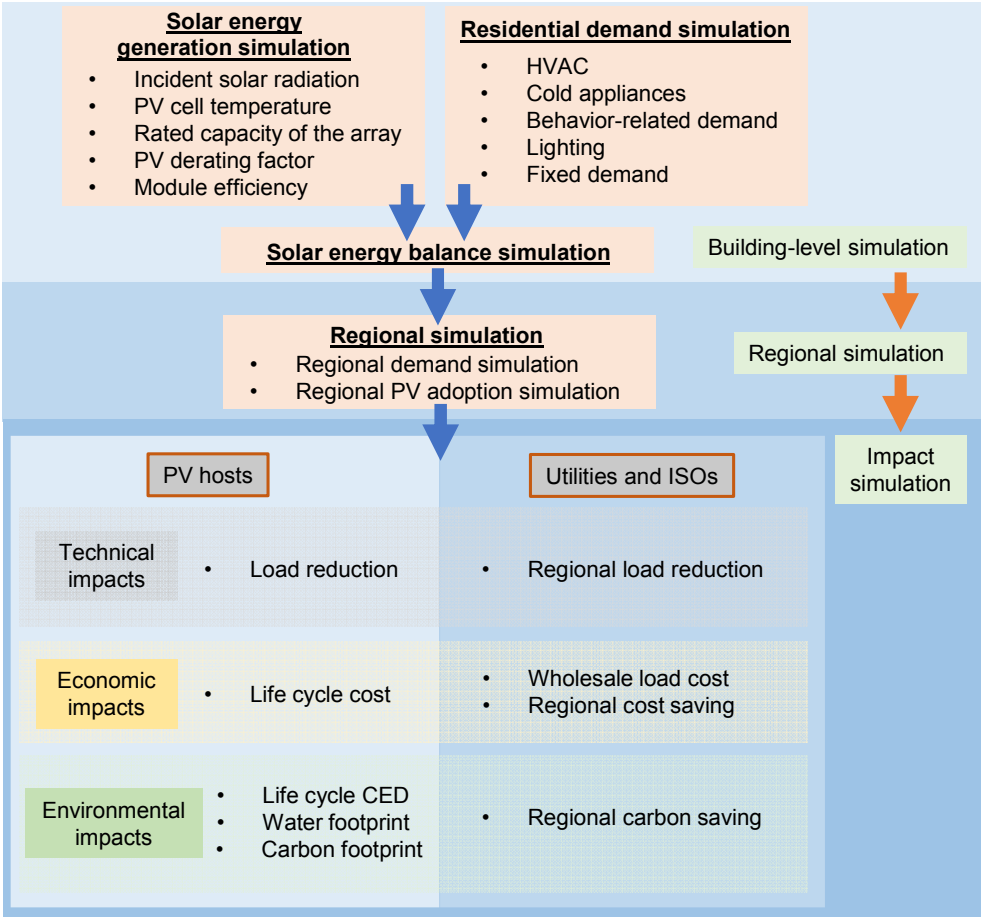

Figure 4-1. The modeling framework of this study

4.2.1. Household solar energy generation simulation

Given the market popularity and cost competitiveness, grid-connected polycrystalline silicon (poly-Si) PV system was selected in this study (Sharma et al., 2015). The optimized PV system configuration (i.e. panel size) was determined for a residential building using a simplified rule-of-thumb engineering optimization based upon the available rooftop size following (Ren et al., 2020).

The solar energy generation model was developed by referring to the method that was applied in the HOMER software (HOMER, 2018). However, we have modified our model to incorporate the cooling influence by wind. Three time-varying input variables including solar radiation, ambient

temperature, and wind speed were utilized (NREL, 2015). The PV system degradation effect was also considered in the model by using annual degradation rate. The energy loss of the PV system during the operation was also estimated based upon the module and inverter efficiencies. This section aims to provide a brief overview of the PV generation model. The detailed modeling description was provided in Ren et al. (2020).

4.2.2. Household energy demand simulation

In order to capture time-varying interactions between the residential demand and power supply (PV generation and grid supply), this study developed Python-based models to simulate major residential demand components using thirty-minute time step and one-year time horizon. The electricity demand of one household is estimated based upon five major components including: HVAC (maintain the desired thermal comfort in the house), cold appliances (e.g., refrigerators and freezers), activities of the household (e.g., cooking, dishwashing etc.), lighting, and fixed use following the suggestion from (Muratori, 2018; Muratori et al., 2013). The total electricity demand D of one household is calculated as Equation 4-2.

$$D = D_{HVAC} + D_{cold} + D_{act} + D_{light} + D_{fix} \quad \text{Equation 4-2}$$

Where,

D is the total electricity demand, kWh;

D_{HVAC} represents the electricity demand of the HVAC system, kWh;

D_{cold} represents the electricity demand of cold appliances, kWh;

D_{act} represents the electricity use related to activities of the household occupants, kWh;

D_{light} is the electricity demand of lighting, kWh;

D_{fix} is the time-invariant power demand that represents ubiquitous electricity use (e.g., lighting during other activities and stand-by electricity consumption of appliances), kWh.

Power losses as a result of system inefficiencies, thermal dissipation, and electrical losses were considered in the demand simulation categories as further described in the following subsections. The detailed modeling of each demand category is presented in the following sections.

4.2.2.1. HVAC demand

In this study, the energy demand of HVAC includes the heating, ventilation, and air conditioning of a household. This demand is estimated based upon the manufactural characteristics of the selected HVAC system, the thermal comfort required by the occupants, climate characteristics (e.g., weather conditions), and the physical properties of the house (e.g., wall and window areas). Specifically, a typical air-based HVAC system was selected for the simulation due to the popularity of the system (U.S. Census Bureau, 2005). An approach based upon overall thermal resistance theory was applied to simulate the behavior of this system following (American Society of Heating, 2009). Python models were used for our simulation using minutely time step. The output was later scaled up to thirty-minute time step to fit the overarching modeling framework.

Equation 4-3 presents the equation of thermal model of a house unit. The room air temperature (T_{room}) was determined based upon the heat input from the heater and HVAC air flow rate capacity (M_{HVAC}).

$$\left(\frac{dQ}{dt}\right)_{heater} = (T_{heater} - T_{room}) \cdot c_p \cdot M_{HVAC} \quad \text{Equation 4-3}$$

Where,

$\left(\frac{dQ}{dt}\right)_{heater}$ represents the heat flow from the heater into the room, kJ/hour;

T_{heater} is the temperature of hot air from heater, 50 °C;

T_{room} is the current room air temperature, °C;

c_p is the heat capacity of air at constant pressure, kJ/kg·°C;

M_{HVAC} represents the air mass flow rate through heater, kg/hour.

The thermal loss of a building was also estimated in each time step using Equation 4-4.

$$\left(\frac{dQ}{dt}\right)_{losses} = \frac{T_{room} - T_{out}}{R} \cdot 3.6 \quad \text{Equation 4-4}$$

Where,

$\left(\frac{dQ}{dt}\right)_{losses}$ represents the heat loss flow from the room into the outside, kJ/hour (1W=3.6 kJ/hour);

T_{room} is the current room air temperature, °C;

T_{out} represents the time varying outside environment temperature, °C;

R represents the equivalent thermal resistance of the house, K/W.

Equation 4-5 presents the overarching guiding equation for HVAC-heating simulation. This equation reflects the thermal dynamic interactions between inside room and HVAC heater considering the thermal loss to the environment.

$$\frac{dT_{room}}{dt} = \frac{1}{M_{air} \cdot c_p} \cdot \left[\left(\frac{dQ}{dt}\right)_{heater} - \left(\frac{dQ}{dt}\right)_{losses}\right] \quad \text{Equation 4-5}$$

Where,

$\frac{dT_{room}}{dt}$ represents the temperature change of the room, °C/hour;

M_{air} is the mass of air inside the house, kg;

c_p is the heat capacity of air at constant pressure, kJ/kg·°C;

$\left(\frac{dQ}{dt}\right)_{heater}$ represents the heat flow from the heater into the room, kJ/hour;

$\left(\frac{dQ}{dt}\right)_{losses}$ represents the heat loss flow from the room into the outside, kJ/hour.

The air flow rate through HVAC (M_{HVAC}) is estimated using equation 4-6.

$$M_{HVAC} = \frac{1}{c_p \cdot (T_{HVAC} - T_{desire})} \cdot \frac{T_{desire} - T_{out}}{R}$$ Equation 4-6

Where,

c_p is the heat capacity of air at constant pressure, kJ/kg·°C;

T_{desire} is the desire temperature inside the house, 21.1·°C;

T_{out} represents the hottest or coldest outside environment temperature when sizing HVAC, °C;

R represents the equivalent thermal resistance of the house, K/W.

R is calculated using Equation 4-7.

$$R = \left[\frac{R_{ground}}{A_{floor}} + \left(\frac{1}{h_{out} \cdot A_{wall}} + \frac{R_{wall}}{A_{wall}} + \frac{1}{h_{in} \cdot A_{wall}}\right)^{-1} + \left(\frac{1}{h_{out} \cdot A_{window}} + \frac{R_{window}}{A_{window}} + \frac{1}{h_{in} \cdot A_{window}}\right)^{-1} + \left(\frac{1}{h_{out} \cdot A_{ceiling}} + \frac{R_{ceil}}{A_{ceil}} + \frac{1}{h_{in} \cdot A_{ceil}}\right)^{-1}\right]^{-1}$$ Equation 4-7

Where,

h_{out} and h_{in} are the outside and inside convective coefficients respectively;

A_{wall} and A_{window} are the surface of walls and windows of the house in contact with the environment respectively;

R_{wall} and R_{window} are the thermal resistances of the windows and walls respectively.

The values of the above parameters used in this study are provided in the Table C-4 of the SI. The surface of walls and windows is estimated using the building information (including building stories and living area) from the City of Boston's open-sourced GIS portal (COB, 2019). The air mass of the HVAC control volume of each building was estimated based upon the household living area and height.

The worst summer and winter conditions (described in Table C-4 of the SI) were considered for validating the air flow rate through HVAC (M_{HVAC}) and determining the target resulting temperature of the air from the HVAC furnace (showed in Table C-5 of the SI). The temperature of the air from the HVAC system during the summer was assumed to be 13°C following the suggestions from (American Society of Heating, 2009; Muratori et al., 2013). The HVAC model determines that each day simulated is either a heating or cooling day. This study also assumed that a tolerance of ±1°C of the desired temperature (21.1 °C/70 °F) was applied for simulating the control strategy (Muratori et al., 2013).

Energy consumption of fans (cooling mode) for ventilation was estimated. The power absorbed by the HVAC equipment was estimated using motor efficiency (η_{motor}). The energy consumed by the fans was estimated using Equation 4-8 and 4-9.

$$D_{fan} = \frac{m_{HVAC} \cdot \Delta p_{tot}}{\eta_{fan} \cdot \eta_{motor}}$$ Equation 4-8

$$\Delta p_{tot} = p_{static} + \rho \frac{v^2}{2}$$ Equation 4-9

Where,

D_{fan} is the power consumption of the fans, kWh;

m_{HVAC} is the HVAC air flow rate, kg/s;

Δp_{tot} represents the total pressure drop, Pa;

η_{fan} and η_{motor} are the efficiencies of the fan and motor respectively, and $(\eta_{fan} \cdot \eta_{motor})$ is assumed to be 0.15 (Walker et al., 2003);

p_{static} is the static pressure drop, 135 Pa (Muratori et al., 2013);

ρ is the air density, 1.225 kg/m^3;

v is the air velocity, 4m/s (American Society of Heating, 2009).

The operation of heating or cooling mode of the HVAC system presents different energy consumptions. In the heating mode, the power needed to generate the heat can be used from either traditional furnace heating using fuels (e.g., natural gas, fuel oil) or electricity. When the traditional furnace heating is selected, the electricity consumption of the HVAC system is assumed to be 0.

When the electric HVAC heating system is applied, the energy/electricity needed for heating is calculated using Equation 4-10.

$$E_{electric}(D_{heating}) = \frac{m_{HVAC} \cdot c_p \cdot (T_{HVAC} - T_a)}{1 + COP}$$ Equation 4-10

Where,

$E_{electric}$ and $D_{heating}$ both represent the energy needed or electricity consumption of heating, kWh;

m_{HVAC} is the HVAC air flow rate, kg/s;

c_p is the air specific heat, kJ/kg K;

T_{HVAC} is the HVAC supply air temperature, °C;

T_a is the air temperature inside the house, °C;

COP is the coefficient of performance which represents the thermal energy added to the house per unit of electric energy absorbed by the HVAC system, 2.5 (Muratori et al., 2013).

During the summer operation, the HVAC system provides the functions of cooling and air humidity reduction. The total energy needed for these two functions is determined by the sensible heat ratio (SHR). SHR is the ratio between the sensible heat load (e.g., energy used for cooling) and total heat load. SHR was assumed to be 0.7 in this study (Llc, 2003). The electricity consumption of cooling in the summer is calculated through Equation 4-11.

$$D_{cooling} = \frac{m_{HVAC} \cdot c_p \cdot (T_a - T_{HVAC})}{SHR \cdot \mathrm{COP}} \quad \text{Equation 4-11}$$

Where,

$D_{cooling}$ is the electricity consumption of cooling, kWh;

m_{HVAC} is the HVAC air flow rate, kg/s;

c_p is the air specific heat, kJ/kg K;

T_a is the air temperature inside the house, °C;

T_{HVAC} is the HVAC supply air temperature, °C;

SHR is the sensible heat ratio, 0.7;

COP is the coefficient of performance, 2.5.

The total HVAC electricity consumption during the cooling days is therefore the sum of D_{fan} and $D_{cooling}$. The HVAC simulation results as well as validation have been provided in the Section 3.1 Residential demand simulation of the SI.

4.2.2.2. Cold appliances demand

The demand modeling of household cold appliances utilizes a similar method referred to (Muratori et al., 2013). The size (average nominal power rating) and number of the refrigerators or freezers in the house were used to estimate the electricity consumption and demand patterns of cold appliances. The impacts of external temperature and occupants opening the doors of those cold appliances were neglected following (Muratori et al., 2013).

The average nominal power rating of a refrigerator was assumed to be 725W based upon the published statistics from the U.S. Department of Energy (Muratori et al., 2013). The overall annual electricity consumed by refrigeration in U.S. homes was estimated to be 6% of total residential electricity consumption in 2019 (EIA, 2020b). Moreover, the average annual electricity consumption for a U.S. residential utility customer was 10649 kWh in 2019 (EIA, 2020c). This study therefore assumed 639 kWh (6% of 10649 kWh) of annual energy consumption of cold appliances for one household. This work also assumed that a refrigerator is an on/off device that operates at its nominal power when on. Hence, the average operating time was estimated by dividing annual energy consumption by nominal power, which implies the cold appliance operates 881 hours every year.

To simulate the electricity consumption of cold appliance, a Bernoulli distribution approach was applied (Weisstein, 2002). Specifically, the operation of cold appliance was assumed to be evenly distributed over one year, which takes around 10% of a year (881 hours/8760 hours). Therefore, a cold appliance was assumed running for three random 10-min intervals every 5 hours. As a result, daily energy consumption of about 1.74 kWh was yielded. Figure C-13 of the SI presents a simulated 1-day energy consumption profile of cold appliances in a household.

4.2.2.3. Behavior-related demand

The electricity consumption of activities of building occupants was estimated based upon the occupant behaviors simulation using the Markov chain model and power conversion factors (i.e., the wattage of appliances used when energy-related activities are conducted) (Muratori et al., 2013). The following behaviors are simulated: sleeping, no-power activity, cleaning, laundry, cooking, automatic dishwashing, leisure, away (working), and away (not working). This study assumed that each household occupant is in one of these nine activity in every discrete time step following (Muratori et al., 2013). The change of an activity is determined by the transition probabilities at a certain time step. At each time step, a pseudorandom number is generated to determine which activity takes place.

The number of household members, the transition probabilities for each occupant, and power conversion factors were model inputs in our behavior-related energy consumption model. The transition probabilities are derived from the American Time Use Survey (ATUS) data. Five typical

occupant types (including working males, non-working males, working females, non-working females, and children) with different associated transition probabilities are modeled.

Specifically, the ATUS is conducted annually from a subsample of participants in the Consumer Preferences Survey administrated by the U.S. Bureau of Labor Statistics. The detailed data regarding the time allocation of American adults is publicly available through this survey. Daily activities of ATUS respondents were recorded in a minute timestep starting at 4 a.m. and ending at midnight. The information in terms of sex, age, working condition, and the number of the ATUS respondents for this study were provided in the Table C-7 of the SI. The percentage distributions of nine activities of five types of occupants over a day were presented in the Figure C-2 of the SI cleaned from the raw ATUS dataset.

The transition probability for weekdays and weekends and for each minute of a day of one occupant type was estimated using Equation 4-12.

$$p_{i,j}^{d,m} = \frac{w_k \cdot n_{i,j,k}^{d,m}}{\sum_k \sum_j w_k \cdot n_{i,j,k}^{d,m}} \quad \text{Equation 4-12}$$

Where,

p represents the transition probability;

d indicates either weekdays (d = 1) or weekends (d = 0);

m represents minutes of a day (m = 1,2,…,1440);

i and j are the states of the occupant (activity transition from i to j) and j = 1, 2, …, 9 (1. Sleep, 2. No-power activity, 3. Cleaning, 4. Laundry, 5. Cooking, 6. Automatic dishwashing, 7. Leisure, 8. Away, working, and 9. Away, not working);

k represents the identification of the respondent/occupant type;

w_k is the weight placed on the respondent/occupant type from the ATUS (the weight of data relative to the total population);

$n_{i,j,k}^{d,m}$ is the number of transitions that respondent k makes from state i to state j during minute m of day d.

The number of transitions of each 1-min timestep is counted. Sixty 1-min observations were counted for each occupant type for each hour. The transition probability metrices were generated for each 1-min time step. Later, 30 one-minute transition probability metrices were multiplied together to generate a 30-minute transition probability metric.

In order to estimate the power demands of nine activities, the power conversion factors were applied to translate activity behaviors into electricity demands as presented in Table C-6 of the SI. The results and validation of the behavior-related demand simulation were provided in the Section C3.1. Residential demand simulation, Behavior-related energy consumption simulation of the SI. The simulated annual and typical daily behavior-related demand patterns of the selected community were presented in the Figure C-14 of the SI. Our simulation results were also compared with the ATUS dataset using regression analysis (Figure C-15 of the SI). Ten simulated one-day activity profiles of five types of occupants in a weekday and a weekend day were also presented in the Figure C-14 of the SI. Overall, our model provides ideal simulation results using ATUS data input to reflect human activities over time.

4.2.2.4. Lighting and fixed demand

The energy consumption of lighting was also modeled based upon the amount of available natural lighting and building occupancy for each building. Two levels of electricity consumption for lighting (i.e., lighting power conversion factors) were considered (varied from day to night). This study assumed that electricity for lighting was consumed when there was at least one occupant in the house and doing activities other than sleeping. When there was no occupant in the house, the lighting demand was assumed to be zero. Occupants in the house or not and doing which activity depended on the previous activity simulation.

Daily sunrise and sunset time of the city of Boston was obtained from NOAA (NOAA, 2021). Daytime lighting power conversion factor was used between the sunrise and sunset time, while nighttime lighting power conversion factor was used for the rest of the day (Figure C-3 of the SI). Daytime and nighttime lighting power conversion factors were assumed to be 125W and 330W respectively. The power conversion factor of fixed demand (i.e. constant electric consumption) was assumed to be 230W. Simulated one-day lighting electricity consumption patterns of the selected community in both weekday and weekend days were presented in the Figure C-17 of the SI.

4.2.3. Household energy balance simulation

The household energy balance simulation intends to allocate the generated solar energy to meet residential demand and sell to the grid. The generated solar energy was prioritized to meet the residential local demand. When there is surplus energy after meeting the local demand, the excess energy will be sold to the grid. This study assumes that this priority does not change during on-,

mid-, and on-peak periods. Grid sell was assumed to be unconstrainted following the current Massachusetts Net Metering policy (Mass.gov, 2020b). A more detailed model description can be found in Ren et al. (2020, 2021).

4.2.4. Approach for scaling up

The city of Boston, Massachusetts (MA) was selected as our testbed due to its solar potential and strong policy incentives. Specifically, information for the residential buildings selected and analyzed were obtained from the City of Boston's open-sourced GIS data portal (COB, 2019). Key attributes including street name and number, living area, number of floors, and number of household units were obtained from this GIS data portal (COB, 2019). Around 68,000 residential buildings were investigated after the removal of the buildings that has more than 60 floors or without floor information following (Wikipedia, 2021), as presented in Figure C-1 (a) in the SI. Due to the high computational cost for simulation, a community located in the city of Boston was further selected for modeling (Figure C-1 (b) and (c) of the SI). This community was selected due to its similar household type percentages compared with the average household type percentages of the city of Boston (Table C-2 of the SI). Table C-3 in the SI presents the relevant residential information of the simulated community. Later, this community was scaled up to the Boston city level based upon the population proportion.

The total rooftop area of each building was calculated using the living area divided by the number of floors obtained from the GIS data portal (COB, 2019). Later, the available rooftop for PV adoption of each building was estimated. The percentage of the total rooftop area on residential buildings that is suitable for PV adoption was assumed to be 26% following the suggestions from

the National Renewable Energy Laboratory (NREL) reports (Gagnon et al., 2016; Melius et al., 2013).

In order to simulate the demand pattern of each residential building in the selected community, the type(s) of household (types of occupant) in each building unit was determined using the 2010 U.S. Census Survey data. The percentages of various household types of the selected community were obtained from the 2010 U.S. Census Survey data. Eight household types including single-male household, single-female household, husband-wife family with one child, husband-wife family without child, single-male family with one child, singe-female family with one child, two-male household, and two-female household were considered. We randomly assigned a household type to a household unit in a residential building following these household type percentages (this process is presented in the Figure C-4 of the SI). The numbers and percentages of eight household types of the simulated community are provided in the Table C-8 of the SI. A total number of 209 households with 370 occupants in 145 buildings were simulated. The working and non-working conditions of each simulated occupant was randomly assigned based upon the labor force participation rate. In this study, the labor force participation rates for males and females were assumed to be 69.2% and 57.4% respectively reported from the 2019 U.S. Bureau of Labor Statistics (BLS, 2020).

In terms of regional HVAC demand simulation, the selected residential buildings using electric heater was determined based upon the random assigned function following the percentage of 15.3% (percentage of households using electric heating in Massachusetts) (Mass.gov, 2018). The buildings using cooling HVAC were randomly assigned proportionally following the suggestion

that 79% of the residential buildings use cooling equipment in Massachusetts (EIA, 2009). The simulated annual regional HVAC electricity consumption result of the selected community was presented in the Figure C-10 and Figure C-11 of the SI.

The simulated overall regional residential demand of the community was later scaled up to the Boston city scale based upon the population proportion (Table C-3 of the SI). The average monthly electricity consumption per simulated household was estimated to be 596.03 kWh in our simulation, which is within the range of 583.0-887.4 kWh per U.S. household reported from EIA (EIA, 2020c). Another study reported the average monthly residential electricity consumption per Massachusetts housing unit is 583 kWh (EIA, 2018; PP-MASS, 2021). Moreover, the percentages of simulated electricity consumption of five categories were later calculated to compare with the real reported electricity use percentages in U.S. homes (EIA, 2015a). As shown in Table 4-1, our simulation results ideally reflect the electricity consumption contributions of a residential household.

Table 4-1. Residential site electricity consumption by end use in this study and EIA report

Source	Cold appliances	Behavior-related demand	Fixed use	HVAC	Lighting
This study	7.6%	24.6%	24.3%	34.4%	9.1%
EIA	7.0%	51.0%		31.7%	10.3%

The simulated results of the overall residential demand were provided in the Section C3.1. Overall residential demand of the SI (Figure C-18 of the SI). Overall, by comparing our simulated demand results with ISO-NE residential demand dataset, we found our simulation could effectively capture the features of the real reported demand pattern in terms of monthly average household electricity consumption and pattern seasonality (Figure C-19 of the SI).

The energy balance analysis and impact assessments were conducted for each selected individual building. For the purpose of determining the priority of residential buildings to install PV systems, we sorted the buildings based upon their available rooftop area for PV installation. The buildings with a larger available rooftop area for PV installation were assumed to install the system earlier. A larger rooftop area for PV installation usually represents a higher technical potential for solar generation, therefore may lead to a higher economic and environmental benefits incentivizing the PV hosts (Gagnon et al., 2016; Ren et al., 2020). We then calculated the total impacts for the target community. Lastly, the result was extrapolated from the selected community level to the whole Boston city level based upon the building number ratio. In this study, incremental percentages of PV adoptions at a city level was simulated. 25%, 50%, 75%, and 100% PV adoption percentages were used for result discussion.

In this study, electricity rate designs of net metering and wholesale pricing were considered. Net metering represents the rates of the electricity used from the grid and sold to the grid from the PV systems were the same using the retail rate. In this study, a flat rate structure which utilizes a constant rate of 14.9 cents/kWh was used in this study for Boston area based upon National Renewable Energy Laboratory (NREL) and U.S. Energy Information Administration (EIA) estimations (EL, 2021). The wholesale pricing design reflects the scenario when the distributed residential solar PV systems enter the wholesale electricity market. The price for the sell to the grid from the solar generation is determined by the time-varying wholesale electricity rate. In this study, the wholesale electricity rates were estimated under different levels of PV adoption. The simulated new electricity retail rate was assumed to be the sum of new estimated wholesale

electricity rate, constant distribution energy charge (7.04 cents/kWh), and constant transmission charge (3.52 cents/kWh) reported from Eversource in Boston service area (Eversource, 2021).

The impact of PV adoption on the wholesale electricity prices was estimated using an empirical equation. The wholesale electricity prices were referred to wholesale load costs as mentioned in ISO-NE database, which represent the large portion of total costs related to the provision of wholesale electricity including energy, capacity, ancillary, administration and other charges (ISO-NE, 2020a). Compared with other types of electricity costs, the wholesale load cost was also selected as a popular indicator for electricity cost estimation (ISO-NE, 2020b). In this study, an empirical equation of the wholesale load cost was obtained based upon the historical minutely grid mix, daily generation by fuel type, and hourly wholesale load costs from the ISO-NE database as well as the monthly prices and revenue of fuels (for electric power) in the grid mix (Equation 13). All data was modified to a monthly time step. The grid fuel mix, daily generation by fuel type, and wholesale load costs of New England from October 2015 to October 2020 were collected from the ISO-NE databases (ISO-NE, 2020c, 2020d, 2020e). The fuel prices including natural gas, coal, petroleum liquids, nuclear, hydro-electric, and centralized renewables for electric power sector were collected from EIA 2015-2019 database (EIA, 2020d) (as provided in Table S091009 of the SI). The fuel revenue is assumed to be the product of the fuel price and the amount of fuel consumption. Since natural gas is the dominant marginal fuel use for power generation at the wholesale market based upon the ISO-NE grid mix database observation, this study assumed that the increase of solar penetration from decentralized PVs into the grid would lead to a decrease of natural gas usage (ISO-NE, 2020d).

Specifically, the linear regression was conducted using JMP® Pro 15.0.0 software. The minimum Akaike Information Criterion (AIC) was selected as the stopping rule. Both forward and backward directions were tested for the regression model. The regression result was presented as Equation 4-13.

$$\widehat{P_t} = -9.34 + 3.03\mathrm{e}^{-6}P_{Wind,t}Use_{Wind,t} + 1.30\mathrm{e}^{-6}P_{Oil,t}Use_{Oil,t} + 5.92\mathrm{e}^{-7}P_{NG,t}Use_{NG,t}$$

Equation 4-13

Summary of Regression Fit	
R Square	0.833
Adjusted R Square	0.824
P Value	< .0001

Where,

P_t is the wholesale load cost in the month *t*, \$/kWh,

t represents the month in a year, *t*=1, 2, 3, 4 …12,

$P_{Wind,t}$, $P_{Oil,t}$, and $P_{NG,t}$ represent the U.S. electric power generation unit costs from wind source, petroleum oil, and natural gas fuels respectively in the month *t*, \$/MWh,

$Use_{Wind,t}$, $Use_{Oil,t}$, and $Use_{NG,t}$ are the total electricity consumed from wind, oil, and natural gas power generation respectively in the month *t*, MWh.

4.2.5. Technical impact assessment

In order to assess the PV generation penetration into the grid during different time windows, off-, mid-, and on-peak periods were utilized in this study following a pilot study conducted by the Liberty Utilities. Three time periods including off-peak (0:00–8:00 and 19:00–24:00), mid-peak

(8:00–14:00), and on-peak (14:00–19:00) were applied for results presentation. Load reductions (kWh) in these three peak time periods were calculated using Equation 4-1.

$$R_{load} = \int_{t_0}^{t} (E_{solar} + E_{sell}) dt \quad \text{Equation 4-1}$$

Where,

R_{load} represents the load reduction of the grid, kWh;

E_{solar} is the direct solar energy consumption to meet building demand, kW;

E_{sell} is the grid sell from the PV system, kW.

The percentage of solar energy use onsite was also calculated to reflect the energy reliance to the centralized utilities for the PV adopters in this study. The solar energy use onsite percentage was estimated as a percentage of direct solar energy consumption from the PV systems over the overall residential demand of the PV installed buildings.

4.2.6. Economic impact assessment

The life cycle cost (LCC) of the PV system for each selected residential building was estimated. The LCC of a PV system was calculated using the NPV of the capital cost, operation and maintenance (O&M) cost, and federal and state tax credit using Equation 4-14. The capital cost consists of the costs of panels and racking, inverters, permission, and labor. These costs have been reported in the Section B2 of the SI. The O&M cost includes the cost for actual grid use and the saving from sell to the grid from the PV system. All future costs were discounted to the year 2021 using a discount rate of 6% (Freyman, 2021).

$$LCC = C_c - C_t + \sum_{n=0}^{n=L} \left[\frac{r_{use} \int (E_{use}) dt - r_{sell} \int (E_{sell}) dt}{(1+i)^n}\right]$$ Equation 4-14

Where,

LCC represents the LCC of a PV system, $;

C_c is the capital cost of the PV system; $;

C_t includes the federal tax credit (26% of the capital cost) and Massachusetts state tax credit (15% of the capital cost, up to $1000) for the PV system, $;

L is the life span of the PV system, 20 years;

r_{use} is the electricity rate for grid use, $/kWh;

E_{use} is the actual grid use, kW;

r_{sell} is the electricity rate for grid sell from the PV system, $/kWh;

E_{sell} is the grid sell from the PV system, kW;

i is the discount rate, 6%;

n is the year index.

4.2.7. Environmental impact assessment

The environmental impacts of the PV system in terms of cumulative energy demand (CED), water and carbon footprints were simulated. Life cycle stages of manufacturing, transportation, and operation were assessed using Equation 4-15. The manufacturing impacts of the PV system components were estimated using the entries from the EcoInvent 3.0. The operation stage considers the savings from both direct solar energy consumption and grid sell. The end-of-life phase was neglected. SimaPro 8.3 was applied for the characterization of the environmental impacts. The cumulative energy demand V 1.09 method, the Berger et al., 2014 Water Scarcity method, and the IPCC 2013 GWP 20a method were used for estimating CED, water, and carbon

footprints respectively. The SimaPro entries, unit cost and environment impact of the PV system components are provided in the Section B2 of the SI.

$I = I_m + I_t - [f_u \int (E_u + E_s) dt] L$ Equation 4-15

Where,

I represents the life cycle environmental impacts of a PV system, MJ, L, or kg CO_2 eq.;

I_m represents the environmental impacts of the PV manufacturing, MJ, L, or kg CO_2 eq.;

I_t is the environmental impacts of the PV transportation phase, MJ, L, or kg CO_2 eq.;

f_u represents the unit environmental impacts of the replaced grid use by the PV system, MJ/kWh, L/kWh, or kg CO_2 eq./kWh;

E_u is the direct solar energy consumption from the PV system, kW;

E_s is the grid sell the PV system, kW;

L is the life span of the PV system, 20 years.

The f_u of the CED and water footprint were estimated using the U.S. electricity grid supply entry from SimaPro (provided in the section B2 of the SI). To better reflect the dynamics of the carbon intensity of the New England grid, time-varying carbon emission units ($f_{u,carbon}$) of the regional grid supply were used (Figure C-5 of the SI). $f_{u,carbon}$ were calculated based upon the 2019 New England utility fuel mix profile obtained from the Independent System Operator-New England (ISO-NE) database (ISO-NE, 2020d). The unit environmental impacts of each fuel type are provided in the Section B2. Table B-2 of the SI.

4.3. Results and Discussion

4.3.1. Technical results

Figure 4-2 presents the load reductions of 25%, 50%, 75%, and 100% PV adoption percentages. Even under 100% PV adoption scenario, only 39% of residential demand can be met through distributed rooftop PV generation. This indicates that distributed PV generation cannot be self-sufficient to meet city residential demand, and other types of power supplies are indispensable. This also indicates that even smaller contribution of distributed solar generation can be used to commercial or industrial sectors. Moreover, the increase of load reduction benefit has been much constrained especially in high PV adoption rates. For example, the load reduction increased by only 87.7% when the PV adoption rate increased from 25% to 50%. This is because late PV adopters usually have a smaller PV system capacity due to a smaller available rooftop area for PV installation compared with the early adopters. Figure 4-3 further presents the load reduction change rates under varied adoption percentages. We found that load reduction performance increases dramatically during the initial 5.5% of PV adoption. Then this increase rate drops stably between the adoption rate of 5.5% to around 90% and later drops dramatically. This indicates that although 100% PV adoption provides the largest load reduction, the initial 5.5% PV adoption presents the most effective load reduction performance than later adoptions.

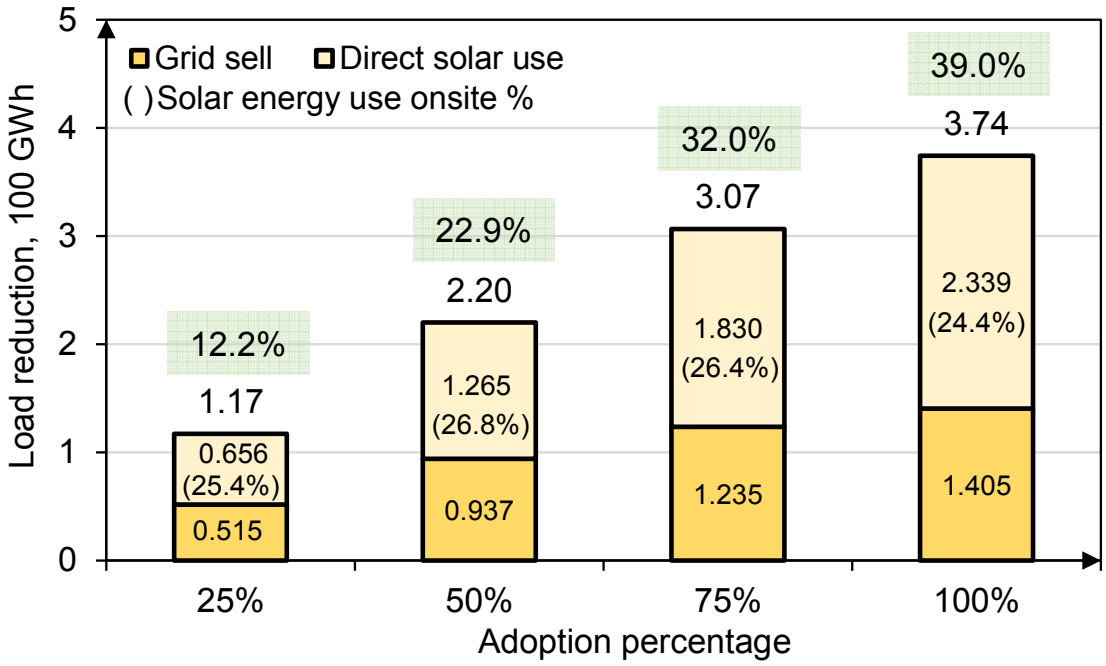

Figure 4-2. Load reductions of 25%, 50%, 75%, and 100% PV adoption percentages

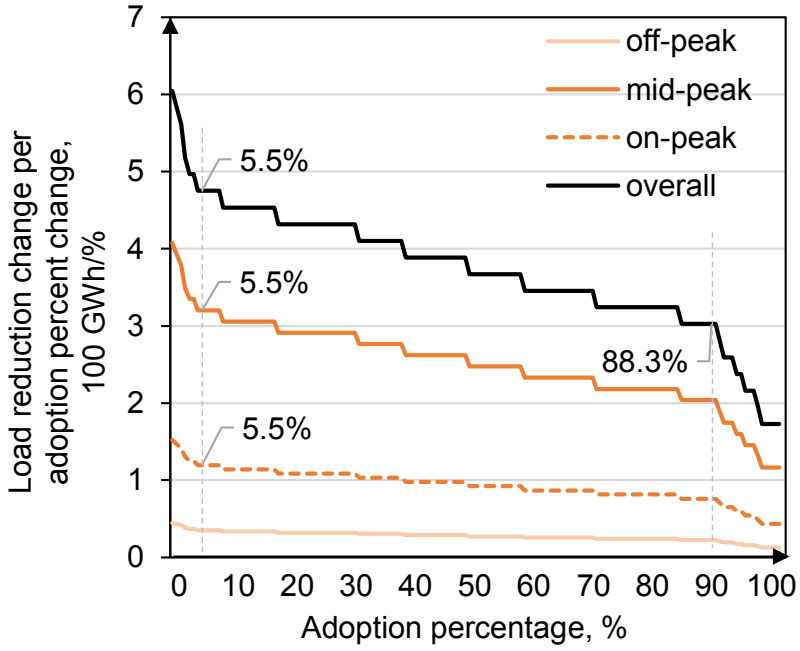

Figure 4-3. Load reduction change rates under different adoption percentages

Figure 4-4 presents the load reductions and percentages of solar energy use onsite during off-peak, mid-peak, and on-peak periods under four PV adoption rates. Mid-peak hours present the highest load reduction and solar energy use onsite percentage (63.5%-69.5%); however, on-peak load reduction and solar energy use onsite percent (19.8%-22.8%) are largely limited, and off-peak load reduction and solar energy use onsite percent (5.0%-5.5%) are the lowest. This is because mid-peak period has the largest amount of solar generation that was used locally and sold to the grid. On-peak and off-peak hours are usually in the late afternoon and early morning/night respectively when the solar radiation is much limited. For the ISOs, this indicates the importance of implementing energy storage and time-varying energy system control to match the solar use and solar grid feed-in time with the on-peak window to achieve the optimal on-peak grid load reduction. Moreover, the percentage of solar energy use onsite is in the range of 24.4%-26.8% with an average percent of 25.8% and decreases with the increase of PV adoption rate. This implies only around 26% of the local demand of the PV-installed households can be met by their PV system. Increasing PV adoption rate may increase the energy reliance to the centralized grid for the PV-aggregated community. However, this increase is not significant. This indicates implementing uncontrolled PVs without energy storage may not be the optimal solution for the energy users who intend to increase energy security through eliminating grid reliance by PV adoption.

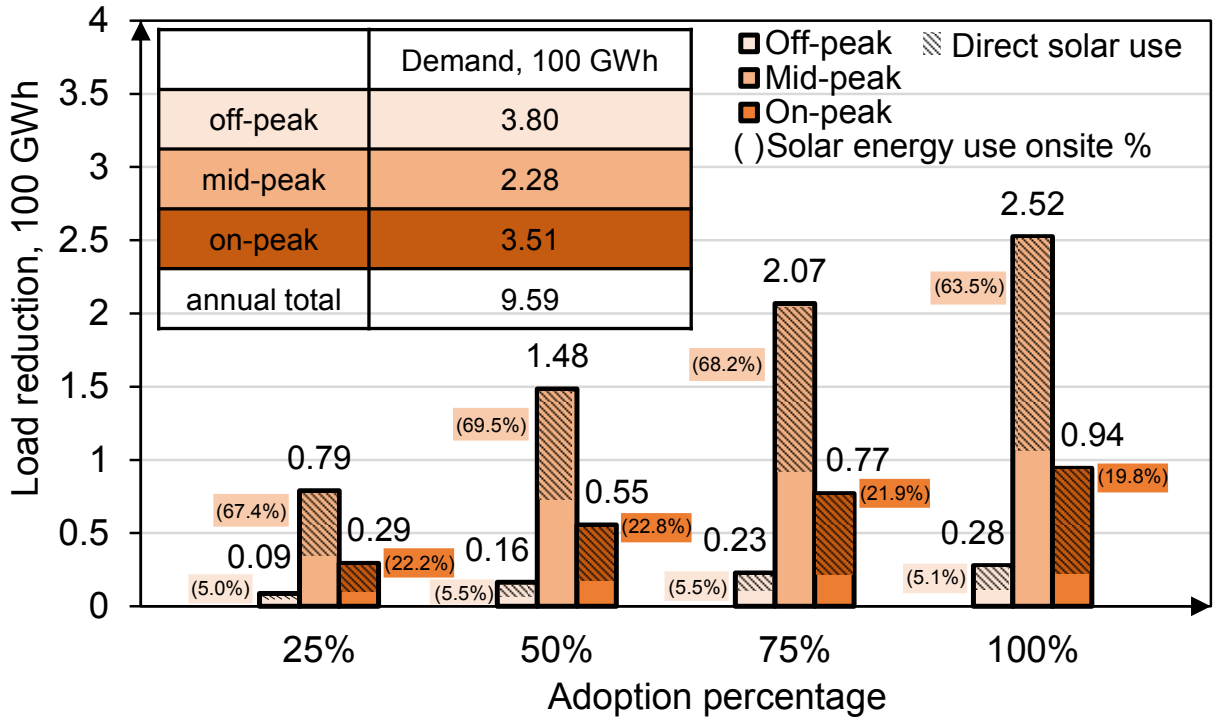

Figure 4-4. Load reductions of four PV adoption percentages during off-, mid-, and on-peak periods

Figure 4-5 further presents the simulated residential grid use under varied adoption percentage scenarios. Figure 4-5 (a) shows that increasing PV adoption effectively decreases the monthly residential grid use over a year, especially during the summer months due to the higher PV generation capacity compared with other months. Figure 4-5 (b) presents the simulated residential grid use in a typical winter day under varied PV adoption rates. Our results show that although mid-peak presents a significantly large load reduction, such PV penetration leads to a steeper ramp-up curve of the residential grid demand due to the very limited on- and off-peak load reductions. However, figure 4-5 (c) shows that the increasing PV adoption effectively flattens the previous peak load curve in a typical summer day. This reveals that increasing residential PV adoption could either ramp up or flatten the residential grid demand load curve given the demand and solar generation seasonality. This indicates the significance of implementing seasonal time-of-use rate

designs to match the local demand with PV generation (especially during the winter months) to achieve an optimal peak shave outcome for the utilities.

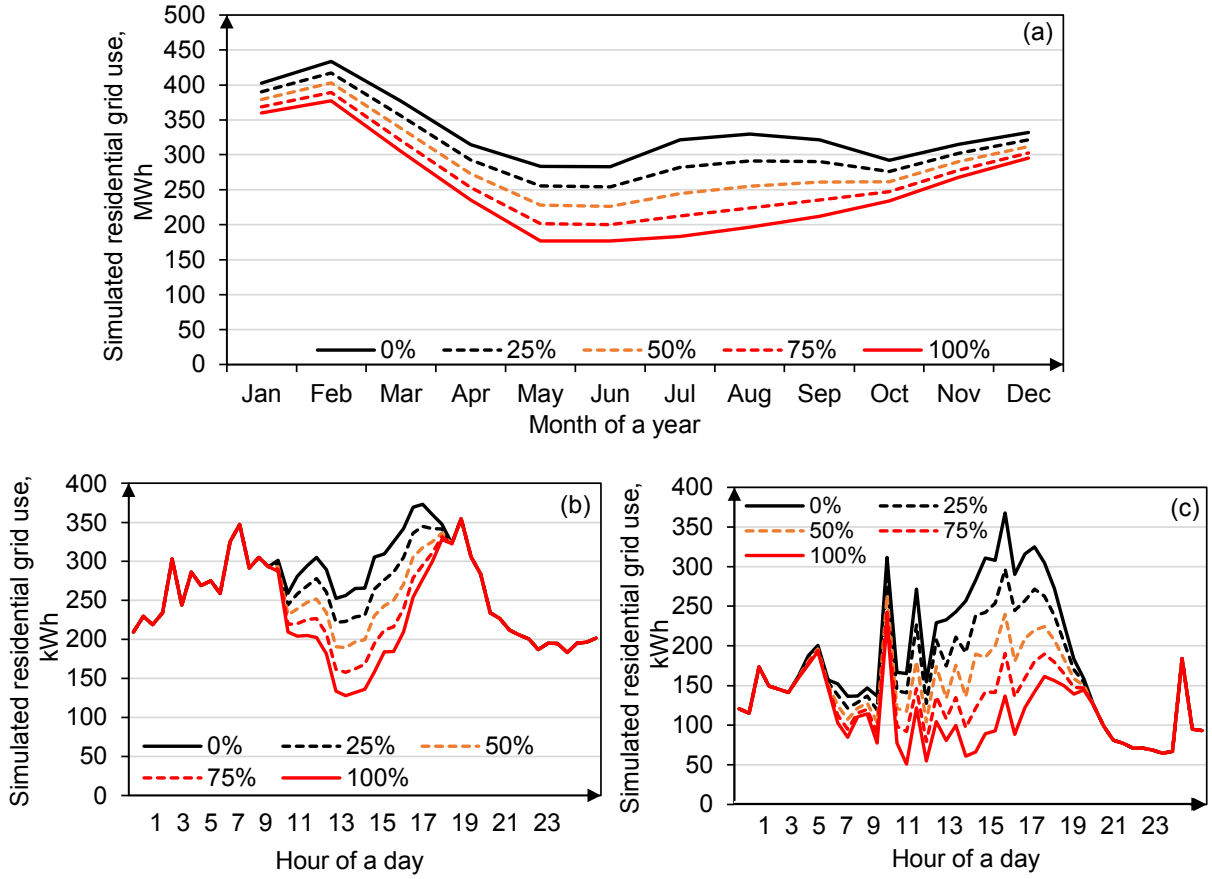

Figure 4-5. Simulated residential grid use by months (a), in a typical winder day (b), and a typical summer day (c) under different PV adoption percentages

4.3.2. Economic results

Figure 4-6 presents the average LCC of the simulated PV systems of all PV-adopted buildings under different adoption percentages. The NM rate design consistently presents the lowest LCC (average of $19.99K) regardless of adoption percentage compared with the WS rate design (average LCC of $23.27K). This is because the PV hosts using the NM design take advantage of a constant higher solar grid sell price (usually retail rate) compared with the time-varying WS rates.

However, the differences of the LCCs under these two rate designs are not significant, especially at the early adoption rate. This implies a potential equivalent economic interest in both NM and WS markets to the individual PV adopters. Our study also found the time-varying WS rate decreases with the increase of PV adoption percentages (as shown in the Figure C-24 of the SI) due to the replacement of natural gas fuel generation by distributed solar generation. However, compared with the overall electricity rate including the transmission and distribution rates, this WS rate change present insignificant impact to the overall rate in WS scenarios. When the PV adoption percentage is relatively small (0-10%), the NM and WS designs present similarly higher LCC compared with larger adoption scenarios. This is because although early PV adopters have a larger available rooftop area for PV installation (i.e. larger system generation capacity), they also present a higher utility cost for meeting larger local demand, and therefore lead to limited surplus solar generation to feed into the grid. When the PV adoption percentage is relatively large (10-100%), the lowest LCC is achieved at around 70% adoption rate. This is because the PV systems adopted from 10-70% present lower LCCs compared with other adoption percent. These buildings usually have relatively large rooftop area for PV installation and low demand. Single-family low-rise buildings are typically observed in this category. When the PV adoption percentage is larger than 70%, the LCC slightly increases with the increase of adoption rate. These late adopters usually have a limited rooftop size with a large demand. Residential multi-family and high-rise complex buildings are typical examples from our observation. Such results indicate that future guidance for the aggregation of distributed PV systems to enter the wholesale market may differ the residential building types to be able to achieve an optimal life cycle cost for the aggregated PV hosts. This also indicates potential different preferences for different types of house owners to install and aggregate PVs to join the WS market in terms of different LCCs.

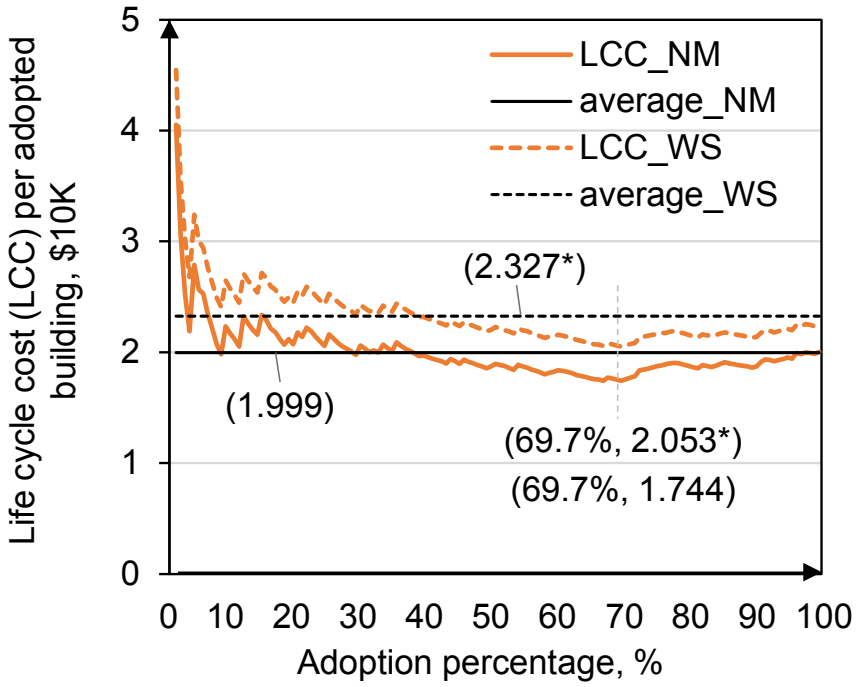

Figure 4-6. Life cycle cost per PV-adopted building under different adoption percentages (the value in parentheses represents the LCC; asterisk represents the value of wholesale scenario)

4.3.3. Environmental results

Figure 4-7 presents the average life cycle CED, water consumption, and carbon emission effects of the simulated PV systems of all adopted building under varied adoption percentages. Results show all simulated PV systems present negative life cycle environmental impacts. This indicates all simulated PV systems regardless of adoption percentage and sequence could provide ideal environmental benefits from their system life cycle. However, when the PV adoption percentage is relatively small (0-16.6%), the life cycle environmental impacts increase dramatically due to the decreasing environmental savings during the operational phase of the PV systems. After the critical point of 16.6%, these impacts increase slowly to the 100% adoption scenario. This indicates that early 16.6% PV adoption performs the best environmentally compared with the late adopters, and

this performance may drop into a flatland quickly with the increase of adoption rate. However, overall, the highest environmental benefit is still achieved at 100% adoption rate.

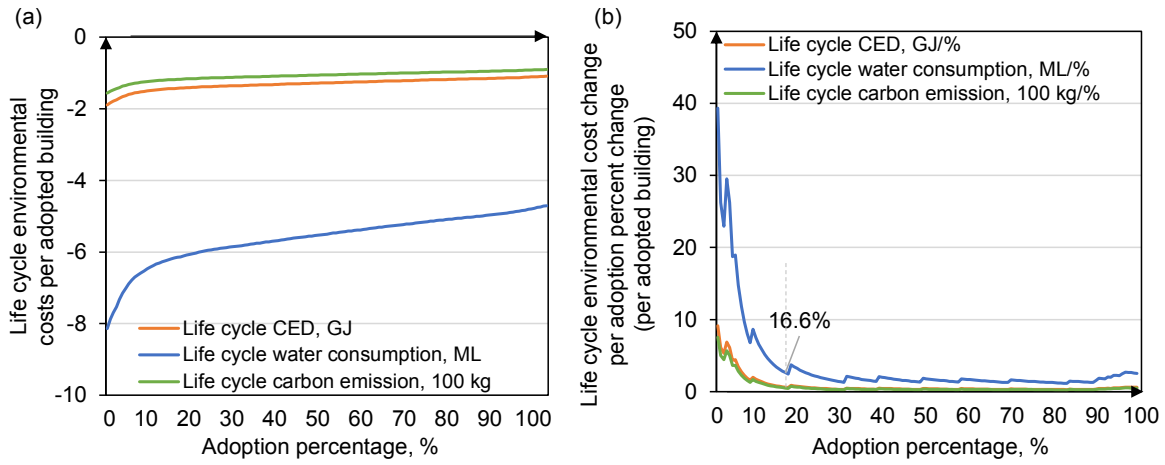

Figure 4-7. (a) Life cycle environmental costs per PV-adopted building under different adoption percentages; (b) life cycle environmental cost change per adoption percent change

When the grid performance and environmental impacts are considered together, the regional load reduction and environmental savings increase with PV adoption rate increase, but the effectiveness of the technical and environmental performances decrease with the increase of PV adoption rate. Our results also show that while the 100% PV adoption clearly provides the largest load reduction and optimal environmental benefits, the energy reliance to the centralized grid supply for PV hosts may slightly increase. More importantly, this 100% penetration of PV generation could largely reduce the mid-peak grid demand which could further lead to a steeper ramp-up curve of the grid load in summer days. However, this consequence may be different in winter when considering the residential demand and solar generation seasonality. Hence, there is a potential tradeoff between the grid performance and environmental benefits under varied PV adoption rates. Moreover, the initial 5.5% PV adoption presents the most effective load reduction performance while the initial 16.6% PV adoption presents the most effective environmental performance. This shows co-

benefited load reduction and environmental performances can be achieved at the early 5% PV adoption indicating the recognition of positive influence of pioneer PV adopters. When the technical, economic, and environmental impacts are considered together, although early PV adoption performs the best technically and environmentally compared with late adoption, early adopters present relatively higher life cycle costs.

4.4. Conclusion

An integrated SDM, LCA, and LCCA modeling framework was developed to investigate the technical, economic, and environmental outcomes of PV implementations on residential building level. This building-level model was then converted into a Python model for regional PV adoption simulation. The feedback loop between the PV adoption and wholesale load cost was considered. The tradeoffs in terms of load reduction, LCC, carbon footprint, CED, and water footprints were assessed under varied PV adoption rates. The city of Boston, MA was selected as our testbed. We found the regional load reduction and environmental savings increase with PV adoption rate increase, but the effectiveness of the technical and environmental performances decreases with the increase of PV adoption rate. Although early PV adoption performs the best technically and environmentally compared with late adoption, early adopters present relatively higher life cycle costs. Moreover, our time-varying observation found a steeper ramp-up curve of the grid load under large penetration of solar PV systems in winter days; however, it provides load-shedding benefits during summer days due to large mid-peak load reduction of the PV adoption. This indicates the significance of implementing energy storage and relevant time-varying energy control strategies. Future studies may further include energy storage installation and related energy system management strategies to allow for a more dynamic simulation of PV adoptions to identify

the potential technical, economic, and environmental tradeoffs and further inform PV planning and management.

5. CHAPTER 5: CONCLUSION

This dissertation proposed and developed a comprehensive modeling framework to investigate the technical, economic, and environmental impacts and tradeoffs of residential PV adoption on both individual building and city scales. A prototype residential building and a residential community located in the metro Boston area, Massachusetts, the United States were selected as our testbeds. System dynamics modeling (SDM) was applied in this study to capture the interactions between PV generation, local demand, and the grid.

In Chapter 2, a dynamic life cycle economic and environmental assessment framework was first developed using SDM with the conventional LCA and LCCA for residential solar PV systems. Two types of PV systems including the GC and the SA systems designs were investigated. This framework was then applied to a prototype residential building located in Boston, MA. Our model effectively captured the direct solar energy use, solar energy store for later consumption, and grid sell or energy waste for the prototype house under the GC or SA system adoption. Solar energy generated, stored, and sold/wasted all present strong seasonal trends. The prototype house has the lowest monthly demand during summer, while the solar energy generation is the highest during the period. Hence, a larger amount of solar energy can be sold or stored during these months. Moreover, the optimized PV-battery system designs for achieving the highest demand met, economic saving, and environmental saving were simulated and compared for this prototype house. For SA systems, we identified the tradeoffs between demand met and life cycle cost, however, these tradeoffs can be best balanced through adjusting the number of PV panels installed. We also found a clear environmental and economic tradeoff when selecting the size of the SA systems. For GC systems, when there is no limit on when and how much excess solar energy can be sold to the

grid, both the economic and environmental benefits are the highest when no battery is installed, and the benefits increase with the increase of panel size. However, when policy constraints such as limitations/caps of grid sell are in place, tradeoffs would present as whether or not to install batteries for excess energy storage. Our results overall indicate the importance of PV-battery system design optimization and tradeoffs assessment to co-optimize the technical, economic, and environmental outcomes of PV adoption.

In Chapter 3, a time-of-use utility rate design and typical PV-battery system control strategies were further implemented into our previous modeling framework to investigate the design and operation of solar PV-battery systems that can achieve grid, environmental, and economic co-benefits under TOU rate design for the prototype residential building. We found scenarios that maximize the selling/use of solar energy during the on-peak hours through battery installation and control can achieve the highest on-peak load reductions and economic benefits under the TOU rate design. However, they do not necessarily provide the highest environmental benefits, as on-peak hours in the New England grid have lower carbon emission and fossil fuel depletion factors as compared with the mid-peak hours. This indicates a potential tradeoff between the need for on-peak load reduction, economic saving, and environmental protection. From an environmental perspective, our finding demonstrates the necessity of better battery control or TOU designs that can effectively incentivize solar energy uses when the grid carbon intensity is the highest. Overall, installing a PV system alone presents relatively strong economic and environmental performances, but its on-peak load reduction is limited. Installing a battery system without an effective control strategy results in relatively weak peak-load reduction, economic, and environmental outcomes. This highlights the importance of effective battery control in the implementation of solar PV-battery systems.

In Chapter 4, we converted our previous building-level modeling framework into a regional-level PV adoption simulation and assessment modeling framework using Python. A residential demand model and a regional scaling up model were incorporated into the modeling framework. The feedback loop between the PV adoption and wholesale load cost was considered. The tradeoffs in terms of load reduction, LCC, carbon footprint, CED, and water footprints were assessed under varied PV adoption rates. The city of Boston, MA was selected as our testbed. We found the regional load reduction and environmental savings increase with the PV adoption rate increase, but the effectiveness of the technical and environmental performances decreases with the increase of the PV adoption rate. Although early PV adoption performs the best technically and environmentally compared with late adoption, early adopters present relatively higher life cycle costs. Moreover, our time-varying observation found a steeper ramp-up curve of the grid load under large penetration of solar PV systems in winter days; however, it provides load-shedding benefits during summer days due to large mid-peak load reduction of the PV adoption. This indicates the significance of implementing energy storage and relevant time-varying energy control strategies.

While the studies presented in this dissertation provide important insights regarding the technical, economic, and social tradeoffs pertain to solar PV adoption at different scales, this research field might benefit from future studies in the following perspectives:

- The technical, economic, and environmental performances and tradeoffs of PV adoptions vary by different local grid mixes, demand patterns, ambient environments, PV installation building

constraints, energy management strategies, solar energy incentives, utility rate designs, federal and state renewable regulations, associated with complex interests of individual energy users, policy makers, electric utilities, and energy balancing authorities. Future studies may investigate the impacts of PV adoption across various municipalities and climate conditions.

- The installation of energy storage systems such as battery systems can be effective to coordinate the PVs, grids, and demand interactions, mitigate the load fluctuation impact from the PV systems, reduce the use of fossil fuel-based supplies, promote cost savings, and increase the energy security. However, the battery sizing and battery control strategies need to be better optimized considering the time-varying feedbacks between the PVs and grids to enhance the battery life cycle performance. Moreover, the improvement of battery technology (e.g., increase of charging and discharging efficiencies, decrease of the battery degradation rate and system component costs) is significant to increase the cost effectiveness of battery systems and reduce the life cycle cost and environmental impacts of PV-battery adoptions.

- The proper selections of the tilt and angle of the PV panel installation are needed to optimize the amount of PV generation for meeting local demand and/or selling to the grid. Future studies may consider these indicators to better optimize the PV-grid balance.

- The increasing applications of new emerging technologies such as the electric vehicles (EVs), vehicle-to-home systems, and heat pump systems could alleviate the reliance on fossil fuel-based energy. However, such implementations potentially increase the need for electricity. It is therefore imperative to examine the performances of distributed PV-battery systems to accommodate these changes in real time.

- The cost saving of individual PV adopters may dissipate due to the increasing PV penetration-induced decreasing grid solar sell prices when the feedback loop between the PV generation and the wholesale electricity cost is considered. It is therefore critical to reflect this changing cost saving in future economic assessment of PV adoptions and inform PV planning and management.

- The impact from the end-of-life phase of the PV adoptions such as toxicity concerns from the disposal material should be considered in the life cycle assessment on a regional level.

- The ongoing COVID epidemic has been affecting the residential demand pattern due to the change of human behaviors (e.g., work from home). It is essential to investigate how the rooftop PV adoptions affect the new demand pattern (e.g., peak time windows and load changes). It is also imperative to optimize the operational strategies of PV-battery systems to achieve the new balance of energy demand and supply (e.g., distributed PV generation and grid supplies) as well as the technical, economic, and environmental co-benefits.

A. APPENDIX A: SUPPORTING INFORMATION FOR CHAPTER 2

Section A1. Literature review of life cycle studies of PV systems

Life cycle cost assessments (LCCA) is a popular approach to assess the economic feasibility of solar PV systems (Adriana et al., 2012; Burns and Kang, 2012; Chandel et al., 2014; De Souza et al., 2017; Gürtürk, 2019; Lai and McCulloch, 2017; Rehman et al., 2007). The common objectives of these studies are assessing the financial viability of the PV systems (Chandel et al., 2014; De Souza et al., 2017; Gürtürk, 2019); informing energy policy and decision making (e.g., feed-in tariffs, net metering) (Burns and Kang, 2012; Carter, 2014; Hsu, 2012; Poullikkas, 2013); comparing PV systems' economic performances at different locations (Rehman et al., 2007); and optimizing the solar PVs' sizes (Adriana et al., 2012; Chel et al., 2009). These studies solely focus on the life cycle economic performance of the solar PV, while the environmental impacts/benefits of the PV systems have been neglected. Economic indicators such as levelized cost of electricity (LCOE) and investment payback time (IPBT) were usually selected for comparison in these studies. The previous reported LCOE ranges from 0.12-0.86 $/kWh, while the IPBT ranges from 7.5-34.2 (Bhandari et al., 2015; K Branker et al., 2011; Price et al., 2010). Energy savings from solar power generation are commonly calculated on an annual or system lifespan basis using averaged data estimated based upon real-time solar radiation data. The dynamic demand and supply relationships were not considered. Due to the ample uncertainty of assessment assumptions in different studies (Darling et al., 2011), it is difficult to compare and evaluate the economic cost and benefit of optimal PV systems from different references (Adriana et al., 2012; Burns and Kang, 2012; Chandel et al., 2014; De Souza et al., 2017; Gürtürk, 2019; Hegedus and Luque, 2010; Lai and McCulloch, 2017; Price et al., 2010; SolarBuzz, 2011; Sutula, 2006). The choices of discount rate in the solar industry, system lifetime, system degradation, capital cost, grid parity, demand profile and financing and incentives including tax credit, tariff and rebate in these studies are constrained in selected geographical and temporal boundaries. This strong spatial and temporal boundedness could lead to a weak extensibility of previous LCCA studies to the future optimization assessment of the PV systems.

Life cycle assessment (LCA) has been widely adopted to assess the environmental performance of solar PV systems (Akinyele et al., 2017; Alsema, 2012; Battisti and Corrado, 2005; Bergerson and Lave, 2002; Bernal-Agustín and Dufo-López, 2006; Beylot et al., 2014; Espinosa et al., 2011; Evans et al., 2009; García-Valverde et al., 2009; Gerbinet et al., 2014; B. Huang et al., 2017; Ito et al., 2008; Jungbluth et al., 2008, 2005; Kannan et al., 2006; Kreith et al., 1990; Kumar and Tiwari, 2009; M. Raugei, 2015; Mason et al., 2006; Meier, 2002; Nawaz and Tiwari, 2006; Nieuwlaar et al., 1996; Pacca et al., 2007; Peng et al., 2013; Raugei et al., 2007; Rawat et al., 2018; Schaefer and Hagedorn, 1992; Sherwani et al., 2010a; Tripanagnostopoulos et al., 2005; Tsang et al., 2016; Wu et al., 2017a; Xu et al., 2018). Carbon emission and cumulative energy demand are most chosen indicators to evaluate the environmental performance of solar PV systems with storage in these studies. Carbon emissions of various solar PV systems range from 9.4-280.0 g-$CO_{2\text{-}eq}$/kWh_e, while cumulative energy demand payback time ranges from 0.8-15.5 years. The purposes of these studies are usually assessing the PVs' environmental impacts at different sites with different environmental conditions (Akinyele et al., 2017; Nawaz and Tiwari, 2006; Rawat et al., 2018); comparing different types of PV modules and system components (Alsema, 2012;

Beylot et al., 2014; Espinosa et al., 2011; Gerbinet et al., 2014; Jungbluth et al., 2008, 2005; M. Raugei, 2015; Mason et al., 2006; Peng et al., 2013; Raugei et al., 2007); comparing the environmental impacts of solar PVs with other types of power supplies (García-Valverde et al., 2009; Kannan et al., 2006; Kreith et al., 1990; Meier, 2002; Nieuwlaar et al., 1996; Schaefer and Hagedorn, 1992; Tsang et al., 2016; Wu et al., 2017a); assessing and comparing environmental impacts of PV lifecycle stages and processes (B. Huang et al., 2017; Xu et al., 2018); and comparing various PV systems' configurations and designs (Battisti and Corrado, 2005; Evans et al., 2009; Gerbinet et al., 2014; Ito et al., 2011, 2008; Laleman et al., 2011; Pacca et al., 2007).

Out of these LCAs, some have assessed the economic and environmental tradeoffs of various PV systems (Bernal-Agustín and Dufo-López, 2006; Ito et al., 2008; Kumar and Tiwari, 2009; Tripanagnostopoulos et al., 2005). The objectives of these studies are comparing different types of PV modules (Ito et al., 2008); testing different values of interest rate and energy tariffs (Bernal-Agustín and Dufo-López, 2006); comparing different PV system configurations (Kumar and Tiwari, 2009); and assessing the PV system performances under the different weather conditions (Tripanagnostopoulos et al., 2005). Most of these studies applied annual and/or monthly average solar radiation and electricity demand data, or experimental observation data to estimate the life cycle economic and environmental impacts of the selected systems, which neglects the diurnal and seasonal patterns of electricity supply and demand (Bernal-Agustín and Dufo-López, 2006; Ito et al., 2008; Kumar and Tiwari, 2009; Tripanagnostopoulos et al., 2005).

Table A-1. Cumulative energy demand (CED) and greenhouse gases (GHG) emissions of photovoltaics (PV) systems in previous studies

Type of PV	Energy factor	GHG factor	Note
2.7 kW grid-connected (GC) mono-crystalline solar PV system	EPBT: 6.74 years	-	System lifetime (years): 25
mono-crystalline solar PV modules	11 - 17.5 MWh/kW	-	Exploitation and preparation of raw materials, process energy, hidden energy of input materials and production equipment
PV module	16 MWh/kW	-	From growth of the silicon crystalline ingot to module fabrication
PV inverters	0.17 MWh/kW	-	-
3 kW mono-crystalline residential rooftop solar PV modules, Japan	17.70 MWh/kW	91 g-CO_2 eq./kWh	From quartz (production of MG silicon) to module fabrication
	EPBT: 15.5 years		for 1427 kWh/m^2/year solar radiation
	12.4 MWh/kW		Off-grade silicon (from semiconductor industry) to module fabrication
35 W mono-crystalline solar PV modules	40.55 MWh/kW, the energy yield ratio (EYR): 1.65-2.6	64.8 g-CO_2/kWh$_e$	India, manufacturing of silicon wafers to modules fabrication, peak output of 35 W and having efficiency of 13%; 20 years
mono-crystalline solar PV modules	13.78 MWh/kW	-	From mineral sand to module fabrication
solar PV system	-	217 g-CO_2/kW h_e	The GHG emission from electricity generation from the solar PV system
oil-fired steam turbine	-	937 g-CO_2/kW h_e	Life cycle cost of electricity generation from the oil-fired steam turbine plant is about 7.03 cents/kWh$_e$ based on current market price of fuel-oil price of 200 US$ per tonne
natural gas-fired combined cycle	-	493 g-CO_2/kW h_e	net efficiency of 50%, including the transmission and distribution loss; a gas price of US$ 5.34 per MMBTU

amorphous PV systems	13,000 to 21,000 kWh/kW	3.360 kg-CO_2/kW_p	The accumulated primary energy consumption for the construction of the photovoltaic power plants; CO_2 for amorphous technology
mono-crystalline solar PV system	3.2 years	60.0 g-CO_2/kWh_e	Efficiency (%): 14; lifetime: 30 years, Netherlands
GC PV systems, rooftop installation	2.5–3 years	50–60 g/kWh_e now and probably 20–30 g/kWh_e in the future	production of PV modules and balance of system (BOS) components
multi-megawatt ground mounted system	3–4 years	-	
PVL62 (photovoltaic laminates) and PVL136 thin film (amorphous) modules	371 MJ (primary energy) in materials; 1490 MJ as process energy	34.3 g-CO_2 eq./kWh_e	including BOS, inverter installations and transportation
100 MW very large-scale PV (VLS-PV) systems (amorphous silicon (a-Si) solar cell modules)	-	15.6-16.5 g-CO_2 eq./kWh_e	Gobi Desert; considering temperature of the desert 5.8 and 30.2 °C
30 m^2 amorphous solar PV system	-	47 g-CO_2/kWh_e	lifetime (years) and efficiency (%): 20, 10; Netherlands
amorphous solar PV system	2.7 years	50 g-CO_2/kWh_e	lifetime (years) and efficiency (%): 30, 7; Netherlands
8 kW amorphous solar PV system	-	39 g-CO_2/kWh_e	lifetime (years) and efficiency (%): 30, 5.7; US
33 kW amorphous solar PV system	3.2 years	34.3 g-CO_2/kWh_e	lifetime (years) and efficiency (%): 20, 6.3; US
100 MW amorphous solar PV system	2.5 years	15.6 g-CO_2/kWh_e	lifetime (years) and efficiency (%): 30, 6.9; China
100 MW poly-crystalline solar PV system	1.9 years	12.1 g-CO_2/kWh_e	lifetime (years) and efficiency (%): 30, 12.8
100 MW poly-crystalline solar PV system	1.5 years	9.4 g-CO_2/kWh_e	lifetime (years) and efficiency (%): 30, 15.8
mono-crystalline silicon technology	-	5.020 kg-CO_2 /kW_p	-
Mono-crystalline wafers of p-type silicon PVS	4 years	-	India
distributed 2.7 kW_p solar PV system	2.2 MJ/kWh_e, EPBT 4.47 years	165 g-CO_2 /kWh_e	Singapore; 36 mono-crystalline silicon modules (12 V, 75 W_p) mounted on a building rooftop with aluminium supporting structures and concrete blocks for the base; lifetime (years) and efficiency (%): 25,10.6
2.7 kW mono-crystalline solar PV system	5.87 years	217 g-CO_2/kWh_e	lifetime (years) and efficiency (%): 25, 7.3-8.9; Singapore
300 kW PV plant	total embodied energy: 16.5 GWh	4205 metric tons of CO_2; 280 g-CO_2 eq./kWh_e	Austin US, 3.5-acre field of 2620 m^2 and having single crystal (mc) silicon cell; lifetime (years) and efficiency (%): 30, 8.5
14.4 kW_p (kW peak) PV system	8 years	44 g-CO_2 eq./kWh_e	UK; nominal area of 160 m^2, less than 11,000 kWh_e AC output would be generated annually; lifetime (years) and efficiency (%): 30, 11.5
1 kW grid-connected multi-crystalline silicon PV system	3.3 years	Carbon payback time (CPBT, years): 4.1; 26.4 g-CO_2/kWh_e	lifetime (years) and efficiency (%): 20, 10.7; Rome, Italy
3 kW_p PV and PV/T system	2.9 years	104 g-CO_2/kWh_e	Greece, 30 m^2 with multi-crystalline (pc) silicon PV modules; lifetime (years): 20
3.5 MW_p multi-crystalline PV	total primary energy 526–542 MJ/m^2; EPBT: 0.21 year	29–31 kg CO_2 eq./m^2	support structures are assumed to be 60 years, inverters and transformers are considered to have life of 30 years

33 kW KC120 multi-crystalline modules (with BOS, inverter)	1000 MJ primary energy in materials and 3020 MJ process energy; EPBT 5.7 years	72.4 g-CO_2 eq./kWh_e (US conditions); 54.6 g-CO_2 eq/kWh_e (European conditions)	lifetime (years) and efficiency (%): 20, 12.92
100 MW large-scale multi-crystalline PV system	1.7 years	12 g-CO_2 eq./kWh_e	Gobi Desert, tilt angle 20°; lifetime (years) and efficiency (%): 30, 12.8
multi-crystalline silicon	-	CBPT: 3.37-8.04	-
3 kW rooftop PV systems (solar-grade poly-crystalline silicon)	-	GHG emission 53.4, 43.9 and 26 g-CO_2 eq./kWh_e	efficiency (%): 17; Japan
12 different 3 kW_p GC PV systems	3–6 years	39-110 g-CO_2 eq./kWh_e (Swiss mix of 79 g-CO_2 eq./kWh_e)	-
Nano-crystalline dye sensitized (NCDSC) system	-	19–47 g-CO_2 eq./kWh_e (20 years);78–188 g-CO_2 eq/kWh_e (5 years)	lifetime (years): 5-30
Amorphous PV system	2.5–3.2 years	15.6–50 g-CO_2 eq./kWh_e	
mono-crystalline type	3.2–15.5 years	44–280 g-CO_2 eq./kWh_e	
poly-crystalline solar PV systems	1.5–5.7 years	9.4–104 g-CO_2 eq./kWh_e	
thin film PV systems	0.75–3.5 years	10.5–50 g-CO_2 eq./kWh	
mono-Si PV systems	1.7 - 2.7 years	29 - 45 g-CO_2 eq./kWh	
high-concentration PV system	0.7-2.0 years	-	-
manufacturing silicon solar cells (terrestrial cells and space cells)	12-24 years	-	-
PV modules in commercial production lines	1.2 (amorphous silicon modules) and 2.1 years (crystalline silicon modules)	-	France
producing PV modules in manufacturing	4 years	-	India
multi-Si PV module	1145 kW h_t/m^2	-	cell accounts for 970 kWh_t/m^2, frame accounts for 175 kWh_t/m^2
crystalline silicon PV modules (mono-Si PV module)	4160 to 15520 MJ/m^2;	-	total energy requirement: 11670 MJ/m^2
open field and roof-top PV systems	1710 and 1380 kWh_e/m^2 (7-26 years)	-	-

Some studies incorporated dynamic process modeling using dynamic supply and demand data/pattern to assess the technical, economic, and/or environmental performances of solar PV systems (Akinyele and Rayudu, 2016a, 2016b; Allouhi et al., 2019, 2016; Berwal et al., 2017; Bilich et al., 2017; Bortolini et al., 2014; Diaf et al., 2008; Hondo, 2005; Jones et al., 2018; Kazem et al., 2017; Lee et al., 2018a; Poullikkas, 2013; Uddin et al., 2017; Zhang et al., 2016). Table 2-1 presents literature review summary of these dynamic life cycle studies.

Several LCCA studies considered the diurnal and seasonal dynamics in their analyses. Kazem (Kazem et al., 2017) used hourly weather data including solar irradiation, temperature, relative humidity and wind speed to estimate the potential energy generation from a 1 MW grid-connected

(GC) power generation plant in Adam, Oman. MATLAB was used to optimize the PV size for the highest economic benefit. This study solely modelled the PV system from power generation side without considering the demand-side dynamics.

Lee et al., (2018) used hourly solar radiation data, building and price information databases, and ArcMap 10.1 to estimate the economic potential of rooftop grid-connected solar PV systems for each building in the urban area of Seoul in South Korea. They found the annual economic potential of the rooftop solar PV system could supply up to 4.48% of the annual electricity consumption in the Gangnam district as of 2016, South Korea (Hong et al., 2017; Lee et al., 2018a).

Uddin et al., (2017) examined the influence of battery degradation on the technical and economic performances of solar PV system with battery storage of a residential mid-size family house in the UK. This study found integrating electric energy storage with solar PV showed no economic benefits due to the degradation caused by high frequency cycling of small 2-kWh battery during operations (Uddin et al., 2017). However, this study did not consider possible control strategies of the solar battery and only one panel size has been tested.

A few LCAs have considered the dynamics involved in the solar PVs' environmental performances. Bilich (2017) applied hourly solar insolation, the average daily electricity demand, and the peak electricity demand to test three smart grids designs for a model village in Kenya. PV-battery, PV-diesel, and PV-hybrid smart-grid designs were tested on the environmental indicators of climate change, particulate matter, photochemical oxidants, and terrestrial acidification for this village. Excel and Gabi were applied to determine the system sizes and further verified using HOMER software. In addition, this study also compared the environmental impacts of Cadmium telluride (CdTe) and Monocrystalline silicon (Mono-Si) PV modules as well as lithium-ion (Li-Ion) and Lead acid (PbA) batteries (Bilich et al., 2017). The system sizing methodology in this study including HOMER is based upon the technical and economic performances of the selected distributed systems, and the environmental concern is not addressed in their sizing simulations.

Akinyele et al. (2016 a&b) applied dynamic life cycle economic and environmental assessments to evaluate the technical, economic, and environmental performances of standalone (SA) solar PV systems in off-grid communities under demand load growth scenarios. Different from other studies, battery storage was modelled. Detailed battery state of charge (SoC) and reliability analysis (using loss of energy probability and the availability as two indicators) were selected as important technical storage indicators. In addition, this study specifically considered temperature losses, losses due to the incomplete utilization of solar irradiation, and balance of system (BOS) losses in the load assessment (Akinyele and Rayudu, 2016a, 2016b). These two studies tested the performance of solar PV considering system losses under demand growths, but the array and battery sizing only considered the loss of energy probability and the availability.

Jones et al. (2018) combined LCIA with discounted cash-flow analysis to assess the carbon footprint and financial impact of battery storage in grid-connected PV systems in a non-domestic building in UK. This study specifically assessed the impact of battery storage within a grid-connected PV system. To reflect the financial attraction to non-domestic building owners, this study tested various cost reduction and rate scenarios. In addition, life cycle emissions of the PV system with and without battery were calculated and compared to better understand the role of

solar battery on environmental benefits. This study found that battery storage does not necessarily increase CO_2 savings and costs of battery need to be reduced rapidly to make solar battery more financially attractive in the UK (Jones et al., 2018). However, only one panel size is modelled and tested. The CO_2 emissions intensity of the electricity grid was based on the yearly average of the UK national grid.

Table A-2. Literature review summary of dynamic life cycle assessment studies

Ref.	(Akinyele and Rayudu, 2016a)	(Akinyele and Rayudu, 2016b)	(Bilich et al., 2017)	(Jones et al., 2018)	(Kazem et al., 2017)	(Lee et al., 2018a)	(Uddin et al., 2017)
Year	2016	2016	2016	2018	2017	2018	2017
Location	Bauchi State, Nigeria	Gusau, Zamfara State, Nigeria	Kenya	UK	Adam city, Oman	Seoul, South Korea	UK
Model objective	24-household community	Small community	Off-grid communities	Non-domestic building	Power generation plant	All building in urban district	3-bedroom house
PV type	SA	SA	SA	GC	GC	GC	GC
PV capacity	40 kW	40.4 kW	6.42 and 1.22 kW	20 kW	1 MW	Solar potential	4kW
Capacity source	IEEE and IEC guidelines	IEEE guideline and Homer	Estimation through Excel, verified by Homer	Given	Given	ArcGIS	Give
Module type	N/A	crystalline	CdTe	Mono-Si	N/A	N/A	Mono-Si
Battery type	N/A	N/A	Li-Ion	Li-Ion	N/A	N/A	Li-Ion
Battery size	N/A	N/A	Homer determined	20 kWh	N/A	N/A	2 kWh
System lifespan	25 years	25 years	25 years	30 years	25 years	25 years	1 year
Battery indicator	Detailed battery state of charge	Detailed battery state of charge	N/A	Battery efficiency, battery energy loss	N/A	N/A	Calendar ageing, capacity throughput, ambient temperature, state of charge, depth of discharge and current rate
Technical indicator	System output, energy production, yield and losses, and efficiency, Reliability analysis: unmet energy demand, loss of energy probability and the availability; temperature losses; losses due to the incomplete utilization of solar irradiation; balance of System (BOS) losses	Load demand, system reliability: the unmet demand, loss of energy probability and the availability (similar indexes as previous)	Unmet demand	N/A	Capacity factor, yield factor (consider wire and temperature inverter losses), optimum system factors including capacity factor, yield factor, PV energy production, optimum inverter were obtained from MATLAB code.	Technical potential assessment through ArcGIS-considering geographic constraints (available rooftop area)	N/A
Economic indicator	Annual life cycle cost including diesel fuel cost; the unit cost of energy	Life cycle cost similar as last Ref.	N/A	Net present value	Life cycle cost, cost of energy	Life cycle cost-profitability and economic potential: return on investment and payback period	annual revenue from installing a PV-battery
Environmental indicator	Life cycle amount of fuel saved, the emissions minimized, the	Life cycle impact: emission rate, GWP, CED, energy payback	Climate change, particulate matter, photochemical	Life cycle carbon emission	N/A	N/A	N/A

	global warming potential	time, energy return on investment	oxidants, and terrestrial acidification				
Other power source	Diesel power plant/generator	Diesel power plant/generator	diesel	UK grid	N/A	N/A	UK grid
Grid mix Info.	N/A	N/A	N/A	UK national grid	N/A	N/A	N/A
Geospatial Info.	N/A	N/A	N/A	N/A	N/A	Spatial diversity	N/A
Scenario setup	Load demand growth	Load demand growth	PV-Battery, PV-Diesel; PV-Hybrid	Cost reduction scenario, electricity; retail price scenario	N/A	Subsidy scenario; self-consumption and business scenarios	N/A
Dynamic process modeling	Battery and system losses modeling	Battery and system losses modeling	Scenario-based simulation	cost reduction and rate scenarios	System optimization algorithm	GIS combined with scenario simulation	Battery degradation model

Section A2. Comparison of typical modeling tools for accessing PV systems

Table A-3. Comparison of SD-based modeling framework (this dissertation), Hybrid Optimization of Multiple Energy Resources (HOMER), and System Advisor Model (SAM)

Method	Dynamic life cycle economic and environmental assessment modeling framework (this study)	HOMER		SAM
		HOMER Pro	HOMER Grid	
Main objective	Comprehensive and integrative technical, economic and environmental decision informing on distributed and grid-connected solar power supply systems	Technical-economic optimization of microgrids, remote utilities, and distributed generation systems	Technical-economic optimization of grid-connected solar plus storage or other hybrid grid-connected distributed generation systems	Techno-economic model that facilitates decision-making for people in the renewable energy industry
Developer		HOMER Energy LLC., U.S. National Renewable Energy Laboratory (NREL)		U.S. Department of Energy and NREL, Sandia National Laboratories; The University of Wisconsin
Year firstly developed	This study	1993		August 2007
Target user	PV hosts, utility operators, energy-related decision makers, system engineers	PV hosts, micro-grid engineers and operators, energy-related decision makers		Project managers and engineers, policy analysts, technology developers, researchers
software	Vensim	HOMER		The SAM Simulation Core (SSC) software development kit (SDK)
Adaptable software		N/A		C/C++, C#, Java, Python, MATLAB, Excel, TRNSYS
Modeled system	Residential standalone and grid-connected solar PV systems with or without battery storage	Solar photovoltaic (PV), wind turbine, generator: diesel, electric utility grid, traditional hydro, run-of-river hydro power, biomass power, generator: gasoline, biogas, alternative and custom fuels, cofired, microturbine, fuel cell; energy storage: flywheels, customizable batteries, flow batteries, hydrogen		Photovoltaic, concentrating solar power, solar water heating, wind, geothermal, biomass, and conventional power systems
Financial model indicator	Life cycle cost (net present value), investment payback period (costs of initial construction, component replacements, maintenance); revenues include income from selling power to the grid	Levelized cost of electricity		Levelized cost of energy
Economic Metrics		life-cycle cost (net present value), levelized cost of energy (costs of initial construction, component replacements, maintenance, fuel, plus the cost of buying power from the grid and miscellaneous costs such as penalties resulting from pollutant emissions; Revenues include		Residential and commercial projects: levelized cost of energy, electricity cost with and without renewable energy system, electricity savings, after-tax net present value, payback period; power purchase agreement (PPA) projects: levelized cost of energy, electricity sales

		income from selling power to the grid, plus any salvage value that occurs at the end of the project lifetime.)	price, internal rate of return, net present value, debt fraction or debt service coverage ratio; project annual cash flows: revenues from electricity sales and incentive payments, installation costs, operating, maintenance, and replacement costs other payments
Environmental indicators	LCA: life cycle CED, carbon, and water footprints	Carbon dioxide (CO_2), carbon monoxide (CO), unburned hydrocarbons (UHC), particulate matter (PM), sulfur dioxide (SO_2), and nitrogen oxides (NO_X)	N/A
Environmental impacts result from	Life cycle stages (from manufacturing to operational stages, end-of-life not considered)	Annual production of electricity/thermal energy by generators/boiler; consumption of grid electricity (if connected) during the system operational stage	N/A
Environmental impacts factor	Environmental impacts factor (CED, water, carbon footprints per unit of grid supply, kWh)	Emissions factor (kg of pollutant emitted per unit of fuel consumed)	N/A
Simplified equation for calculating environmental impacts	life cycle environmental impacts=environmental impacts of systems manufacturing and O&M + grid-related environmental impacts (if connected)	Annual emissions of certain pollutant (kg/yr)=emissions factor * total annual fuel consumption	N/A
Grid-related environmental impacts calculation	Life cycle net grid usage * environmental impacts factors (calculated from Simapro based on chosen grid mix)	Annual net grid purchases (kWh, total annual grid purchases minus the total grid sales) * emission factor (g/kWh) of each pollutant	N/A
Model structure	Solar generation, energy balance and energy storage simulation incorporated with LCCA and LCA	System output, battery performance, and related loads calculations	User interface, calculation engine, programming interface
Examples of input variables	Solar radiation profiles, Energy consomption profiles, environmental profile (ambient temperature, wind speed), utility rate profile	Type of energy source, initial investment, choice of various system components	Weather data, costs data, PV system data, utility data, tax and other incentive variables
Source code availability		Not available. The general description available in online manual	Not available, reference manuals describing the algorithms in each of the performance model modules are available
Time step and horizon	30-minute time step over one year for simulation and 25-year system lifespan for LCCA and LCA	Hourly to minutely time step over one year	Hourly step over one year
Other function		The environmental impacts of chosen systems can be provided (emissions)	Sensitivity analysis
limitation		Technical and economic perspective sizing only	Cannot model hybrid power systems; battery storage not included

Section A3. Additional methodology description

To validate the PV cell temperature (T, °C) calculated through Equation 2-2 in Chapter 2 with the consideration of the cooling effect of wind on PV panels, Sandia Module Temperature Model (Equation A1) and Faiman Module Temperature Model (FMT) (Equation A2) were also implemented in this modeling framework (Faiman, 2008) and wind speed (W, m/s) data of Boston from NSRDB was also applied in the model as the case study.

$T = D(e^{a+bW}) + T_a$ Equation A1

$T = T_a + \left(\frac{D}{U_0 + U_1 W}\right)$ Equation A2

Where, T represents the PV cell temperature in the current time step, °C; T_a is the ambient temperature in the current time step, °C; D is the solar radiation striking the PV array in the current time step, kW/m^2; W is the wind speed (m/s); U_0 is the constant heat transfer component, W/m^{2}K; U_1 is the convective heat transfer component, W/m^{2}K. a and b are parameters that depend on the module construction and materials as well as on the mounting configuration of the module. In this study, a is -3.560 and b is -0.075 (Stein, 2012). Faiman (Faiman, 2008) measured solar irradiance, wind speed, and module temperatures on seven types of modules and found the values of U_0 and U_1. In this study, U_0 is 25 and U_1 is 6.84 W/m^{2}K.

In the battery storage model, this study also applied the Kinetic Battery Model (HOMER, 2017; Manwell and McGowan, 1993) to calculate the electricity energy charging and discharging capacities, which indicate the capacities of absorbing and withdrawing energy from the battery storage at each time step. In the kinetic battery model (Manwell and McGowan, 1993), the total amount of energy stored in the battery at any time (Q, kWh) is the sum of the available (Q_1, kWh) and bound energy (Q_2, kWh) as Equation A3. Q, Q_1 *and* Q_2were assumed to be 0 kWh at the first timestep. The equations to calculate the Q_1 and Q_2 in each time step are provided, Equation A4 and A5. The maximum battery charge capacity (P_k, kW) and maximum battery discharge capacity (P', kW) were calculated in each time step based upon Equation A4 and A5 respectively (Manwell and McGowan, 1993). Q and Q_1 indicate the battery state of charge and reveal the most recent charge and discharge history of the battery. The storage capacity of one battery of 1.02 kWh (B) and the number of batteries installed in the BES (m) indicate the total capacity of the BES. The storage capacity ratio (C) and the storage rate constant (K) were assumed to be 1 (HOMER, 2018, 2017).

$Q = Q_1 + Q_2$ Equation A3

Where, Q represents the total amount of energy stored in the battery, kWh; Q_1 is the available energy, kWh; Q_2 is the bound energy, kWh.

$P_k = \frac{KQ_1e^{-K\Delta t} + QKC(1-e^{-K\Delta t})}{1 - e^{-K\Delta t} + C(K\Delta t - 1 + e^{-K\Delta t})}$ Equation A4

$P' = \frac{-KCBm + KQ_1e^{-K\Delta t} + QKC(1-e^{-K\Delta t})}{1 - e^{-K\Delta t} + C(K\Delta t - 1 + e^{-K\Delta t})}$ Equation A5

Where, P_k represents the maximum battery charge capacity through Kinetic Battery Model, kW; P' represents the maximum battery discharge capacity, kW; Q_1 is the available energy in the storage at the beginning of the time step, kWh; B is the storage capacity of one battery, 1.02 kWh; m is the number of battery installed in the BES; Q is the total amount of energy in the storage at the beginning of the time step, kWh; C is the storage capacity ratio, 1; K is the storage rate constant, 1; Δt is the length of the time step, thirty minutes.

Except Kinetic Battery Model (Manwell and McGowan, 1993), this study also considered other two limitations to calculate the maximum capacity of charging into battery storage, which were battery storage limitation and charge current limitation (HOMER, 2017). Equation A6 presents the calculation of maximum battery charge capacity through battery storage limitation and equation A7 shows the calculation of this capacity with the limitation of charge current. The storage's maximum charge rate of 0.98 A/Ah (α_c), the storage's maximum charge current of 270 A (I_{max}) and the storage's nominal voltage of 3.7 V (V_n) were used in the simulation (HOMER, 2018).

$$P_s = \frac{(Bm-Q)(1-e^{-\alpha_c \Delta t})}{\Delta t} \qquad \text{Equation A6}$$

$$P_c = \frac{mI_{max}V_n}{1000} \qquad \text{Equation A7}$$

Where, P_s represents the maximum battery charge capacity with battery storage limitation, kW; P_c represents the maximum battery charge capacity with charge current limitation, kW; B is the storage capacity of one battery, 1.02 kWh; m is the number of battery installed in the BES; Q is the total amount of energy in the storage at the beginning of the time step, kWh; α_c is the storage's maximum charge rate, 0.98 A/Ah; Δt is the length of the time step, thirty minutes; I_{max} is the storage's maximum charge current, 270 A; V_n is the storage's nominal voltage, 3.7 V.

In our study, the least of three values: P_k, P_s, and P_c, was assumed to be the maximum storage charge capacity after charging losses in the model (HOMER, 2017), as shown in Equation A8. The storage charge efficiency (η) of 89.4% was used (HOMER, 2017).

$$P = \frac{MIN(P_k,P_s,P_c)}{\eta} \qquad \text{Equation A8}$$

Where, P represents the maximum battery charge capacity in the model, kW; η is the storage charge efficiency, 89.4%.

Figure A-1 presents the tiered cost of labor for the installation of solar PV systems (HomeAdvisor, 2019).

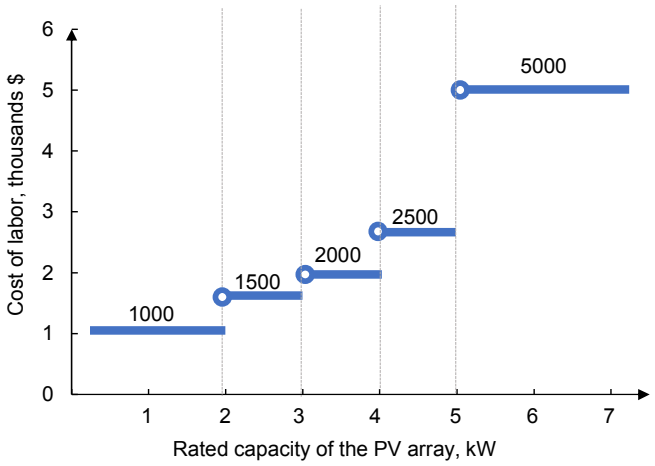

Figure A-1. The tiered cost of labor for solar PV system installation (HomeAdvisor, 2019)

Section A4. Additional results

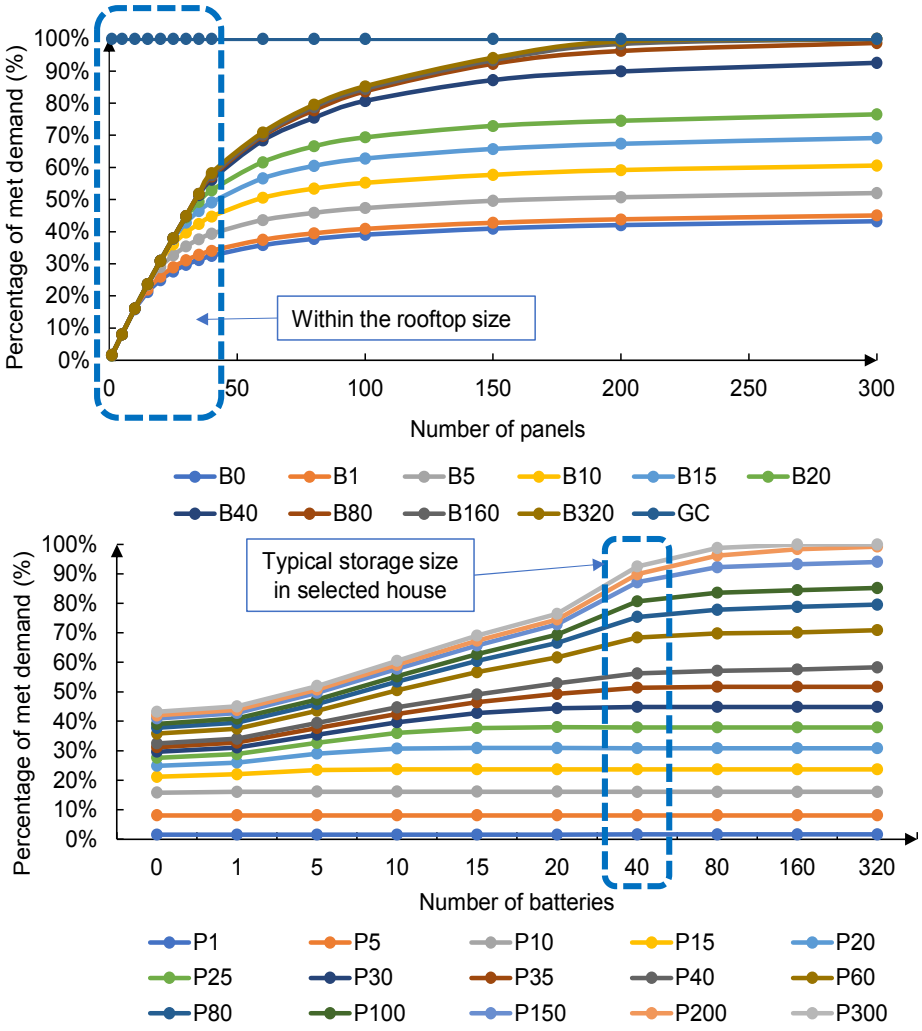

Figure A-2. Percentage of demand met through solar energy in PV systems

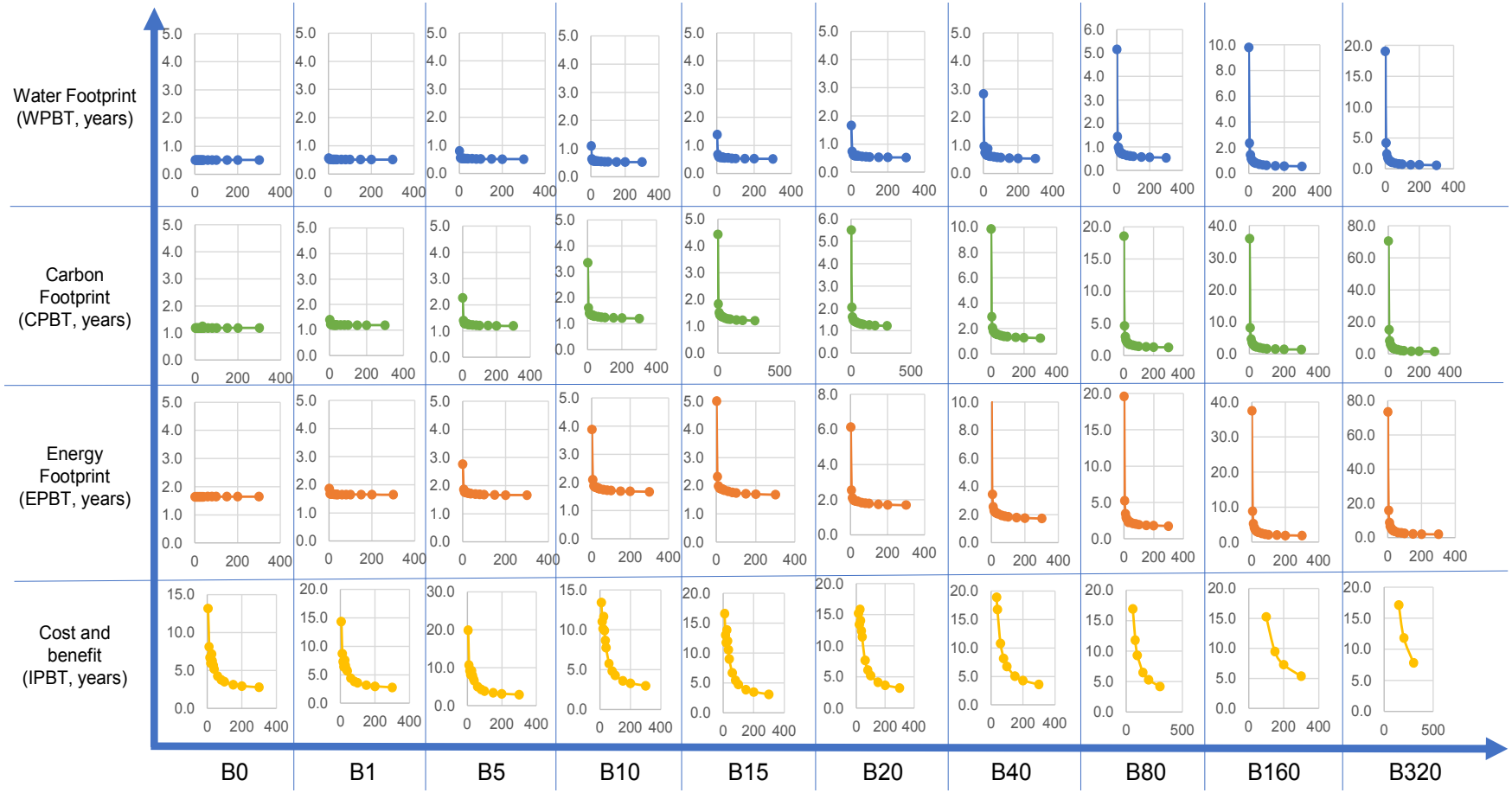

Figure A-3. Environmental and economic payback time of grid-connected (GC) PV systems

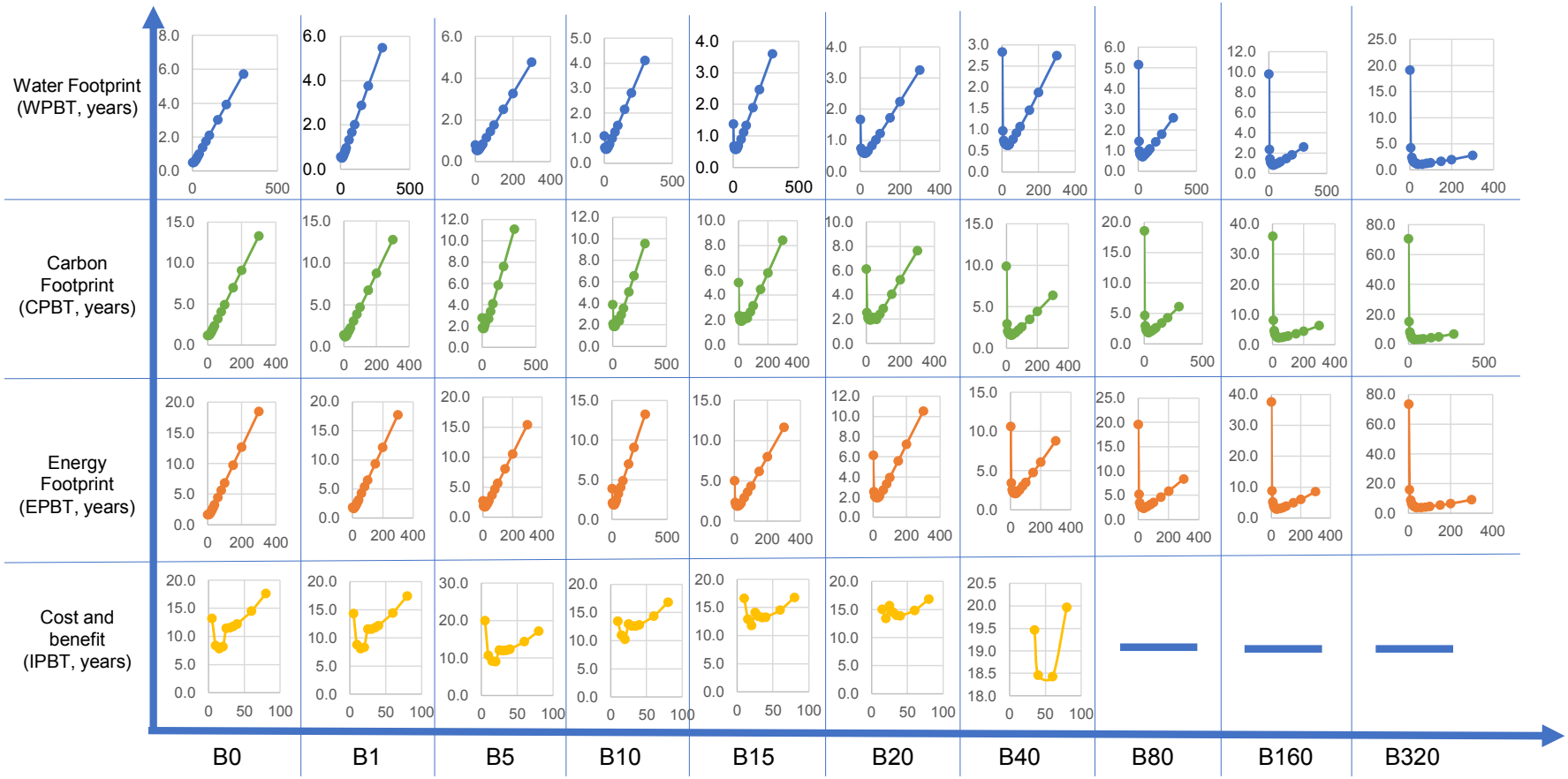

Figure A-4. Environmental and economic payback time of standalone (SA) PV systems

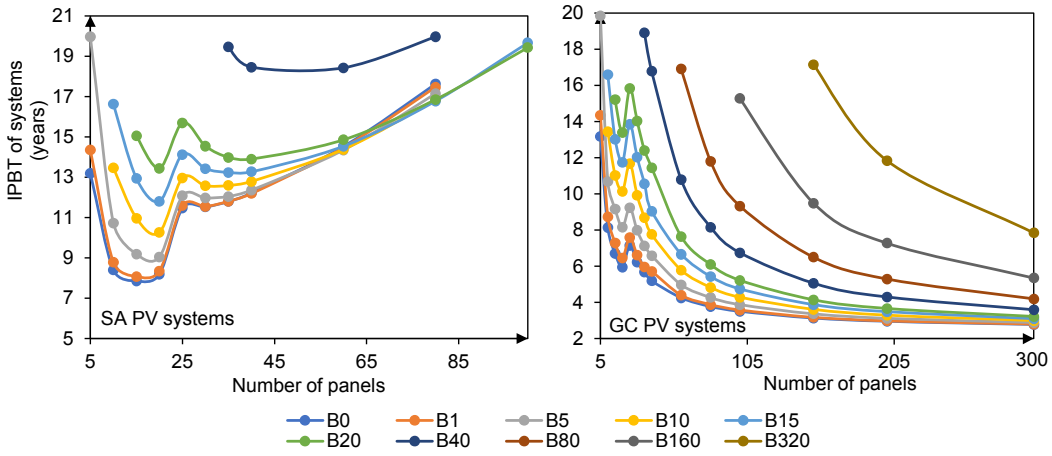

Figure A-5. Investment payback time (IPBT) of SA and GC PV systems

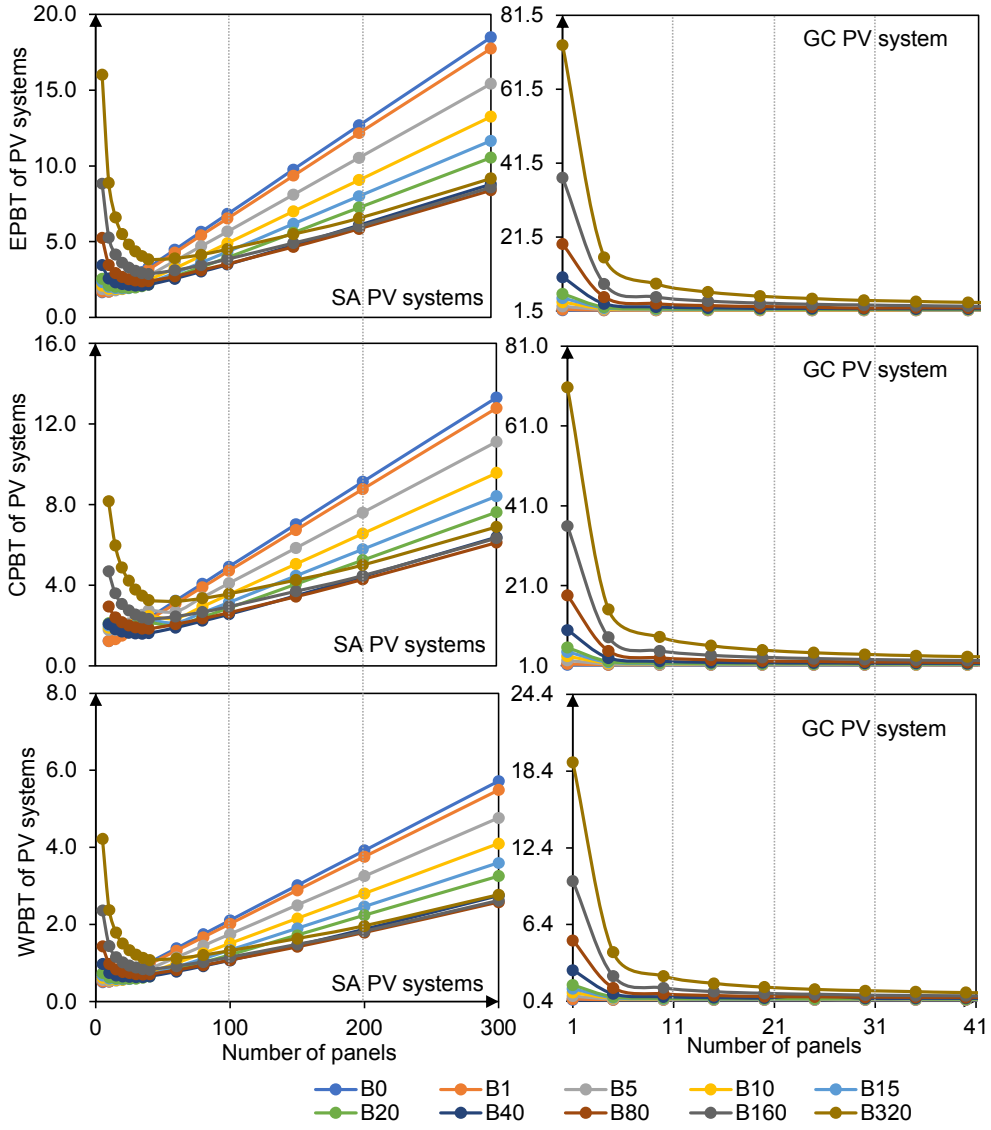

Figure A-6. EPBT, CPBT and WPBT of SA and GC PV systems

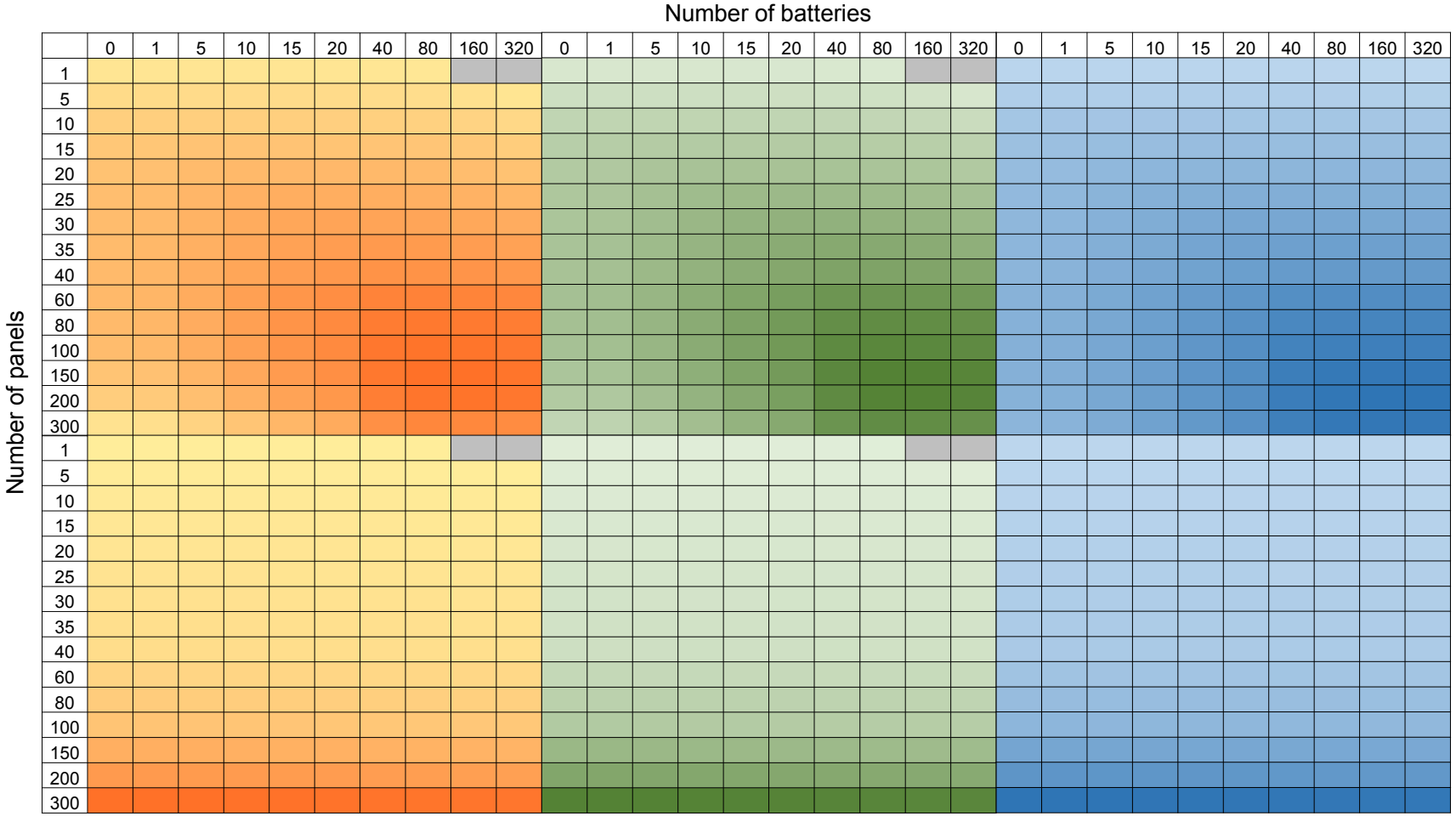

Figure A-7. Environmental impact intensity of SA (upper row) and GC (under row) PV systems (Orange color represents life cycle CED, MJ; green color represents life cycle carbon footprint, kg CO_2 eq; blue color represents life cycle water footprint, L. Lighter color represents larger life cycle environmental impacts. Grey cells represent positive life cycle environmental impacts.)

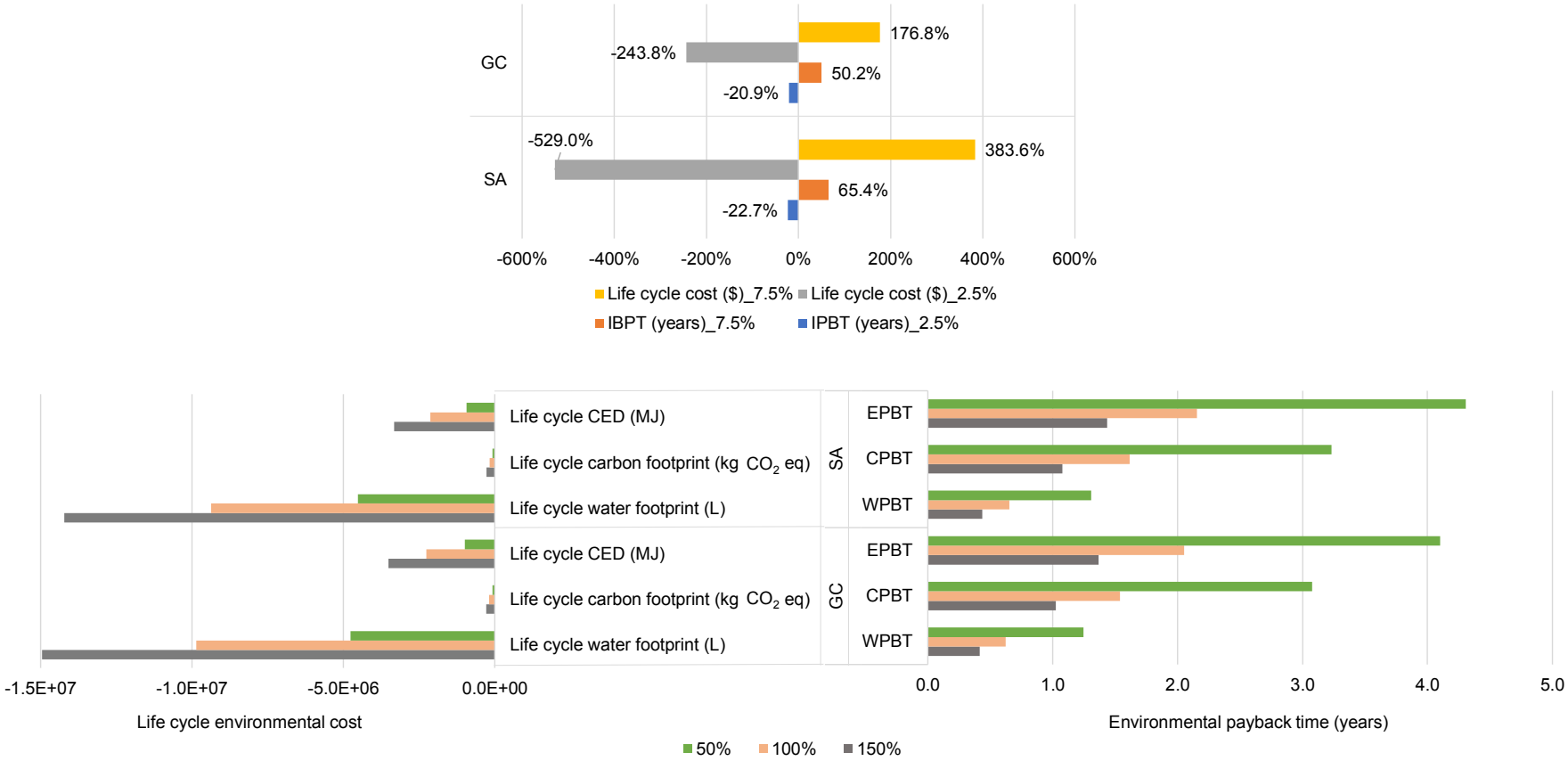

Figure A-8. Effects of increasing and decreasing the discount rate and the environmental impact units by 50% on life cycle costs, IPBT, life cycle environmental costs and environmental payback time

Table A-4. Effects of increasing and decreasing the discount rate (5%) by 50% on IPBT and life cycle cost of SA and GC PV systems

IPBT (years)	SA	GC
NPV 2.5%	14.3	13.3
NPV 5%	18.5	16.8
NPV 7.5%	30.6	25.2

Life cycle cost ($)	SA	GC
NPV 2.5%	-4748.1	-5979.7
NPV 5%	-754.9	-1739.4
NPV 7.5%	2141.1	1335.8

Type of PV system	SA	GC
IPBT (years)_2.5%	-22.7%	-20.9%
IBPT (years)_7.5%	65.4%	50.2%
Life cycle cost ($)_2.5%	-529.0%	-243.8%
Life cycle cost ($)_7.5%	383.6%	176.8%

Table A-5. Effects of increasing and decreasing the environmental impact units by 50% on life cycle environmental savings of GC PV systems

Value change	CED (MJ)	Carbon footprint (kg CO_2 eq)	Water footprint (L)
50%	1.0E+06	8.6E+04	4.8E+06
100%	2.3E+06	1.9E+05	9.9E+06
150%	3.5E+06	2.9E+05	1.5E+07

PBT change	EPBT	CPBT	WPBT
50%	4.10	3.08	1.24
100%	2.05	1.54	0.62
150%	1.37	1.03	0.41

Table A-6. Effects of increasing and decreasing the environmental impact units by 50% on life cycle environmental savings of SA PV systems

	Energy Savings Life Cycle (MJ)	CO2 saving life cycle (kg CO2 eq)	water saving life cycle (L)
50%	9.4E+05	8.1E+04	4.5E+06
100%	2.1E+06	1.8E+05	9.4E+06
150%	3.3E+06	2.7E+05	1.4E+07

	Energy payback time (yr)	Carbon payback time (yr)	Water payback time (yr)
50%	4.31	3.23	1.31
100%	2.15	1.62	0.65
150%	1.44	1.08	0.44

B. APPENDIX B: SUPPORTING INFORMATION FOR CHAPTER 3

Section B1. Solar PV's relevant energy management strategies

Net metering and time-of-use utility rates have been implemented and adjusted to meet the increasing needs of renewable and distributed energy technologies such as solar PV systems in the overall power supply system (Bazmi and Zahedi, 2011; Eid et al., 2014; SEIA, 2019b). Net metering policy is one of the most important incentives that supports residential energy users to implement solar PV systems in their energy systems (Poullikkas, 2013). Massachusetts, as well as most other states in the U.S. which have issued net metering policy, allow property owners to send electricity generated via solar PV system to the grid, and as a return, energy credit will be refunded on future electric bills for the surplus energy produced by the PV (Heeter et al., 2014). Besides, there is also a growing interest in policies and management strategies to reduce peak demand by managing electricity use or shifting the demand to non-peak times (Albadi and El-Saadany, 2008). One of the most effective and popular strategies is the time-of-use (TOU) program. A few states in the U.S. like California have been implementing this policy (Herter et al., 2007; Herter and Wayland, 2010). Because of the differential fluctuate prices during a day, TOU program brings opportunities and incentive to energy users to install solar PV systems and battery storage systems to maximize their economic benefits as well as potential environmental benefits.

Besides the policy-level effort, increasing attention has been paid to the alternative demand response (DR) strategies (Hopper et al., 2006; Karami et al., 2014; Prüggler, 2013; Zheng et al., 2015). DR is a term defined as "*changes in electric usage by end-use customers from their normal consumption patterns in response to changes in the price of electricity over time, or to incentive payments designed to induce lower electricity use at times of high wholesale market prices or when system reliability is jeopardized*" (Erdinc, 2014; Venkatesan et al., 2012; Zhao et al., 2013). These strategies including battery storage dispatch strategies show potential on the alleviation of grid stress from the demand side. Renewable and distributed energy supply systems (e.g., solar PV systems) coupled with battery storage are usually popular choices in current energy markets (Agnew and Dargusch, 2015). Compared with the large-scale, utility-based practice, customized distributed energy systems with storage in residential, commercial, or industrial settings are usually small-scale and more flexible (e.g., flexible customized battery dispatch strategies).

Section B2. Additional methodology description

Figure B-1 presents the revised schematic of the system dynamics model (SDM) developed for Chapter. 3 This SDM consists of three main components: solar energy generation, battery storage, and energy balance simulations.

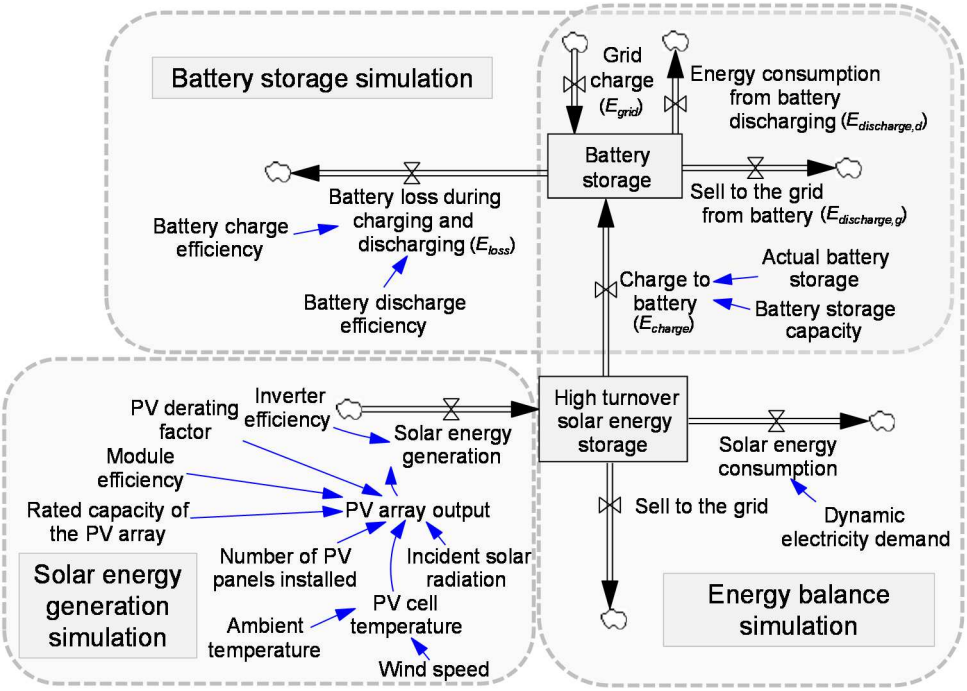

Figure B-1. The system dynamics model structure of the solar PV-battery system

Figure B-2 presents the hourly operation of two typical battery control strategies (scenarios S4A and S4B) simulated in this chapter.

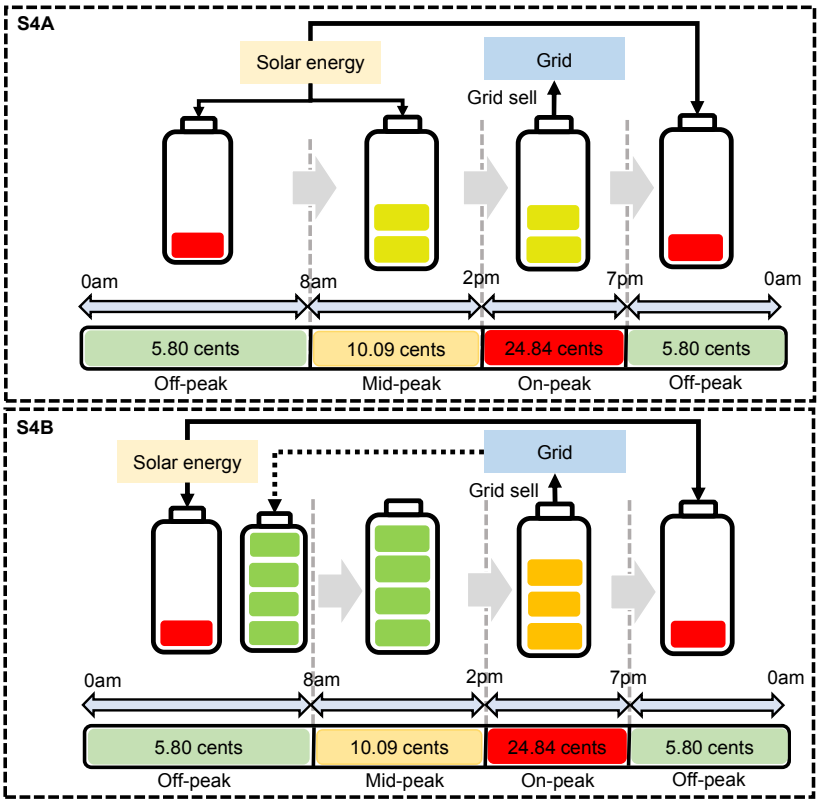

Figure B-2. Two types of battery charge control strategies investigated in Chapter 3

SimaPro 8.3 was used for characterization of the environmental impacts. Table B-1 presents the unit costs and environmental impacts obtained from SimaPro. Carbon footprint, water footprint, and life cycle fossil fuel depletion factors were calculated using ReCiPe Midpoint (H) 1.12 Europe Recipe H method. The references of cost units of PV systems were provided in the main manuscript.

Table B-1. Carbon footprint, water footprint, life cycle fossil fuel depletion, and cost units of selected solar PV systems

Solar PV systems	SimaPro entry	Cost unit	Carbon footprint unit	Water footprint unit	Fossil fuel depletion unit
PV panel	Photovoltaic panel, multi-Si wafer {GLO}| market for | Alloc Def, S	\$1/W	202 kg CO_2 eq/m^2	9860 L/m^2	54.9 kg oil eq/m^2
Battery	Battery, Li-ion, rechargeable, prismatic {GLO}| market for | Alloc Def, S	\$209/kWh_c	6.13 kg CO_2 eq/kg	205 L/kg	1.71 kg oil eq/kg
Inverter	Inverter, 2.5 kW {GLO}| market for | Alloc Def, S	\$300/piece	203.0 kg CO_2 eq/piece	3840 L/piece	53.6 kg oil eq/piece
Mounting and wiring	Photovoltaic mounting system, for flat-roof installation {GLO}| market for | Alloc Def, S	\$450	35.4 kg CO_2 eq/m^2	275 L/m^2	8.67 kg oil eq/m^2

Table B-2 presents the carbon footprint, water footprint, and life cycle fossil fuel depletion factors (per kWh of electricity generated) of different types of fuel use for power generation. Carbon footprint, water footprint, and life cycle fossil fuel depletion factors were calculated using ReCiPe Midpoint (H) 1.12 Europe Recipe H method. No significant difference was found in model output applying the ReCiPe Midpoint (H) 1.12 Europe or IPCC 2013 GWP 100a. Water footprint factors (water depletion) were also compared with the water consumption factors obtained from (Macknick et al., 2011).

Table B-2. The carbon footprint, water footprint, and life cycle fossil fuel depletion factors of different types of fuel for power generation

Type[a]	Carbon footprint factor, kg CO_2 eq./kWh		Life cycle fossil fuel depletion factor, kg oil eq./kWh	Water footprint factor, L/kWh		SimaPro entry
Method	IPCC 2013 GWP 100a	ReCiPe Midpoint (H) 1.12 Europe			Macknick et al., 2011	
Natural gas	0.63	0.62	0.24	3.50	1.78	Electricity, high voltage {NPCC, US only}| electricity production, natural gas, conventional power plant | Alloc Def, S
	0.42	0.41	0.15	0.88		Electricity, high voltage {NPCC, US only}| electricity production, natural gas, combined cycle power plant | Alloc Def, S
Hydropower	0.0045	0.0044	0.0009	0.078	17.0	Electricity, high voltage {NPCC, US only}| electricity production, hydro, run-of-river | Alloc Def, S

	0.44	0.44	0.15	8.80		Electricity, high voltage {NPCC, US only}| electricity production, hydro, pumped storage | Alloc Def, S
	0.0068	0.0067	0.0012	29.3		Electricity, high voltage {NPCC, US only}| electricity production, hydro, reservoir, alpine region | Alloc Def, S
Nuclear	0.013	0.013	0.0032	3.10	2.54	Electricity, high voltage {NPCC, US only}| electricity production, nuclear, boiling water reactor | Alloc Def, S
	0.012	0.012	0.003	3.0		Electricity, high voltage {NPCC, US only}| electricity production, nuclear, pressure water reactor | Alloc Def, S
Coal	1.16	1.16	0.25	1.30	2.35	Electricity, high voltage {NPCC, US only}| electricity production, hard coal | Alloc Def, S
	1.24	1.24	0.28	2.50		Electricity, high voltage {NPCC, US only}| electricity production, lignite | Alloc Def, S
Oil	1.22	1.22	0.41	3.60	N/A	Electricity, high voltage {NPCC, US only}| electricity production, oil | Alloc Def, S
Landfill gas	0.25	0.25	0.05	19.0	0.89	Electricity, high voltage {NPCC, US only}| heat and power co-generation, biogas, gas engine | Alloc Def, S
Wind	0.02	0.02	0.005	0.39	0	Electricity, high voltage {NPCC, US only}| electricity production, wind, >3MW turbine, onshore | Alloc Def, S
	0.012	0.012	0.003	0.24		Electricity, high voltage {NPCC, US only}| electricity production, wind, <1MW turbine, onshore | Alloc Def, S
	0.012	0.012	0.0035	0.22		Electricity, high voltage {NPCC, US only}| electricity production, wind, 1-3MW turbine, onshore | Alloc Def, S
Wood	0.053	0.054	0.014	0.26	N/A	Electricity, high voltage {NPCC, US only}| heat and power co-generation, wood chips, 6667 kW, state-of-the-art 2014 | Alloc Def, S
Refuse	0.46	0.46	0.12	11.0	N/A	Electricity, for reuse in municipal waste incineration only {RoW}| treatment of waste wood, untreated, municipal incineration | Alloc Def, S
	0.18	0.18	0.038	18.0		Electricity, for reuse in municipal waste incineration only {GLO}| treatment of biowaste, municipal incineration | Alloc Def, S
Solar	0.067	0.066	0.017	2.53	0.098	Electricity, low voltage {NPCC, US only}| electricity production, photovoltaic, 570kWp open ground installation, multi-Si | Alloc Def, S

a. The average value was used when there were more than one SimaPro entries investigated.

Table B-3 presents the time of the off-, mid-, and on-peak periods in a day in response to the changes of the on-peak duration in the sensitivity analysis. 24-hour format was used for time display.

Table B-3. The time of the off-, mid-, and on-peak periods in a day in response to decrease and increase of the on-peak duration by 50%

	On-peak duration	Off-peak time	Mid-peak time	On-peak time	Off-peak time
Initial setting	5 hours	0:00 - 8:00	8:00 - 14:00	14:00 - 19:00	19:00 - 24:00

Decrease by 50%	2.5 hours	0:00 - 8:00	8:00 - 15:15	15:15 - 17:45	17:45 - 24:00
Increase by 50%	7.5 hours	0:00 - 8:00	8:00 - 12:45	12:45 - 20:15	20:15 - 24:00

Section B3. Additional results

Sensitivity analysis

Table B-4 presents the percent change and sensitivity index of life cycle cost, carbon footprint, water footprint, and life cycle fossil fuel depletion of PV-battery systems in response to decrease or increase of the sensitive variables by 50%.

Table B-4. Life cycle cost, carbon and water footprints, and life cycle fossil fuel depletion of PV-battery systems in response to decrease or increase of the sensitive variables by 50%

Indicator	Scenario	Variable	decrease by 50%		increase by 50%	
			percent change	sensitivity index	percent change	sensitivity index
LCC	S1	discount rate	25.1%	-0.50	-18.2%	-0.36
		on-peak duration	-17.9%	0.36	21.6%	0.43
		off-peak rate	-13.5%	0.27	13.5%	0.27
		mid-peak rate	-9.6%	0.19	9.6%	0.19
		on-peak rate	-26.9%	0.54	26.9%	0.54
	S2	discount rate	2.9%	-0.06	-2.1%	-0.04
		on-peak duration	-6.4%	0.13	15.8%	0.32
		off-peak rate	-28.6%	0.57	28.6%	0.57
		mid-peak rate	34.3%	-0.69	-34.3%	-0.69
		on-peak rate	-11.5%	0.23	11.5%	0.23
	S3	discount rate	4.0%	-0.08	-2.9%	-0.06
		on-peak duration	-0.7%	0.01	5.6%	0.11
		off-peak rate	-8.6%	0.17	8.6%	0.17
		mid-peak rate	1.6%	-0.03	-1.6%	-0.03
		on-peak rate	-0.9%	0.02	0.9%	0.02
	S4A	discount rate	-13.5%	0.27	9.8%	0.20
		on-peak duration	-11.5%	0.23	25.2%	0.50
		off-peak rate	-22.7%	0.45	22.7%	0.45
		mid-peak rate	-3.2%	0.06	3.2%	0.06
		on-peak rate	52.7%	-1.05	-52.7%	-1.05
	S4B	discount rate	-104.8%	2.10	76.0%	1.52
		on-peak duration	-10.5%	0.21	23.8%	0.48
		off-peak rate	-127.5%	2.55	127.5%	2.55
		mid-peak rate	47.4%	-0.95	-47.4%	-0.95
		on-peak rate	288.9%	-5.78	-288.9%	-5.78
Carbon footprint	S1	on-peak duration	-0.5%	0.01	2.0%	0.04
		on-peak Hydro%	5.5%	0.25	-5.5%	0.28
	S2	on-peak duration	-18.9%	0.38	26.7%	0.53
		on-peak Hydro%	6.6%	0.29	-6.6%	0.33

	S3	on-peak duration	-3.3%	0.07	4.4%	0.09
		on-peak Hydro%	0.4%	0.02	-0.4%	0.02
	S4A	on-peak duration	1.6%	-0.03	3.4%	0.07
		on-peak Hydro%	-18.3%	-0.81	18.3%	-0.91
	S4B	on-peak duration	-18.3%	0.37	26.0%	0.52
		on-peak Hydro%	-119.0%	-5.29	119.1%	-5.95
Water footprint	S1	on-peak duration	-9.8%	0.20	11.0%	0.22
		on-peak Hydro%	-14.0%	0.40	14.0%	0.40
	S2	on-peak duration	0.9%	-0.02	3.4%	0.07
		on-peak Hydro%	-3.4%	0.10	3.4%	0.10
	S3	on-peak duration	0.6%	-0.01	2.0%	0.04
		on-peak Hydro%	-0.5%	0.01	0.5%	0.01
	S4A	on-peak duration	-3.4%	0.07	10.0%	0.20
		on-peak Hydro%	26.3%	-0.75	-26.3%	-0.75
	S4B	on-peak duration	1.0%	-0.02	4.3%	0.09
		on-peak Hydro%	109.4%	-3.11	-109.4%	-3.12
Life cycle fossil fuel	S1	on-peak duration	-0.5%	0.01	2.1%	0.04
		on-peak Hydro%	6.1%	0.30	-6.1%	0.23
	S2	on-peak duration	-35.1%	0.70	49.3%	0.99
		on-peak Hydro%	11.8%	0.59	-11.8%	0.44
	S3	on-peak duration	-4.3%	0.09	5.7%	0.11
		on-peak Hydro%	0.5%	0.03	-0.5%	0.02
	S4A	on-peak duration	1.4%	-0.03	5.1%	0.10
		on-peak Hydro%	-23.7%	-1.19	23.7%	-0.89
	S4B	on-peak duration	-63.1%	1.26	87.7%	1.75
		on-peak Hydro%	-393.2%	-19.66	393.5%	-14.76

C. APPENDIX C: SUPPORTING INFORMATION FOR CHAPTER 4

Section C1. Literature review of the top-down and bottom-up residential demand simulation approaches

Table C-1. summarizes the top-down and bottom-up simulation approaches for modeling/ forecasting the residential demand at either household unit or regional grid levels.

Table C-1. Top-down and bottom-up simulation approaches for residential demand simulation

Reference	Method	Metrics	Input	Output	Resolution	Calibration or validation	Applicable to single and/or group	Top-down or bottom-down
(Arghira et al., 2012)	Predictors and Auto Regressive Moving Average method	performances of predictors: the time when appliances use energy and probability of the service to consume energy	appliances energy consumption and weather conditions (temperature, wind strength, wind direction, humidity) of 100 households in France[1]	energy consumption of each electrical appliance	10 min	demand pattern of recurrence to improve the prediction precision	both	bottom-up
(Muratori et al., 2013)	Markov process	power conversion factors: appliances, HVAC, lighting etc.	weather, temperature, dwelling characteristics, and behavior	electricity demand profile	10 min	time-of-use data from the 2003–2009 American Time Use Survey	both	bottom-up
(Muratori, 2018)	Markov chain behavioral model	power conversion factors: appliances, HVAC, lighting etc.	household occupants' behavior: e.g. hours of working	residential electric power profiles	10 min	time-of-use data from the 2003–2009 American Time Use Survey	both	bottom-up
(Dergiades and Tsoulfidis, 2008)	Autoregressive Distributed Lag (ARDL)	cointegrating relation among the variables	Per capital income, price of electricity, price of oil for heating, weather conditions, stock of housing[2]	per capita consumption of electricity	annual	literature review	group	top-down
(Hirst, 1978; O'Neal and Hirst, 1980)	Quantitative model	Residential use of a type of fuel for an end use in certain housing type for one year	heat retention of housing units, the average annual energy use for the type of equipment,	Annual national energy use by fuel, end use, type of housing, and age groups	annual	historical data	both	top-down

			intensity of the equipment is used					
(Saha and Stephenson, 1980)	An engineering-economic model	Energy uses for space heating, water heating, cooking	household appliance ownership and variations (ownership fraction)	fuel use	annual	historical data	group	top-down
(Jonas Tornberg, 2012)	GIS implemented energy model	Energy use of building types: single family house, blocks of flats, shops and offices, hospitals and education etc.	real estate and building data, energy data (heating and hot-water and type of energy/energy carrier)	Energy (natural gas and electricity) use	annual	N/A	both	both

1. From Residential Monitoring to Decrease Energy Use and Carbon Emissions in Europe (REMODECE)
2. From World Development Indicators (WDI) database, the Energy Information Administration (EIA) database, and the US census bureau.

Section C2. Additional methodology description

Case study description

Figure C-1. presents the map of our case study using ArcMap 10.4.1. The selected study area, community, and residential buildings for simulation were presented in Figure C-1. (a), (b), and (c) respectively. ArcMap 10.4.1 was also used to facilitate the spatial distribution of the solar PV generation capacity in the city of Boston.

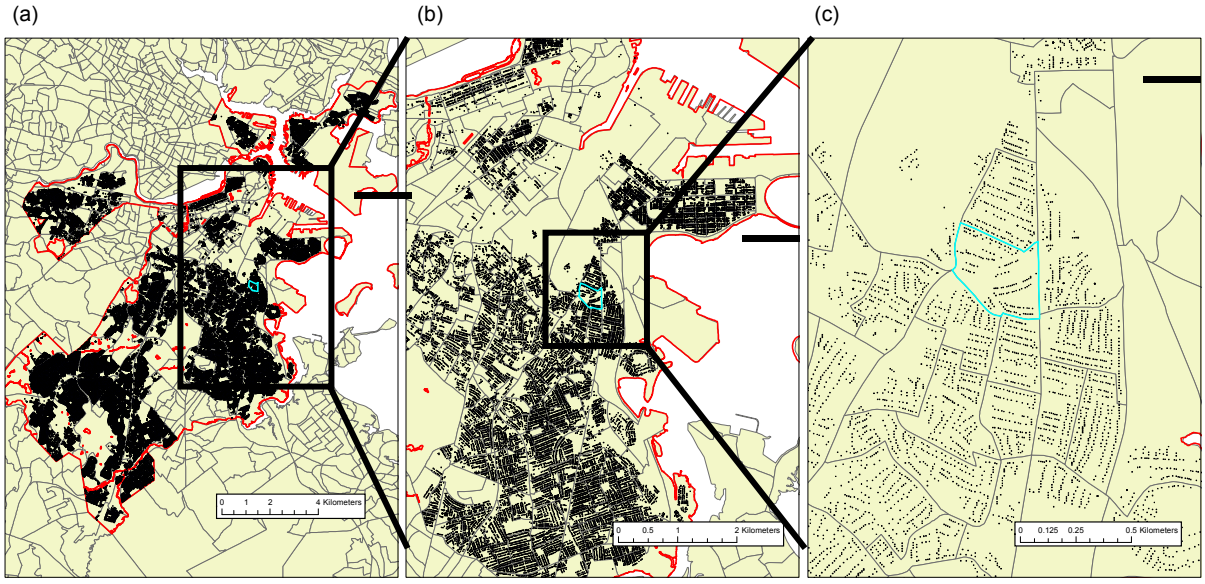

Figure C-1. The map of the (a) selected study area and (b), (c) selected community

In Figure C-1., the black dots represent the residential buildings obtained from the GIS data portal of the City of Boston; the red lines represent the border of the city of Boston; the black lines represent the border of community block groups obtained from the U.S. Census; the blue line represents the border of the simulated community for this study.

Table C-2. presents the average percentages of household types of the simulated community, city of Boston, and state of Massachusetts calculated based upon the U.S. Census data.

Table C-2. Average household type percentages of the selected community, city of Boston, and state of Massachusetts obtained from the U.S. Census

	Household type							
	one-male	one-female	one male one female one child	one male one female no child	one male one child	One female one child	two-male	two-female
the selected community	15.6 %	18.9%	10.5%	17.1%	0.4%	8.2%	15.4 %	13.8%
Boston	15.3 %	18.6%	11.4%	16.3%	1.5%	9.7%	11.0 %	14.8%
Massachusetts	12.0 %	16.2%	19.6%	26.3%	1.8%	7.2%	7.1%	9.8%

Table C-3. presents the residential information of our simulated community provided by the U.S. Census.

Table C-3. The U.S. Census information of the selected community

U.S. Census GEOID	Number of residential buildings selected	Simulated population over city total population
250250907003	145	0.2120%

Section C2.1. Residential demand simulation

HVAC demand simulation

In the work of (Muratori et al., 2013, 2012), the air mass of the control volume is estimated for a residential building with an area of 223 m^2 and a height of 2.44 m. The air flow rate capacity of HVAC is 0.46 kg/s and the nominal power of the coupled furnace is 13.2 kW selected from Table C-4. based upon the optimization of the HVAC system considering the weather conditions. A return air temperature is therefore 50 °C.

Table C-4. Parameter values of the simulated HVAC model (Muratori et al., 2013)

Parameter	Value	Unit
R_{wall}	2.64	m^2 K/W
R_{window}	0.183	m^2 K/W
h_{in}	5	W/m^2 K
h_{out}	30	W/m^2 K
Windows-to-wall ratio	17%	N/A
Desired temperature	21.1	°C
HVAC summer air temperature	13	°C
HVAC winter air temperature	50	°C
Hottest environment temperature	38	°C
Coldest environment temperature	-30	°C

Table C-5. Air flow rates and furnace sizes of commercially available residential HVAC systems and their resulting temperatures of the air (°C) from the furnace (EIA, 2010)

Air flow, cfm	Input capacity, kBTU/h											
	45	50	60	70	75	80	90	100	115	120	125	140
800	50	53	59	66								
1200	40	42	47	51	53	55	59	64				
1600				43	45	47	50	53	58	59	61	
2000							44	47	50	52	53	57

Behavior-related demand

Table C-6. presents the power conversion factors collected from the American appliance stock by the U.S. Department of Energy in February 2012. The laundry activity includes washing machine use (425 W, 39 minutes) and drying use (3400W, 90 minutes). The dishwashing activity is assumed to be one hour. The power consumption of other activities is assumed to be counted only when the occupant is engaged in the activity.

Table C-6. Power conversion factors in the behavioral simulation

Activity	Power consumption (W)
Sleeping	0
No-power activity	0
Cleaning	1250
Laundry	3825
Cooking	1225
Automatic dishwashing	1800
Leisure	300
Away, working	0
Away, not working	0
Day-time lighting power	125
Night-time lighting power	330
Constant electric consumption	230

Table C-7. presents the information of the ATUS respondents selected for this study.

Table C-7. The age, sex, working condition, and number of ATUS respondents selected in this study

	Mean age	Age range	Number of respondents
Male	48.78	18-85	8436
Female	49.93	18-85	9327
Child	8.88	0-17	6561
Overall	38.46	0-85	24324
Working	-	-	5723
Non-working	-	-	3712

Figure C-2. presents the percentage distributions of nine activities of five types of occupants over a day cleaned from the raw ATUS dataset.

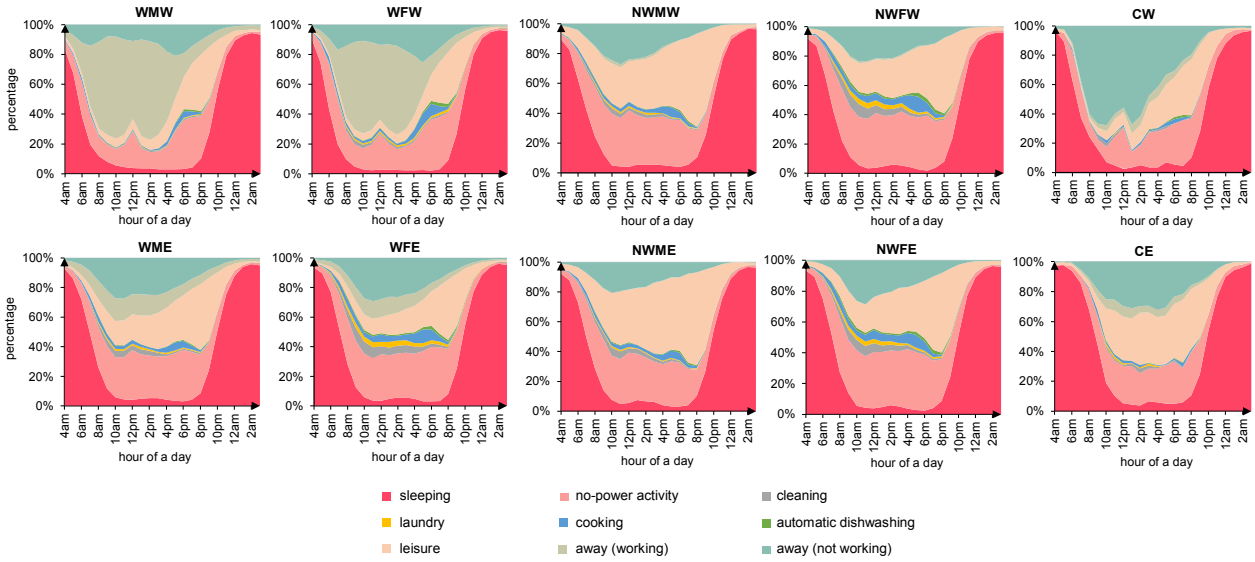

Figure C-2. The percentage distributions of nine activities of five types of occupants over a day

Lighting demand

Figure C-3. presents the sunrise and sunset time of the city of Boston over one year (NOAA, 2021). These two timelines were used to determine the daytime and nighttime for our lighting simulation.

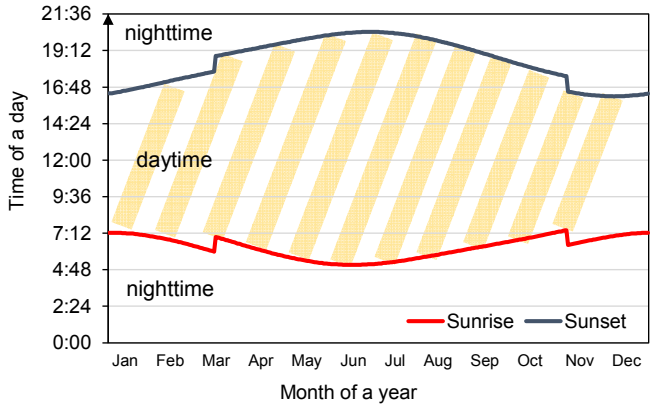

Figure C-3. Sunrise and sunset time of the city of Boston

Regional residential demand simulation

Figure C-4. shows the schematic of the random assigning process to determine the household type of a residential building unit in this study.

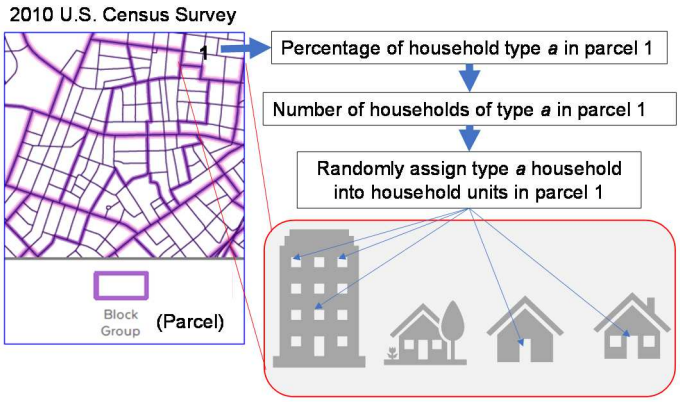

Figure C-4. A schematic of the random assigning process for determining the household type in this study

Table C-8. presents the types, numbers, and percentages of the simulated households in this study.

Table C-8. The types, numbers, and percentages of the simulated households in this study

Household type	Number of the simulated households	Percentage of the simulated households
One-male	30	14.4%
One-female	40	19.1%
One male one female one child	22	10.5%
One male one female no child	35	16.7%
One male one child	2	1.0%
One female one child	13	6.2%
Two-male	36	17.2%
Two-female	31	14.8%
Total	209	100%

Section C2.2. Economic impacts

Wholesale electricity cost simulation

Table C-9. presents the average power plant operating expenses of nuclear, hydro-electric, and other types of power generation.

Table C-9. Average Power Plant Operating Expenses for Major U.S. Investor-Owned Electric Utilities, 2015 through 2019 (Mills per Kilowatt-hour) (EIA, 2020e)

Year	Nuclear	Hydro-electric[1]	Other[2]
2015	25.71	13.42	33.24
2016	25.36	10.98	30.19
2017	24.38	10.29	31.76
2018	23.86	10.65	32.43
2019	23.73	10.80	28.33

1. Hydroelectric category consists of both conventional hydroelectric and pumped storage.
2. Other category consists of photovoltaic, wind, gas turbine, and internal combustion plants.
A mill equals to 1/1000 of the U.S. dollar (equivalent to 1/10 of one cent).
Due to the data availability, the prices of 2020 were assumed to be the same as the prices in 2019.

Section C2.3. Environmental impacts

Figure C-5. presents the carbon emission unit of ISO-NE grid supply over a year. ISO-NE energy system capacities, utility fuel mix, and marginal fuel use

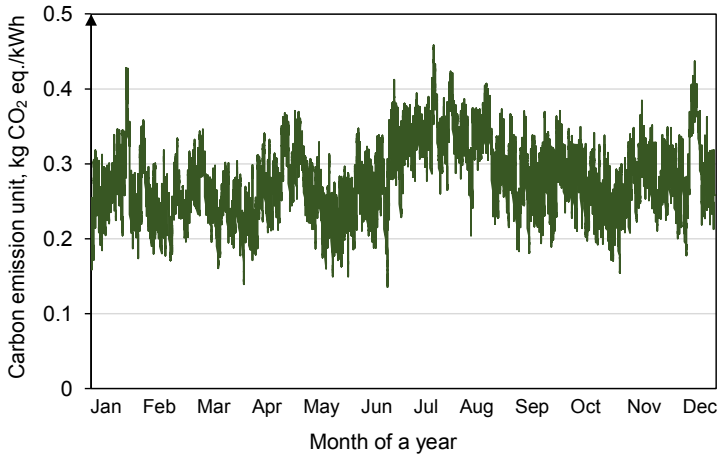

Figure C-5. Carbon emission unit of ISO-NE grid supply over a year

Section C3. Additional results

Solar energy generation

The Massachusetts Commonwealth Solar Program set a statewide target of installing 1600 MW of solar PV by 2020 (Mass.gov, 2021), which 160 MW (approximately 10%) would be the city of Boston's contribution to the state target based upon the proportional estimation of the city population over the state's population. However, our study found the total potential rated capacity of all residential buildings was estimated to be 254.7 MW in the city of Boston. The average potential rated capacity for each building was estimated to be 3.7 kW (Figure C-6.), which is 0.74 times as large as the average size of a residential PV system in the U.S. of 5 kW (EIA, 2015b; SEIA, 2021). In Boston, we found 99.8% of the potential PV systems were smaller than 10 kW. And only less than 0.2% of these buildings may not be available to unlimited Net Metering due to the current utility policy (EnergySage, 2021; Eversource, 2020). More than 85.3% of the buildings present the potential to install a PV system smaller than 5 kW.

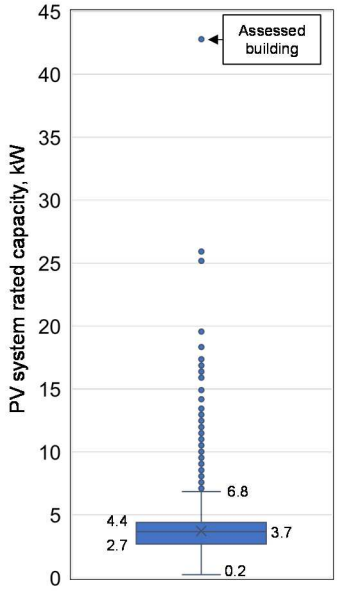

Figure C-6. Distribution of the rated capacities of PV systems of all residential buildings

Figure C-7. (a). presents the annul solar energy generation potential of all residential buildings in the city of Boston. Figure C-7. (b) shows the spatial distribution of the solar energy generation potential by block groups in the city of Boston.

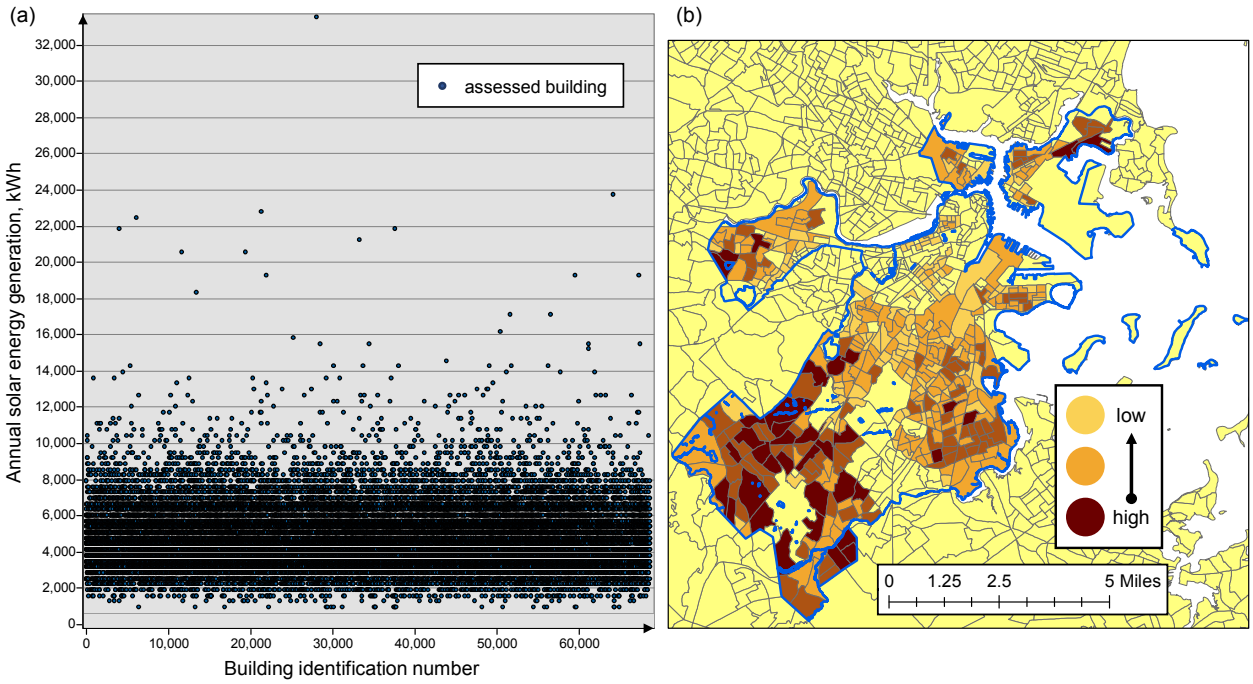

Figure C-7. (a) Annual solar energy generation of all residential buildings; (b) solar potential density map (potential rated capacity of PV systems) of the block groups in the city of Boston

Section C3.1. Residential demand simulation

HVAC simulation

In order to present and validate the output of HVAC simulation, a typical residential building in the city of Boston was selected. Figure C-8. illustrates the geographical location of this selected typical residential building (Maps, 2020). The building information as well as the estimated PV and HVAC systems' parameters were presented in Table C-10.

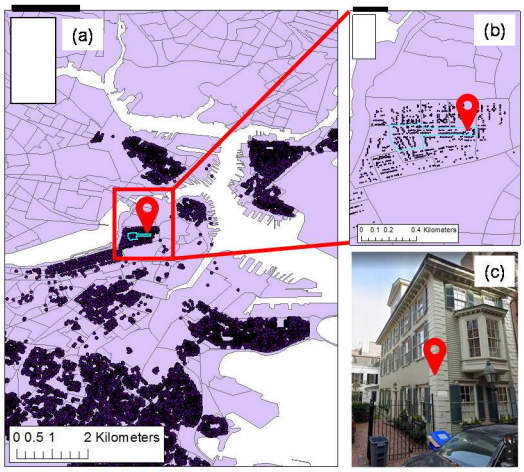

Figure C-8. (a) and (b) Geographical location of the selected typical residential building in the city of Boston; (c) street photo of the selected residential building

Table C-10. Building information of the selected typical residential building

U.S. Census ID	address	Cumulative solar energy generation	Number of floors	Living area	Number of family units	Building thermal resistance, K/W	Optimal HVAC air flow rate, kg/hour	Air Mass Inside Building, kg
250250 201014	17 PINCK NEY	5060.96	3	3428	1	0.00445	4878.2	956.8

Figure C-9. presents the outside, inside room temperatures, and HVAC consumption in a typical winter day and a typical summer day through the HVAC simulation. We found our simulated optimized HVAC system provides ideal thermal performance in terms of maintaining the inside building temperature in a comfort range.

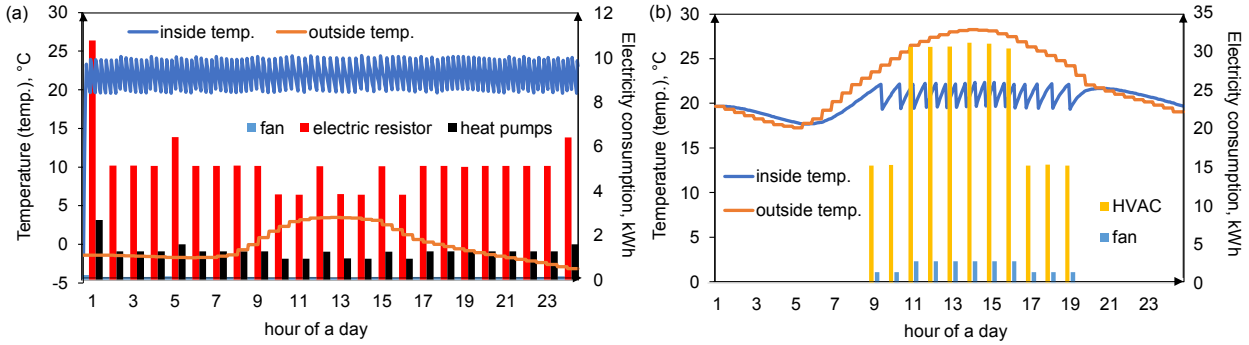

Figure C-9. Outside, inside room temperatures, and HVAC consumption in (a) a typical winter day and (b) a typical summer day

Figure C-10. presents the HVAC electricity consumption simulation results of the selected community over a year. Three types of HVAC systems were investigated under 100% HVAC adoption scenarios including air-conditioner coupled with electric resister heater system (AC-ER), heat pump (AC-HP), and fossil fuel-based heater system (AC-FF).

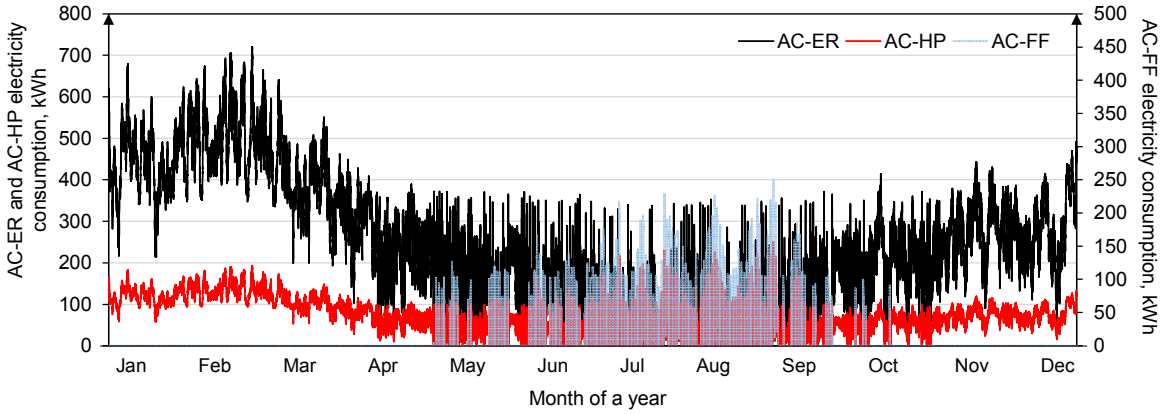

Figure C-10. Simulated annual HVAC electricity consumption of air-conditioner coupled with electric resister heater (AC-ER), heat pump (AC-HP), or fossil fuel-based heater (AC-FF) of the selected community using 30-minute time steps

Figure C-11. presents the HVAC electricity consumption of the simulated community over one year.

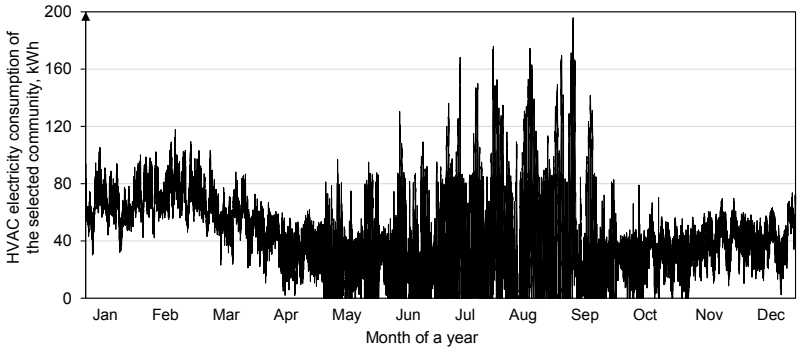

Figure C-11. Simulated HVAC electricity consumption pattern of the selected community using 30-minute time steps

Figure C-12. presents the simulated HVAC electricity consumption pattern of the selected community using daily time steps.

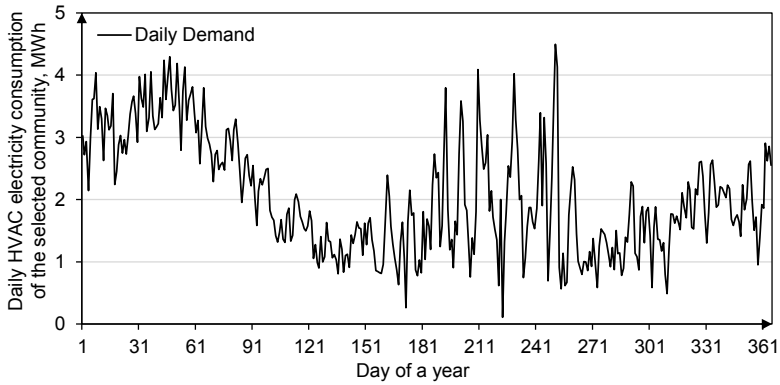

Figure C-12. Simulated HVAC electricity consumption pattern of the selected community using 30-minute time steps

Cold appliances simulation

Figure C-13. presents an example of a 1-day simulated profile of cold appliance energy consumption of one household in this study.

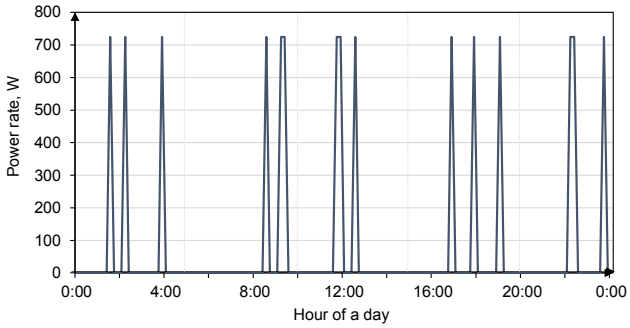

Figure C-13. A one-day energy consumption pattern of the simulated cold appliance

Behavior-related energy consumption simulation

Figure C-14. presents the simulated annual and typical daily behavior-related demand patterns of the selected community using thirty-minute time steps.

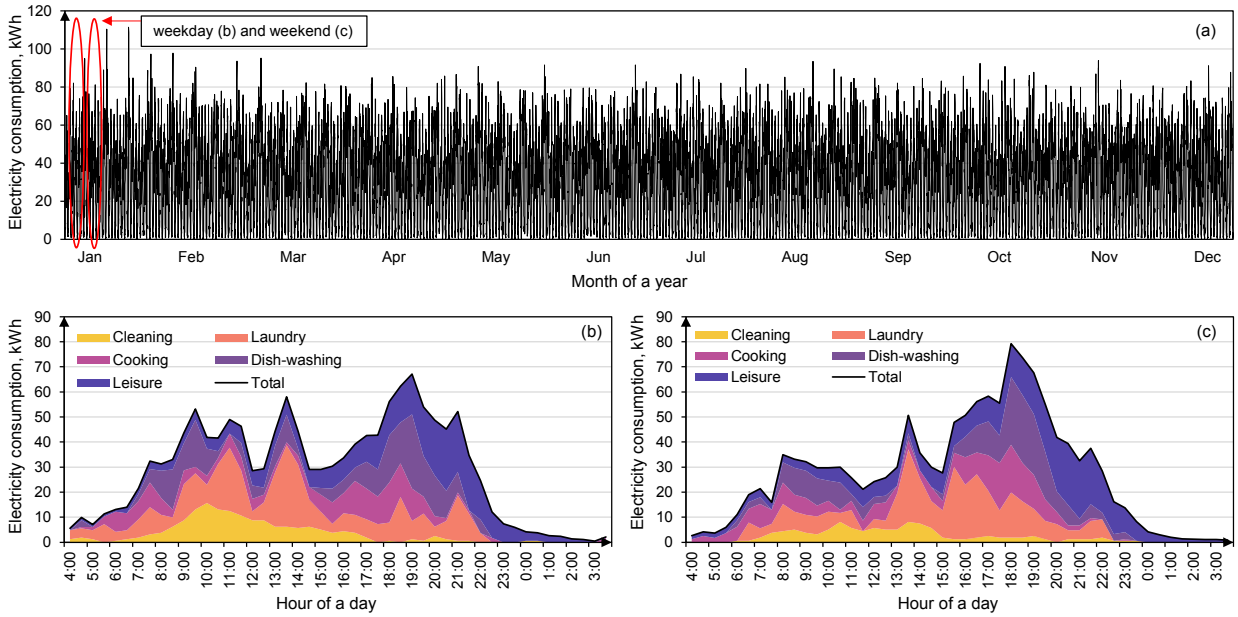

Figure C-14. Simulated behavior-related demand patterns of a year (a), a weekday (b), and a weekend (c) of the selected community using 30-minutes time steps

Figure C-15. presents the regression analysis results comparing the simulated results with the ATUS data.

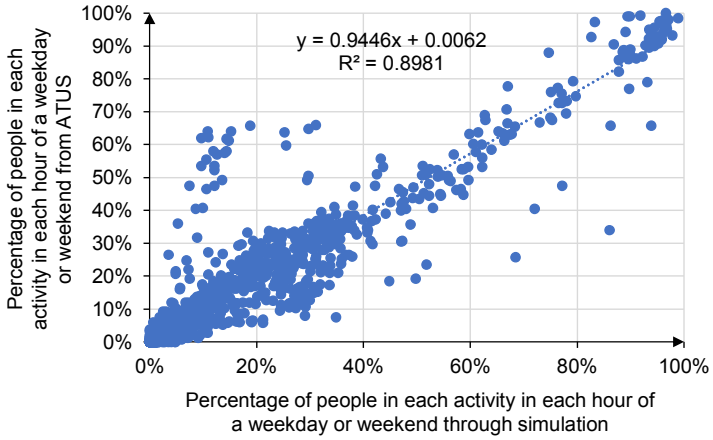

Figure C-15. Linear regression analysis results comparing the simulated activity results with the ATUS activity dataset

Figure C-16. presents simulated one-day activity profiles of five types of occupants in a weekday and a weekend day.

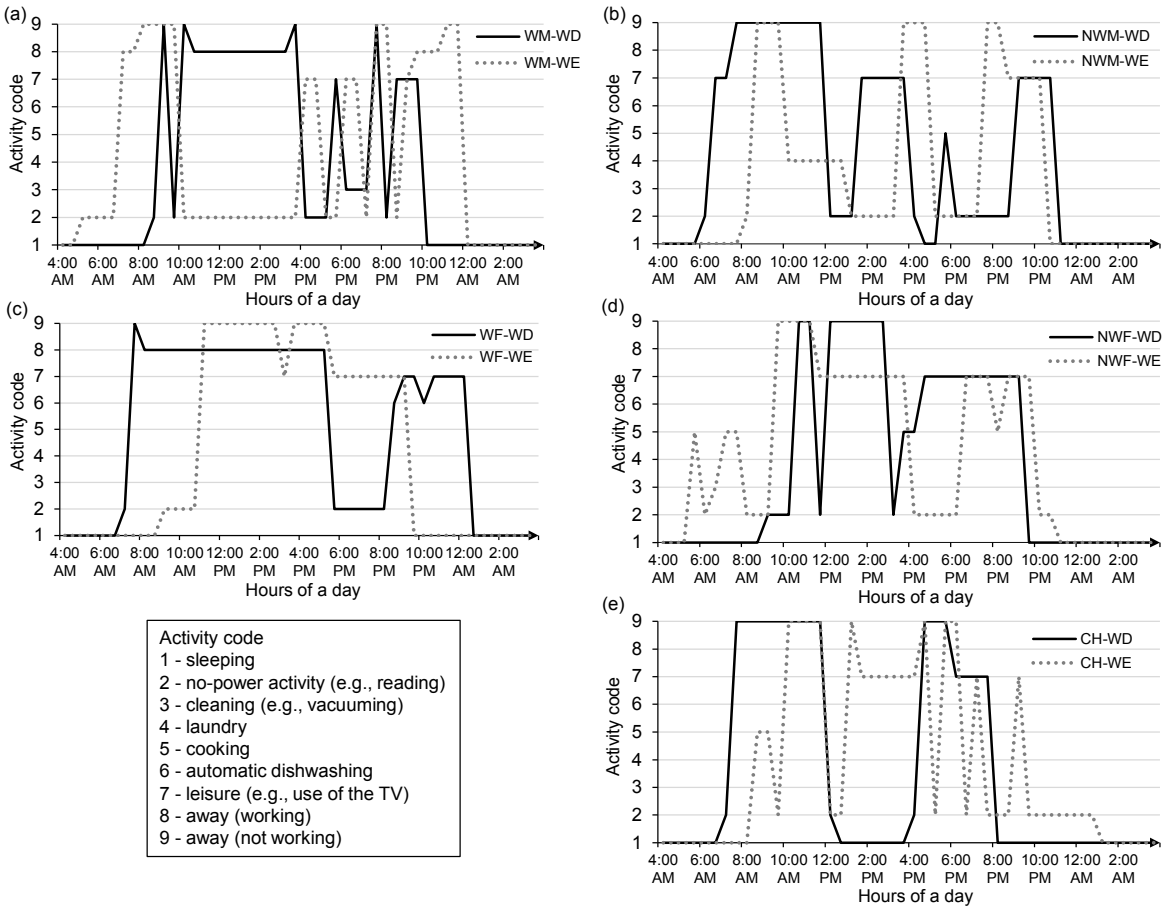

Figure C-16. Simulated one-day activity profiles of five types of occupants in a weekday and a weekend day

Lighting demand

Figure C-17. presents simulated one-day lighting electricity consumption patterns of the selected community in a typical weekday and a weekend day in January.

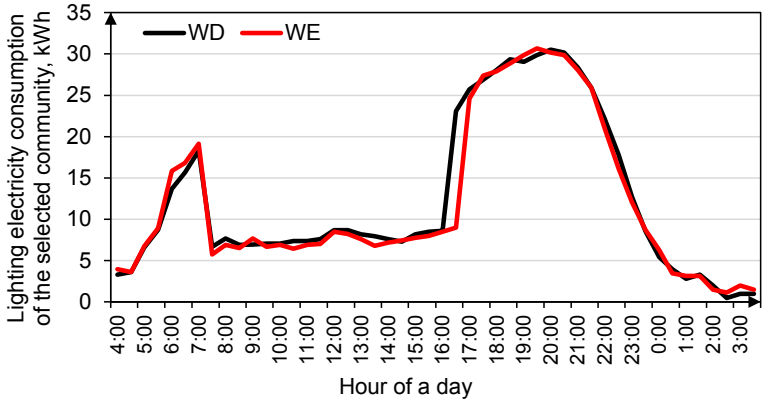

Figure C-17. Simulated daily lighting electricity consumption of a typical weekday (WD) and a weekend day (WE) in January of the selected community

Overall residential demand

Figure C-18. presents the simulated overall electricity demand of the selected community in a year (a), a typical weekday (b), and a weekend day (c) in January using thirty-minute time step.

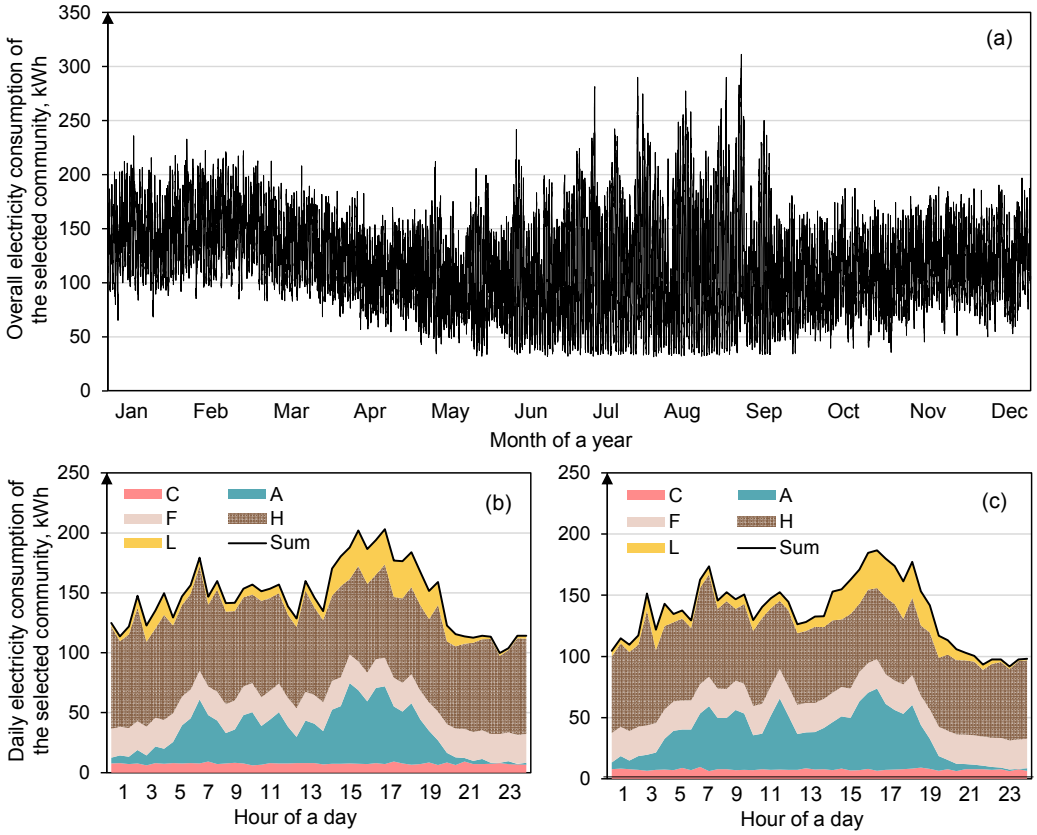

Figure C-18. Simulated overall electricity consumption of the selected community in a year (a), a January weekend day (b), and a January weekday (c)
("C"-cold appliance; "A"-power-related activity; "F"-constant use; "H"-HVAC; "L"-lighting; "Sum"-overall demand)

Figure C-19. presents the simulated overall electricity demand of the selected community in a year using daily time steps. We compared the simulated overall demand pattern with the ISO-NE reported residential demand patterns (Figure C-19. (b)). We found our simulation results could effectively represent the real reported data in terms of monthly average household electricity consumption and demand seasonality.

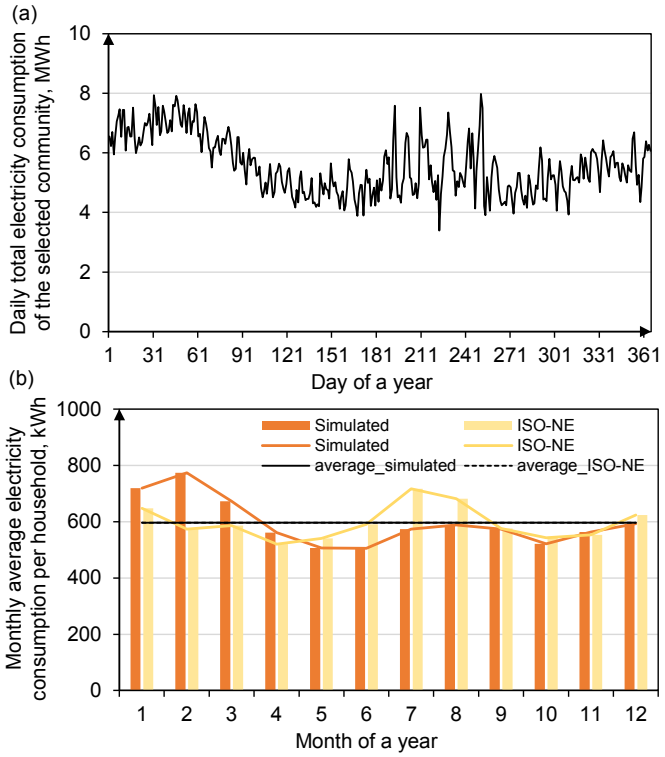

Figure C-19. Simulated overall electricity demand of the selected community in a year (a), a typical winter day (b), and a typical summer day (c)

Section C3.2. Additional technical, economic, and environmental results

Technical results

Additional technical results are presented in this section. Figure C-20. presents the load reductions and load reduction change rates of off-, mid-, and on-peak periods under different PV adoption percentages.

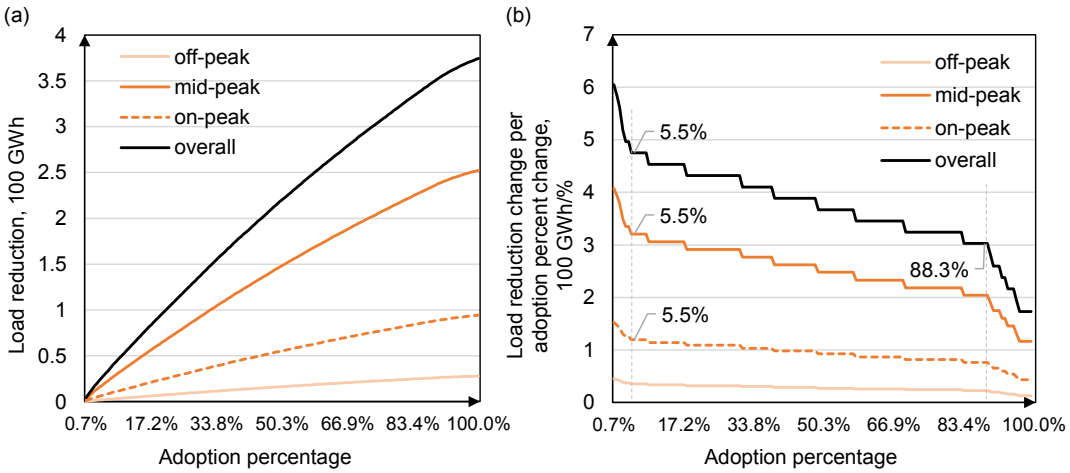

Figure C-20. Load reductions and load reduction change rates of off-, mid-, and on-peak periods under different PV adoption percentages

Figure C-21. presents the number of simulated residential buildings that installed PV systems and their grid use under different PV adoption percentages.

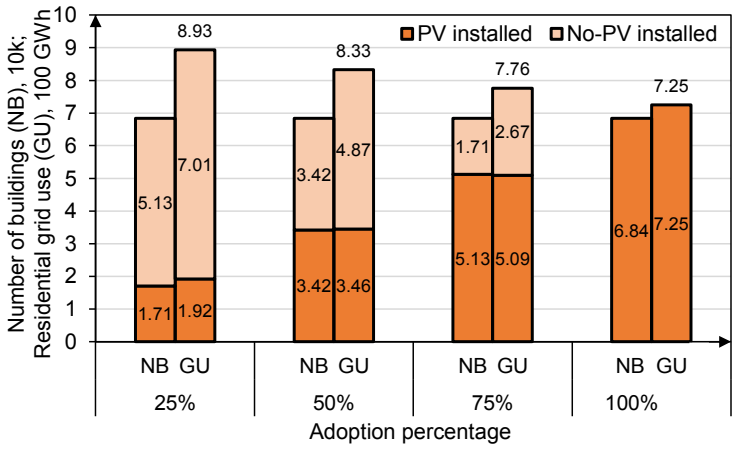

Figure C-21. Number of simulated residential buildings installed PV systems and their grid use under different PV adoption percentages

Figure C-22. presents the energy independence (reliance) indexes of off-, mid-, and on-peak periods under different PV adoption percentages.

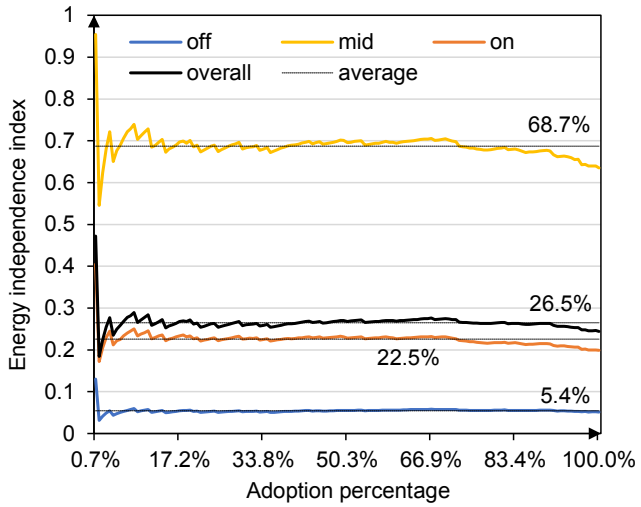

Figure C-22. Energy independence (reliance) indexes of off-, mid-, and on-peak periods under different PV adoption percentages

Economic results

Figure C-23. Operational cost savings and cost saving change rates of the net metering (NM) and wholesale (WS) price designs under different PV adoption percentages

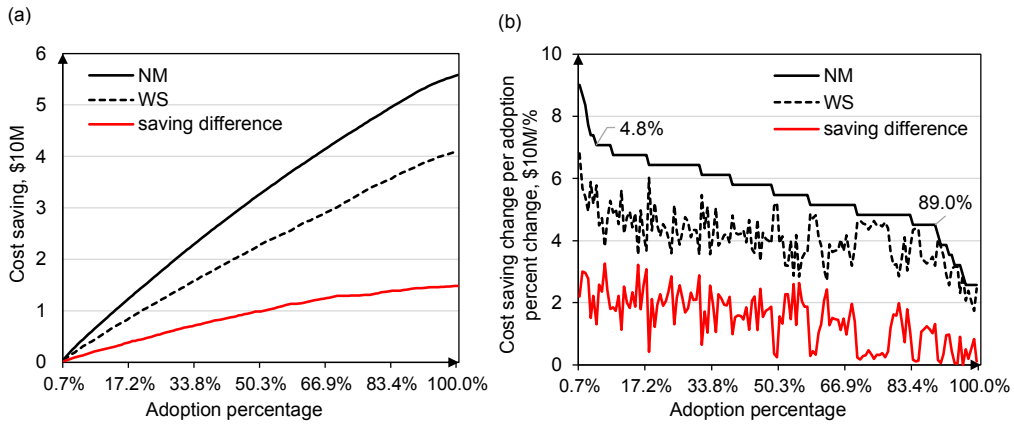

Figure C-23. Operational cost savings and cost saving change rates of the net metering (NM) and wholesale (WS) price designs under different PV adoption percentages

Figure C-24. presents the operational cost savings and wholesale load costs under different PV adoption percentages.

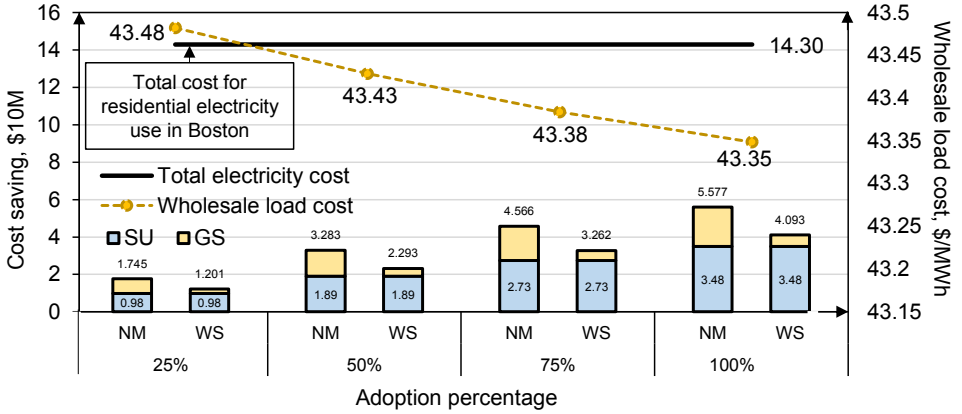

Figure C-24. Operational cost savings and wholesale load costs under different PV adoption percentages

Figure C-25. (a) presents the annual electricity costs and (b) presents the electricity costs per kWh of grid use for both PV-adopted and no-PV buildings under different PV adoption percentages. Annual electricity cost represents the electric bill of residential energy users in a year.

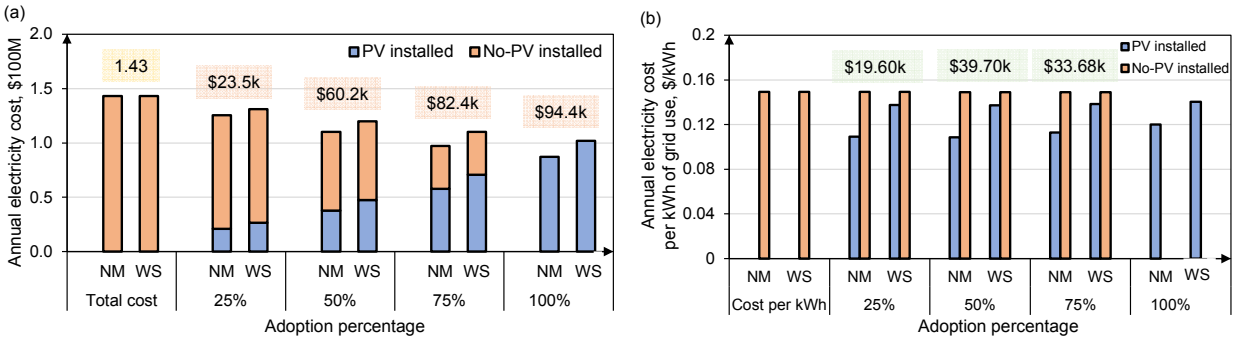

Figure C-25. (a) Annual electricity costs and (b) electricity costs per kWh of grid use for PV adopted and no-PV buildings under different PV adoption percentages

Figure C-26. presents the wholesale load costs in different months under 100% PV adoption simulation.

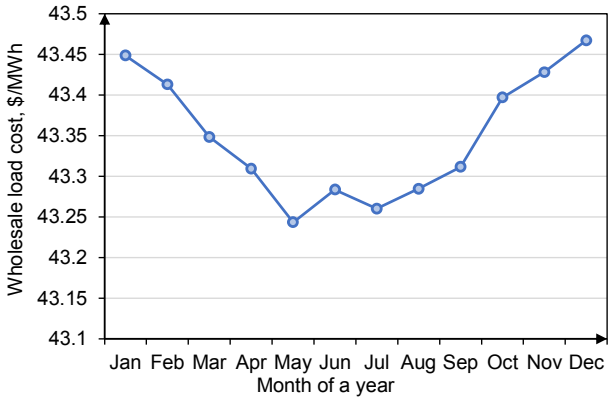

Figure C-26. Wholesale load costs in different months under 100% PV adoption

Table C-11. presents the annual electricity costs (electric utility bill) for both PV and No-PV energy users.

Table C-11. Annual electricity costs for PV and No-PV energy users, $100M

		PV installed	No-PV installed	Total
Total cost	NM	-	1.4300	1.4300
	NM*	-	1.4300	1.4300
	WS	-	1.4300	1.4300
	WS*	-	1.4300	1.4300
25%	NM	0.2100	1.0454	1.2554
	NM*	0.2100	1.0452	1.2552
	WS	0.2644	1.0454	1.3098
	WS*	0.2644	1.0452	1.3096
50%	NM	0.3755	0.7260	1.1015
	NM*	0.3753	0.7256	1.1009
	WS	0.4745	0.7260	1.2005
	WS*	0.4743	0.7256	1.1999
75%	NM	0.5753	0.3977	0.9730
	NM*	0.5748	0.3973	0.9721
	WS	0.7057	0.3977	1.1033
	WS*	0.7052	0.3973	1.1025
100%	NM	0.8717	-	0.8717
	NM*	0.8707	-	0.8707
	WS	1.0201	-	1.0201
	WS*	1.0191	-	1.0191

Table C-12. presents the annual electricity costs per kWh of grid use for both PV-installed and no-PV installed residential buildings.

Table C-12. Annual electricity cost per kWh of grid use, $/kWh

		PV installed	No-PV installed
Cost per kWh	NM	-	0.1491
	NM*	-	0.1491
	WS	-	0.1491
	WS*	-	0.1491
25%	NM	0.1092	0.1491
	NM*	0.1092	0.1491
	WS	0.1375	0.1491
	WS*	0.1374	0.1491
50%	NM	0.1087	0.1491
	NM*	0.1086	0.1490
	WS	0.1373	0.1491
	WS*	0.1372	0.1490
75%	NM	0.1130	0.1491
	NM*	0.1129	0.1490
	WS	0.1386	0.1491
	WS*	0.1385	0.1489
100%	NM	0.1202	-
	NM*	0.1201	-
	WS	0.1407	-
	WS*	0.1405	-

Environmental results

Figure C-27. presents the operational carbon savings and carbon benefit unit costs under different PV adoption percentages. The operational carbon saving was estimated using load reduction of PV adoption and the carbon emission impact unit of the ISO-NE grid mix (kg CO_2 eq./kWh). The carbon benefit unit cost was estimated using the annual saving of no-PV installed buildings (a decreasing electricity retail rate for the overall grid users due to the increasing PV adoption which lowers the wholesale electricity rate) divided by the total operational carbon saving by PV adopters (cent/kg CO_2 eq.). The annual saving of no-PV installed buildings under certain PV adoption percentage was estimated using the different of residential electricity costs under no PV adoption and that PV adoption percentage.

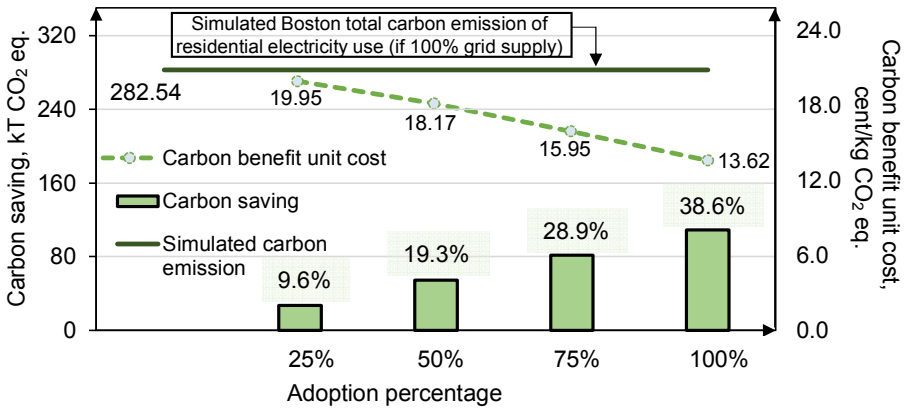

Figure C-27. Operational carbon savings and carbon benefit unit costs under different PV adoption percentages

Figure C-28. present (a) the daily carbon emission and (b) the monthly carbon emission of residential grid use over a year under different PV adoption percentages. Figure C-28. further shows the carbon emission of residential grid use (c) in a typical winter day and (d) a typical summer day under different PV adoptions percentages.

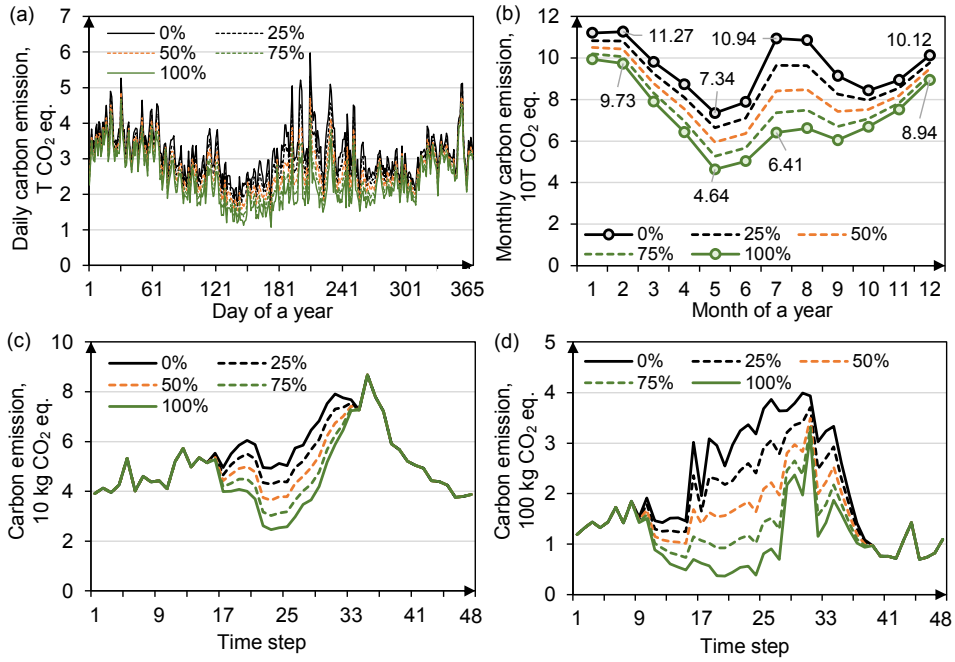

Figure C-28. (a) Daily carbon emission and (b) monthly carbon emission of residential grid use over a year under different PV adoption percentages; carbon emission of grid use (c) in a typical winter day and (d) a typical summer day under different PV adoptions

LIST OF REFERENCES

Abu-jasser, A., 2010. a Stand-Alone Photovoltaic System , Case Study : a Residence in Gaza. Appl. Sci. Environ. Sanit. 5, 81–91.

Adriana, C., Antošová, M., Andrea, S., Čulková, K., 2012. Economical Analysis of the Photovoltaic Systems - Case Study Slovakia. AASRI Procedia 2, 186–191. https://doi.org/10.1016/j.aasri.2012.09.033

Aghaei, J., Alizadeh, M.-I.I., 2013. Demand response in smart electricity grids equipped with renewable energy sources: A review. Renew. Sustain. Energy Rev. 18, 64–72. https://doi.org/10.1016/j.rser.2012.09.019

Agnew, S., Dargusch, P., 2015. Effect of residential solar and storage on centralized electricity supply systems. Nat. Clim. Chang. 5, 315–318. https://doi.org/10.1038/nclimate2523

Agnew, S., Smith, C., Dargusch, P., 2019. Understanding transformational complexity in centralized electricity supply systems: Modelling residential solar and battery adoption dynamics. Renew. Sustain. Energy Rev. 116, 109437. https://doi.org/10.1016/j.rser.2019.109437

Akinyele, D.O., Rayudu, R.K., 2016a. Comprehensive techno-economic and environmental impact study of a localised photovoltaic power system (PPS) for off-grid communities. Energy Convers. Manag. 124, 266–279. https://doi.org/10.1016/j.enconman.2016.07.022

Akinyele, D.O., Rayudu, R.K., 2016b. Techno-economic and life cycle environmental performance analyses of a solar photovoltaic microgrid system for developing countries. Energy 109, 160–179. https://doi.org/10.1016/j.energy.2016.04.061

Akinyele, D.O., Rayudu, R.K., Nair, N.K.C., 2017. Life cycle impact assessment of photovoltaic power generation from crystalline silicon-based solar modules in Nigeria. Renew. Energy 101, 537–549. https://doi.org/https://doi.org/10.1016/j.renene.2016.09.017

Alam, M.J.E., Muttaqi, K.M., Sutanto, D., 2016. Effective Utilization of Available PEV Battery Capacity for Mitigation of Solar PV Impact and Grid Support with Integrated V2G Functionality. IEEE Trans. Smart Grid 7, 1562–1571. https://doi.org/10.1109/TSG.2015.2487514

Alam, M.J.E., Muttaqi, K.M., Sutanto, D., 2014. A novel approach for ramp-rate control of solar PV using energy storage to mitigate output fluctuations caused by cloud passing. IEEE Trans. Energy Convers. 29, 507–518. https://doi.org/10.1109/TEC.2014.2304951

Alam, M.J.E., Muttaqi, K.M., Sutanto, D., 2013. Mitigation of rooftop solar PV impacts and evening peak support by managing available capacity of distributed energy storage systems. IEEE Trans. power Syst. 28, 3874–3884.

Albadi, M.H., El-Saadany, E.F., 2008. A summary of demand response in electricity markets. Electr. Power Syst. Res. 78, 1989–1996. https://doi.org/https://doi.org/10.1016/j.epsr.2008.04.002

Aleem, S.A., Suhail Hussain, S.M., Ustun, T.S., 2020. A review of strategies to increase PV penetration level in smart grids. Energies 13. https://doi.org/10.3390/en13030636

Allouhi, A., Saadani, R., Buker, M.S., Kousksou, T., Jamil, A., Rahmoune, M., 2019. Energetic, economic and environmental (3E) analyses and LCOE estimation of three technologies of PV grid-connected systems under different climates. Sol. Energy 178, 25–36. https://doi.org/10.1016/j.solener.2018.11.060

Allouhi, A., Saadani, R., Kousksou, T., Saidur, R., Jamil, A., Rahmoune, M., 2016. Grid-connected PV systems installed on institutional buildings: Technology comparison, energy

analysis and economic performance. Energy Build. 130, 188–201. https://doi.org/10.1016/j.enbuild.2016.08.054
Alramlawi, M., Gabash, A., Mohagheghi, E., Li, P., 2018. Optimal operation of hybrid PV-battery system considering grid scheduled blackouts and battery lifetime. Sol. Energy 161, 125–137. https://doi.org/10.1016/j.solener.2017.12.022
Alsema, E., 2012. Energy Payback Time and CO2 Emissions of PV Systems, Practical Handbook of Photovoltaics. Elsevier Ltd. https://doi.org/10.1016/B978-0-12-385934-1.00037-4
American Society of Heating, 2009. American Society of Heating, Refrigerating and Air-Conditioning Engineers, Inc., 2009 ASHRAE Handbook-Fundamentals, I-P edition [WWW Document]. URL https://www.academia.edu/39168321/Inch_Pound_Edition_2009_ASHRAE_HANDBOOK_FUNDAMENTALS
Antonanzas, J., Quinn, J.C., 2021. Net environmental impact of the PV industry from 2000-2025. J. Clean. Prod. 311, 127791. https://doi.org/10.1016/j.jclepro.2021.127791
Arcos-Vargas, A., Cansino, J.M., Román-Collado, R., 2018. Economic and environmental analysis of a residential PV system: A profitable contribution to the Paris agreement. Renew. Sustain. Energy Rev. 94, 1024–1035. https://doi.org/10.1016/j.rser.2018.06.023
Arghira, N., Hawarah, L., Ploix, S., Jacomino, M., 2012. Prediction of appliances energy use in smart homes. Energy 48, 128–134. https://doi.org/10.1016/j.energy.2012.04.010
Azzopardi, B., Mutale, J., 2010. Life cycle analysis for future photovoltaic systems using hybrid solar cells. Renew. Sustain. Energy Rev. 14, 1130–1134. https://doi.org/https://doi.org/10.1016/j.rser.2009.10.016
Battisti, R., Corrado, A., 2005. Evaluation of technical improvements of photovoltaic systems through life cycle assessment methodology. Energy 30, 952–967. https://doi.org/10.1016/j.energy.2004.07.011
Bazmi, A.A., Zahedi, G., 2011. Sustainable energy systems: Role of optimization modeling techniques in power generation and supply—A review. Renew. Sustain. Energy Rev. 15, 3480–3500. https://doi.org/https://doi.org/10.1016/j.rser.2011.05.003
Bellocchi, S., Manno, M., Noussan, M., Vellini, M., 2019. Impact of grid-scale electricity storage and electric vehicles on renewable energy penetration: A case study for Italy. Energies 12. https://doi.org/10.3390/en12071303
Bergerson, J., Lave, L., 2002. A life cycle analysis of electricity generation technologies. Heal. Environ. Implic. Altern. Fuels Technol.
Bernal-Agustín, J.L., Dufo-López, R., 2006. Economical and environmental analysis of grid connected photovoltaic systems in Spain. Renew. energy 31, 1107–1128. https://doi.org/10.1016/j.renene.2005.06.004
Bernardes, A.M., Espinosa, D.C.R., Tenório, J.A.S., 2004. Recycling of batteries: a review of current processes and technologies. J. Power Sources 130, 291–298. https://doi.org/https://doi.org/10.1016/j.jpowsour.2003.12.026
Berwal, A.K., Kumar, S., Kumari, N., Kumar, V., Haleem, A., 2017. Design and analysis of rooftop grid tied 50 kW capacity Solar Photovoltaic (SPV) power plant. Renew. Sustain. Energy Rev. 77, 1288–1299. https://doi.org/10.1016/j.rser.2017.03.017
Beylot, A., Payet, J.Ô., Puech, C., Adra, N., Jacquin, P., Blanc, I., Beloin-Saint-Pierre, D., 2014. Environmental impacts of large-scale grid-connected ground-mounted PV installations. Renew. Energy 61, 2–6. https://doi.org/10.1016/j.renene.2012.04.051

Bhandari, K.P., Collier, J.M., Ellingson, R.J., Apul, D.S., 2015. Energy payback time (EPBT) and energy return on energy invested (EROI) of solar photovoltaic systems: A systematic review and meta-analysis. Renew. Sustain. Energy Rev. 47, 133–141. https://doi.org/https://doi.org/10.1016/j.rser.2015.02.057

Bilich, A., Langham, K., Geyer, R., Goyal, L., Hansen, J., Krishnan, A., Bergesen, J., Sinha, P., 2017. Life cycle assessment of solar photovoltaic microgrid systems in off-grid communities. Environ. Sci. Technol. 51, 1043–1052. https://doi.org/10.1021/acs.est.6b05455

Blanc, I., Belloin-Saint-Pierre, D., Payet, J., Jacquin, P., Adra, N., Mayer, D., 2008. Espace-PV: Key Sensitive Parameters for Environmental Impacts of Grid-Connected PV Systems With LCA. 23rd Eur. Photovolt. Sol. Energy Conf. Exhib. 3779.

BLS, 2020. U.S. Bureau of Labor Statistics, Employment Projections, Civilian labor force participation rate by age, sex, race, and ethnicity [WWW Document]. URL https://www.bls.gov/emp/tables/civilian-labor-force-participation-rate.htm

Bortolini, M., Gamberi, M., Graziani, A., 2014. Technical and economic design of photovoltaic and battery energy storage system. Energy Convers. Manag. 86, 81–92. https://doi.org/10.1016/j.enconman.2014.04.089

Boulay, A.-M., Bare, J., Benini, L., Berger, M., Lathuillière, M.J., Manzardo, A., Margni, M., Motoshita, M., Núñez, M., Pastor, A.V., 2018. The WULCA consensus characterization model for water scarcity footprints: assessing impacts of water consumption based on available water remaining (AWARE). Int. J. Life Cycle Assess. 23, 368–378.

Branker, K, Pathak, M.J.M., Pearce, J.M., 2011. A review of solar photovoltaic levelized cost of electricity. Renew. Sustain. Energy Rev. 15, 4470–4482. https://doi.org/https://doi.org/10.1016/j.rser.2011.07.104

Branker, K., Pathak, M.J.M.M., Pearce, J.M., 2011. A review of solar photovoltaic levelized cost of electricity. Renew. Sustain. Energy Rev. 15, 4470–4482. https://doi.org/10.1016/j.rser.2011.07.104

Brown, M.A., Johnson, E., Matisoff, D., Staver, B., Beppler, R., 2016. Impacts of Solar Power on Electricity Rates and Bills. ACEEE Summer Study Energy Effic. Build. 6, 1–13.

Brown, P.R., O'Sullivan, F.M., 2019. Shaping photovoltaic array output to align with changing wholesale electricity price profiles. Appl. Energy 256, 113734. https://doi.org/10.1016/j.apenergy.2019.113734

Burns, J.E., Kang, J.-S.S., 2012. Comparative economic analysis of supporting policies for residential solar PV in the United States: Solar Renewable Energy Credit (SREC) potential. Energy Policy 44, 217–225. https://doi.org/10.1016/j.enpol.2012.01.045

Cai, D.W.H., Adlakha, S., Low, S.H., De Martini, P., Mani Chandy, K., 2013. Impact of residential PV adoption on Retail Electricity Rates. Energy Policy 62, 830–843. https://doi.org/10.1016/j.enpol.2013.07.009

Carter, N.T., 2014. Energy-water nexus: The energy sector's water use. Energy Water Sect. Interdepend. A Prim. 17–34.

Chandel, M., Agrawal, G.D., Mathur, S., Mathur, A., 2014. Techno-economic analysis of solar photovoltaic power plant for garment zone of Jaipur city. Case Stud. Therm. Eng. 2, 1–7. https://doi.org/10.1016/j.csite.2013.10.002

Chel, A., Tiwari, G.N., Chandra, A., 2009. Simplified method of sizing and life cycle cost assessment of building integrated photovoltaic system. Energy Build. 41, 1172–1180. https://doi.org/https://doi.org/10.1016/j.enbuild.2009.06.004

Cheng, D., Mather, B., Seguin, R., Hambrick, J., Broadwater, R.P., 2015. PV impact assessment for very high penetration levels. 2015 IEEE 42nd Photovolt. Spec. Conf. PVSC 2015 6, 295–300. https://doi.org/10.1109/PVSC.2015.7356170
Chesser, M., Hanly, J., Cassells, D., Apergis, N., 2018. The positive feedback cycle in the electricity market: Residential solar PV adoption, electricity demand and prices. Energy Policy 122, 36–44. https://doi.org/10.1016/j.enpol.2018.07.032
COB, 2019. Boston Maps Open Data Geospatial Datasets [WWW Document]. URL http://bostonopendata-boston.opendata.arcgis.com
Connolly, D., Lund, H., Mathiesen, B.V., Leahy, M., 2010. A review of computer tools for analysing the integration of renewable energy into various energy systems. Appl. Energy 87, 1059–1082.
Curry, C., 2017. Lithium-ion battery costs and market. Bloom. New Energy Financ. 5.
Darling, S.B., You, F., Veselka, T., Velosa, A., 2011. Assumptions and the levelized cost of energy for photovoltaics. Energy Environ. Sci. 4, 3133–3139.
De Souza, M.A., Farias, F.S., Costa, J.C.W.A., Cardoso, D.L., 2017. Technical Economic Analysis of Photovoltaic Systems in Heterogeneous Mobile Networks. Procedia Comput. Sci. 109, 825–832. https://doi.org/10.1016/j.procs.2017.05.346
Deltenre, Q., De Troyer, T., Runacres, M.C., 2020. Performance assessment of hybrid PV-wind systems on high-rise rooftops in the Brussels-Capital Region. Energy Build. 224, 110137. https://doi.org/10.1016/j.enbuild.2020.110137
Dergiades, T., Tsoulfidis, L., 2008. Estimating residential demand for electricity in the United States, 1965-2006. Energy Econ. 30, 2722–2730. https://doi.org/10.1016/j.eneco.2008.05.005
Devices—Part, P., 1AD. Measurement of Photovoltaic Current-Voltage Characteristics. CEI/IEC 60901–60904.
Diaf, S., Belhamel, M., Haddadi, M., Louche, A., 2008. Technical and economic assessment of hybrid photovoltaic/wind system with battery storage in Corsica island. Energy Policy 36, 743–754. https://doi.org/https://doi.org/10.1016/j.enpol.2007.10.028
Dincer, I., 2000. Renewable energy and sustainable development: a crucial review. Renew. Sustain. Energy Rev. 4, 157–175. https://doi.org/https://doi.org/10.1016/S1364-0321(99)00011-8
DOE, 2021. United States Department of Energy, Solar Energy Potential [WWW Document]. Natl. Renew. Energy Lab. URL https://www.energy.gov/maps/solar-energy-potential
Duffie, J.A., Beckman, W.A., 1991. Radiation characteristics of opaque materials. Sol. Eng. Therm. Process. 184.
Dufo-López, R., Bernal-Agustín, J.L., 2015. Techno-economic analysis of grid-connected battery storage. Energy Convers. Manag. 91, 394–404. https://doi.org/10.1016/j.enconman.2014.12.038
Durairaj, S.K., Ong, S.K., Nee, A.Y.C., Tan, R.B.H., 2002. Evaluation of life cycle cost analysis methodologies. Corp. Environ. Strateg. 9, 30–39. https://doi.org/10.1016/S1066-7938(01)00141-5
Edalati, S., Ameri, M., Iranmanesh, M., Tarmahi, H., Gholampour, M., 2016. Technical and economic assessments of grid-connected photovoltaic power plants: Iran case study. Energy 114, 923–934. https://doi.org/10.1016/j.energy.2016.08.041
Eftekharnejad, S., Vittal, V., Heydt, G.T., Keel, B., Loehr, J., 2013. Impact of increased penetration of photovoltaic generation on power systems. IEEE Trans. Power Syst. 28, 893–

901. https://doi.org/10.1109/TPWRS.2012.2216294
Eftekharnejad, S., Vittal, V., Heydt, G.T., Keel, B., Loehr, J., 2012. Impact of increased penetration of photovoltaic generation on power systems. IEEE Trans. power Syst. 28, 893–901.
EIA, 2021a. U.S. Energy Information Administration, Today in Energy, U.S. solar photovoltaic module shipments up 33% in 2020 [WWW Document]. URL https://www.eia.gov/todayinenergy/detail.php?id=49396
EIA, 2021b. U.S. Energy Information Administration, Electricity explained, Electricity generation, capacity, and sales in the United States [WWW Document]. URL https://www.eia.gov/energyexplained/electricity/electricity-in-the-us-generation-capacity-and-sales.php
EIA, 2020a. U.S. Energy Information Administration, Net Generation from Renewable Sources: Total (All Sectors), 2010-February 2020 [WWW Document]. URL https://www.eia.gov/electricity/monthly/epm_table_grapher.php?t=epmt_1_01_a
EIA, 2020b. EIA, U.S. Energy Information Administration, How is electricity used in U.S. homes? [WWW Document]. URL https://www.eia.gov/tools/faqs/faq.php?id=96&t=3
EIA, 2020c. EIA, U.S. Energy Information Administration, How much electricity does an American home use? [WWW Document]. URL https://www.eia.gov/tools/faqs/faq.php?id=97&t=3
EIA, 2020d. U.S. Energy Information Administration, Natural Gas, Natural Gas Monthly [WWW Document]. URL https://www.eia.gov/naturalgas/monthly/
EIA, 2020e. U.S. Energy Information Administration, Average Power Plant Operating Expenses for Major U.S. Investor-Owned Electric Utilities, 2009 through 2019 (Mills per Kilowatthour) [WWW Document]. URL https://www.eia.gov/electricity/annual/html/epa_08_04.html
EIA, 2019a. U.S. Energy Information Administration, Electricity explained, Electricity in the United States [WWW Document]. URL https://www.eia.gov/energyexplained/electricity/electricity-in-the-us.php
EIA, 2019b. U.S. Energy Information Administration, Electric Power Monthly [WWW Document]. URL https://www.eia.gov/electricity/monthly/epm_table_grapher.php?t=epmt_1_17_a
EIA, 2019c. U.S. Energy Information Administration, Electric Power Monthly [WWW Document]. URL https://www.eia.gov/electricity/monthly/#generation
EIA, 2019d. U.S. Energy Information Administration, Electric Power Annual [WWW Document]. URL https://www.eia.gov/electricity/annual/customersales-map3.php
EIA, 2018. U.S. Energy Information Administration, U.S. STATES, State Profiles and Energy Estimates [WWW Document]. URL https://www.eia.gov/state/rankings/?sid=US#/series/12
EIA, 2017. Institute for 21st Century Energy, U.S. CHAMBER OF COMMERCE, 2016 U.S. Average Electricity Retail Prices [WWW Document]. U.S. Energy Inf. Adm. Electr. Power Mon. 2017. URL https://www.globalenergyinstitute.org/sites/default/files/023162_EI21_AverageElectricRetail_Map_2016 Final.pdf
EIA, 2015a. EIA, U.S. Energy Information Administration, Use of energy explained, 2015 Residential Energy Consumption Survey [WWW Document]. URL https://www.eia.gov/energyexplained/use-of-energy/electricity-use-in-homes.php
EIA, 2015b. U.S. Energy Information Administration, Today in Energy [WWW Document].

URL https://www.eia.gov/todayinenergy/detail.php?id=23972
EIA, 2011. U.S. Energy Information Administration, Electricity demand changes in predictable patterns [WWW Document]. URL https://www.eia.gov/todayinenergy/detail.php?id=4190
EIA, 2010. U.S. Energy Information Administration, Annual energy review 2009, DOE/EIA-0384 edition, August.
EIA, 2009. Household Energy Use in Massachusetts [WWW Document]. URL https://www.eia.gov/consumption/residential/reports/2009/state_briefs/pdf/ma.pdf
Eid, C., Guillén, J.R., Marín, P.F., Hakvoort, R., 2014. The economic effect of electricity net-metering with solar PV: Consequences for network cost recovery, cross subsidies and policy objectives. Energy Policy 75, 244–254.
EL, 2021. Electricity Local, Boston Electricity Rates [WWW Document]. URL https://www.electricitylocal.com/states/massachusetts/boston/#ref
Elhodeiby, A.S., Metwally, H.M.B., Farahat, M.A., 2011. performance analysis of 3.6 kW roof top grid connected photovoltaic system in egypt, in: International Conference on Energy Systems and Technologies (ICEST 2011), Cairo, Egypt. pp. 11–14.
Eltawil, M.A., Zhao, Z., 2010. Grid-connected photovoltaic power systems: Technical and potential problems-A review. Renew. Sustain. Energy Rev. 14, 112–129. https://doi.org/10.1016/j.rser.2009.07.015
Energy, H., 2017. How HOMER Calculates the Maximum Battery Charge Power [WWW Document]. URL https://www.homerenergy.com/products/grid/docs/latest/how_homer_calculates_the_maximum_battery_charge_power.html
EnergySage, 2021. EnergySage, Eversource Net Metering [WWW Document].
EPA, 2019. United States Environmental Protection Agency, Electric Power Generation, Transmission and Distribution (NAICS 2211) [WWW Document]. URL https://www.epa.gov/regulatory-information-sector/electric-power-generation-transmission-and-distribution-naics-2211
Erdinc, O., 2014. Economic impacts of small-scale own generating and storage units, and electric vehicles under different demand response strategies for smart households. Appl. Energy 126, 142–150. https://doi.org/https://doi.org/10.1016/j.apenergy.2014.04.010
Espinosa, N., García-Valverde, R., Urbina, A., Krebs, F.C., 2011. A life cycle analysis of polymer solar cell modules prepared using roll-to-roll methods under ambient conditions. Sol. Energy Mater. Sol. Cells 95, 1293–1302. https://doi.org/10.1016/j.solmat.2010.08.020
Evans, A., Strezov, V., Evans, T.J., 2009. Assessment of sustainability indicators for renewable energy technologies. Renew. Sustain. Energy Rev. 13, 1082–1088. https://doi.org/https://doi.org/10.1016/j.rser.2008.03.008
Eversource, 2021. 2021 Summary of Eastern Massachusetts Electric Rates for Cambridge Service Area [WWW Document]. URL https://www.eversource.com/content/docs/default-source/rates-tariffs/ema-cambridge-rates.pdf?sfvrsn=c17ef362_48
Eversource, 2020. Net Metering [WWW Document]. URL https://www.eversource.com/content/ema-c/residential/save-money-energy/explore-alternatives/learn-about-solar-energy/net-metering
Eversource, 2018. Eversource, Massachusetts Application to Connect [WWW Document]. URL https://www.eversource.com/content/ct-c/about/about-us/doing-business-with-us/builders-contractors/interconnections/massachusetts-application-to-connect
Faiman, D., 2008. Assessing the outdoor operating temperature of photovoltaic modules. Prog.

Photovoltaics Res. Appl. 16, 307–315.
Fares, R.L., Webber, M.E., 2017. Reduce Reliance on the Utility. Nat. Energy 2. https://doi.org/10.1038/nenergy.2017.1
FERC, 2020. Federal Energy Regulatory Commission, News Media Contact : Craig Cano , mediadl@ferc.gov, Docket No . RM18-9-000 FERC Order No . 2222 : A New Day for Distributed Energy Resources.
Ford, A., Ford, F.A., 1999. Modeling the environment: an introduction to system dynamics models of environmental systems. Island press.
Forrester, J.W., 1997. Industrial dynamics. J. Oper. Res. Soc. 48, 1037–1041.
Freyman, T., 2021. How do you value a renewable energy project? [WWW Document]. URL https://www.ivsc.org/news/article/how-do-you-value-a-renewable-energy-project
Fthenakis, V., Kim, H.C., 2010a. Life-cycle uses of water in U.S. electricity generation. Renew. Sustain. Energy Rev. 14, 2039–2048. https://doi.org/10.1016/J.RSER.2010.03.008
Fthenakis, V., Kim, H.C., 2010b. Life-cycle uses of water in U.S. electricity generation. Renew. Sustain. Energy Rev. 14, 2039–2048. https://doi.org/10.1016/j.rser.2010.03.008
Fthenakis, V.M., Kim, H.C., 2011. Photovoltaics: Life-cycle analyses. Sol. Energy 85, 1609–1628. https://doi.org/10.1016/j.solener.2009.10.002
Fu, R., Margolis, R.M., Feldman, D.J., 2018. US Solar Photovoltaic System Cost Benchmark: Q1 2018. National Renewable Energy Lab.(NREL), Golden, CO (United States).
Gagnon, P., Margolis, R., Melius, J., Phillips, C., Elmore, R., 2016. Rooftop solar photovoltaic technical potential in the united states. A detailed assessment. National Renewable Energy Lab.(NREL), Golden, CO (United States).
García-Valverde, R., Miguel, C., Martínez-Béjar, R., Urbina, A., 2009. Life cycle assessment study of a 4.2 kWp stand-alone photovoltaic system. Sol. Energy 83, 1434–1445. https://doi.org/10.1016/j.solener.2009.03.012
García, M.C.A., Balenzategui, J.L., 2004. Estimation of photovoltaic module yearly temperature and performance based on nominal operation cell temperature calculations. Renew. energy 29, 1997–2010.
Gelazanskas, L., Gamage, K.A.A., 2014. Demand side management in smart grid: A review and proposals for future direction. Sustain. Cities Soc. 11, 22–30. https://doi.org/10.1016/j.scs.2013.11.001
Gerbinet, S., Belboom, S., Léonard, A., 2014. Life Cycle Analysis (LCA) of photovoltaic panels: A review. Renew. Sustain. Energy Rev. 38, 747–753. https://doi.org/10.1016/j.rser.2014.07.043
Grant, C.A., Hicks, A.L., 2020. Effect of manufacturing and installation location on environmental impact payback time of solar power. Clean Technol. Environ. Policy 22, 187–196.
Grinenko, T., 2018. Solar Panel Recycling 101 [WWW Document]. URL https://www.renvu.com/Learn/Solar-Panel-Recycling-101
Gürtürk, M., 2019. Economic feasibility of solar power plants based on PV module with levelized cost analysis. Energy 171, 866–878. https://doi.org/10.1016/j.energy.2019.01.090
Haider, H.T., See, O.H., Elmenreich, W., 2016. A review of residential demand response of smart grid. Renew. Sustain. Energy Rev. 59, 166–178. https://doi.org/10.1016/j.rser.2016.01.016
Heeter, J., Gelman, R., Bird, L., 2014. Status of net metering: Assessing the potential to reach program caps. National Renewable Energy Lab.(NREL), Golden, CO (United States).

Hegedus, S., Luque, A., 2010. Achievements and challenges of solar electricity from photovoltaics. Handb. Photovolt. Sci. Eng. 1–38.
Herter, K., McAuliffe, P., Rosenfeld, A., 2007. An exploratory analysis of California residential customer response to critical peak pricing of electricity. Energy 32, 25–34.
Herter, K., Wayland, S., 2010. Residential response to critical-peak pricing of electricity: California evidence. Energy 35, 1561–1567.
Hiremath, M., Derendorf, K., Vogt, T., 2015. Comparative life cycle assessment of battery storage systems for stationary applications. Environ. Sci. Technol. 49, 4825–4833. https://doi.org/10.1021/es504572q
Hirst, E., 1978. A model of residential energy use. Simulation 30, 69–74. https://doi.org/10.1177/003754977803000301
Hofierka, J., Kaňuk, J., 2009. Assessment of photovoltaic potential in urban areas using open-source solar radiation tools. Renew. Energy 34, 2206–2214. https://doi.org/10.1016/j.renene.2009.02.021
HomeAdvisor, I., 2019. 2019 Solar Panel Cost Guide, Home Solar System Installation Prices [WWW Document]. URL https://www.homeadvisor.com/cost/heating-and-cooling/install-solar-panels/
HOMER, 2018. HOMER Energy, HOMER Pro 3.11 [WWW Document]. URL https://www.homerenergy.com/products/pro/docs/3.11/index.html
HOMER, 2017. HOMER Energy, HOMER Grid 1.1 [WWW Document]. URL https://www.homerenergy.com/products/grid/docs/1.1/index.html
Hondo, H., 2005. Life cycle GHG emission analysis of power generation systems: Japanese case. Energy 30, 2042–2056. https://doi.org/https://doi.org/10.1016/j.energy.2004.07.020
Hong, T., Lee, M., Koo, C., Jeong, K., Kim, J., 2017. Development of a method for estimating the rooftop solar photovoltaic (PV) potential by analyzing the available rooftop area using Hillshade analysis. Appl. Energy 194, 320–332. https://doi.org/10.1016/j.apenergy.2016.07.001
Hopper, N., Goldman, C., Neenan, B., 2006. Demand Response from Day-Ahead Hourly Pricing for Large Customers. Electr. J. 19, 52–63. https://doi.org/https://doi.org/10.1016/j.tej.2006.02.002
Hosenuzzaman, M., Rahim, N.A., Selvaraj, J., Hasanuzzaman, M., Malek, A.B.M.A., Nahar, A., 2015. Global prospects, progress, policies, and environmental impact of solar photovoltaic power generation. Renew. Sustain. Energy Rev. 41, 284–297. https://doi.org/10.1016/j.rser.2014.08.046
Hsu, C.-W.W., 2012. Using a system dynamics model to assess the effects of capital subsidies and feed-in tariffs on solar PV installations. Appl. Energy 100, 205–217. https://doi.org/https://doi.org/10.1016/j.apenergy.2012.02.039
Huang, B., Zhao, J., Chai, J., Xue, B., Zhao, F., Wang, X., 2017. Environmental influence assessment of China's multi-crystalline silicon (multi-Si) photovoltaic modules considering recycling process. Sol. Energy 143, 132–141. https://doi.org/10.1016/j.solener.2016.12.038
Huang, H., Cai, Y., Xu, H., Yu, H., 2017. A multiagent minority-game-based demand-response management of smart buildings toward peak load reduction. IEEE Trans. Comput. Des. Integr. Circuits Syst. 36, 573–585. https://doi.org/10.1109/TCAD.2016.2571847
Imam, A.A., Al-Turki, Y.A., Sreerama Kumar, R., 2020. Techno-economic feasibility assessment of grid-connected PV systems for residential buildings in Saudi Arabia-A case study. Sustain. 12. https://doi.org/10.3390/su12010262

IRENA, 2019. International Renewable Energy Agency, Behind-The-Meter Batteries, Innovation Landscape Brief.
IRS, 2019. U.S. Internal Revenue Service, Residential Renewable Energy Tax Credit [WWW Document]. URL https://www.energy.gov/savings/residential-renewable-energy-tax-credit
ISO-NE, 2020a. ISO-New England, Markets and Operations, Market Performance, Load Costs [WWW Document]. URL https://www.iso-ne.com/markets-operations/market-performance/load-costs/?publish-date=[2015-11-01T00:00:00Z TO 2020-11-01T23:59:59Z]&document-type=Load Cost Components
ISO-NE, 2020b. ISO-New England, Wholesale Load Cost Estimator [WWW Document]. URL https://www.iso-ne.com/markets-operations/market-performance/load-costs/wholesale-electricty-cost-estimator
ISO-NE, 2020c. ISO-New England, Markets and Operations, ISO Express, Energy, Load, and Demand Reports [WWW Document]. URL https://www.iso-ne.com/isoexpress/web/reports/load-and-demand/-/tree/whlsecost-hourly-system
ISO-NE, 2020d. ISO-New England, Operations Reports, Dispatch Fuel Mix [WWW Document]. URL https://www.iso-ne.com/isoexpress/web/reports/operations/-/tree/gen-fuel-mix
ISO-NE, 2020e. ISO-New England, Operations Reports, Daily Generation by Fuel Type [WWW Document]. URL https://www.iso-ne.com/isoexpress/web/reports/operations/-/tree/daily-gen-fuel-type
ISO-NE, 2018a. ISO-New England, Energy, Load, and Demand Reports [WWW Document]. URL https://www.iso-ne.com/isoexpress/web/reports/load-and-demand/-/tree/net-ener-peak-load
ISO-NE, 2018b. ISO New England, Energy, Load, and Demand Reports [WWW Document]. URL https://www.iso-ne.com/isoexpress/web/reports/load-and-demand/-/tree/net-ener-peak-load
Ito, M., Kato, K., Komoto, K., Kichimi, T., Kurokawa, K., 2008. A comparative study on cost and life-cycle analysis for 100 MW very large-scale PV (VLS-PV) systems in deserts using m-Si, a-Si, CdTe, and CIS modules. Prog. Photovoltaics Res. Appl. 16, 17–30.
Ito, M., Kudo, M., Nagura, M., Kurokawa, K., 2011. A comparative study on life cycle analysis of 20 different PV modules installed at the Hokuto mega-solar plant. Prog. Photovoltaics Res. Appl. 19, 878–886.
Jenniches, S., Worrell, E., 2019. Regional economic and environmental impacts of renewable energy developments: Solar PV in the Aachen Region. Energy Sustain. Dev. 48, 11–24. https://doi.org/10.1016/j.esd.2018.10.004
Jeong, Y.-C., Lee, E.-B., Alleman, D., 2019. Reducing voltage volatility with step voltage regulators: A life-cycle cost analysis of Korean solar photovoltaic distributed generation. Energies 12, 652.
Jonas Tornberg, L.T.A., 2012. A GIS energy model for the building stock of Goteborg Jonas.
Jones, C., Peshev, V., Gilbert, P., Mander, S., 2018. Battery storage for post-incentive PV uptake? A financial and life cycle carbon assessment of a non-domestic building. J. Clean. Prod. 167, 447–458. https://doi.org/10.1016/j.jclepro.2017.08.191
Jungbluth, N., Bauer, C., Dones, R., Frischknecht, R., 2005. Life cycle assessment for emerging technologies: Case studies for photovoltaic and wind power. Int. J. Life Cycle Assess. 10, 24–34. https://doi.org/10.1065/lca2004.11.181.3
Jungbluth, N., Tuchschmid, M., de Wild-Scholten, M., 2008. Life Cycle Assessment of Photovoltaics: update of ecoinvent data V2. 0. ESU-services Ltd.

Jurasz, J., Ceran, B., Orłowska, A., 2020. Component degradation in small-scale off-grid PV-battery systems operation in terms of reliability, environmental impact and economic performance. Sustain. Energy Technol. Assessments 38, 100647. https://doi.org/10.1016/j.seta.2020.100647

Kannan, R., Leong, K.C., Osman, R., Ho, H.K., Tso, C.P., 2006. Life cycle assessment study of solar PV systems: An example of a 2.7 kW(p) distributed solar PV system in Singapore. Sol. Energy 80, 555–563. https://doi.org/10.1016/j.solener.2005.04.008

Karami, H., Sanjari, M.J., Hosseinian, S.H., Gharehpetian, G.B., 2014. An optimal dispatch algorithm for managing residential distributed energy resources. IEEE Trans. Smart Grid 5, 2360–2367.

Kaundinya, D.P., Balachandra, P., Ravindranath, N.H., 2009. Grid-connected versus stand-alone energy systems for decentralized power—A review of literature. Renew. Sustain. Energy Rev. 13, 2041–2050. https://doi.org/https://doi.org/10.1016/j.rser.2009.02.002

Kazem, H.A., Albadi, M.H., Al-Waeli, A.H.A., Al-Busaidi, A.H., Chaichan, M.T., 2017. Techno-economic feasibility analysis of 1MW photovoltaic grid connected system in Oman. Case Stud. Therm. Eng. 10, 131–141. https://doi.org/10.1016/j.csite.2017.05.008

Khalilpour, R., Vassallo, A., 2016. Planning and operation scheduling of PV-battery systems: A novel methodology. Renew. Sustain. Energy Rev. 53, 194–208. https://doi.org/10.1016/j.rser.2015.08.015

Khoury, J., Mbayed, R., Salloum, G., Monmasson, E., 2016. Design and implementation of a real time demand side management under intermittent primary energy source conditions with a PV-battery backup system. Energy Build. 133, 122–130. https://doi.org/10.1016/j.enbuild.2016.09.036

Kim, H., Cha, K., Fthenakis, V.M., Sinha, P., Hur, T., 2014. Life cycle assessment of cadmium telluride photovoltaic (CdTe PV) systems. Sol. Energy 103, 78–88. https://doi.org/https://doi.org/10.1016/j.solener.2014.02.008

Klass, D.L., 1998. Biomass for renewable energy, fuels, and chemicals. Elsevier.

Koehl, M., Heck, M., Wiesmeier, S., Wirth, J., 2011. Modeling of the nominal operating cell temperature based on outdoor weathering. Sol. Energy Mater. Sol. Cells 95, 1638–1646.

Köntges, M., Altmann, S., Heimberg, T., Jahn, U., Berger, K.A., 2016. Mean degradation rates in PV systems for various kinds of PV module failures, in: Proc. of the 32nd European Photovoltaic Solar Energy Conference and Exhibition, München: WIP. pp. 1435–1443.

Korsavi, S.S., Zomorodian, Z.S., Tahsildoost, M., 2018. Energy and economic performance of rooftop PV panels in the hot and dry climate of Iran. J. Clean. Prod. 174, 1204–1214. https://doi.org/10.1016/j.jclepro.2017.11.026

Kottek, M., Grieser, J., Beck, C., Rudolf, B., Rubel, F., 2006. World map of the Köppen-Geiger climate classification updated. Meteorol. Zeitschrift 15, 259–263.

Kreith, F., Norton, P., Brown, D., 1990. A comparison of CO2 emissions from fossil and solar power plants in the United States. Energy 15, 1181–1198. https://doi.org/10.1016/0360-5442(90)90110-N

Kumar, S., Tiwari, G.N., 2009. Life cycle cost analysis of single slope hybrid (PV/T) active solar still. Appl. Energy 86, 1995–2004. https://doi.org/10.1016/j.apenergy.2009.03.005

Lai, C.S., McCulloch, M.D., 2017. Levelized cost of electricity for solar photovoltaic and electrical energy storage. Appl. Energy 190, 191–203. https://doi.org/10.1016/j.apenergy.2016.12.153

Laleman, R., Albrecht, J., Dewulf, J., 2011. Life Cycle Analysis to estimate the environmental

impact of residential photovoltaic systems in regions with a low solar irradiation. Renew. Sustain. Energy Rev. 15, 267–281. https://doi.org/https://doi.org/10.1016/j.rser.2010.09.025
Lamnatou, C., Baig, H., Chemisana, D., Mallick, T.K., 2016. Environmental assessment of a building-integrated linear dielectric-based concentrating photovoltaic according to multiple life-cycle indicators. J. Clean. Prod. 131, 773–784. https://doi.org/10.1016/j.jclepro.2016.04.094
Larsen, M.A.D., Drews, M., 2019. Water use in electricity generation for water-energy nexus analyses: The European case. Sci. Total Environ. 651, 2044–2058. https://doi.org/10.1016/j.scitotenv.2018.10.045
Lazzeroni, P., Olivero, S., Stirano, F., Repetto, M., 2015. Impact of PV penetration in a distribution grid: A Middle-East study case. 2015 IEEE 1st Int. Forum Res. Technol. Soc. Ind. RTSI 2015 - Proc. 353–358. https://doi.org/10.1109/RTSI.2015.7325123
Leckner, M., Zmeureanu, R., 2011. Life cycle cost and energy analysis of a Net Zero Energy House with solar combisystem. Appl. Energy 88, 232–241. https://doi.org/10.1016/j.apenergy.2010.07.031
Lee, M., Hong, T., Jeong, K., Kim, J., 2018a. A bottom-up approach for estimating the economic potential of the rooftop solar photovoltaic system considering the spatial and temporal diversity. Appl. Energy 232, 640–656. https://doi.org/10.1016/j.apenergy.2018.09.176
Lee, M., Hong, T., Jeong, K., Kim, J., 2018b. A bottom-up approach for estimating the economic potential of the rooftop solar photovoltaic system considering the spatial and temporal diversity. Appl. Energy 232, 640–656. https://doi.org/10.1016/j.apenergy.2018.09.176
Legere, L., 2016. Government Technology, Pennsylvania PUC Drops Net-Metering Cap for Alternate Energy Users [WWW Document]. URL https://www.govtech.com/fs/Pennsylvania-PUC-Drops-Net-Metering-Cap-for-Alternate-Energy-Users.html
Li, C., Zhou, D., Zheng, Y., 2018. Techno-economic comparative study of grid-connected PV power systems in five climate zones, China. Energy 165, 1352–1369. https://doi.org/10.1016/j.energy.2018.10.062
Li, H., Yi, H., 2014. Multilevel governance and deployment of solar PV panels in U.S. cities. Energy Policy 69, 19–27. https://doi.org/10.1016/j.enpol.2014.03.006
Linssen, J., Stenzel, P., Fleer, J., 2017. Techno-economic analysis of photovoltaic battery systems and the influence of different consumer load profiles. Appl. Energy 185, 2019–2025. https://doi.org/10.1016/j.apenergy.2015.11.088
Litjens, G.B.M.A., Worrell, E., van Sark, W.G.J.H.M., 2018. Lowering greenhouse gas emissions in the built environment by combining ground source heat pumps, photovoltaics and battery storage. Energy Build. 180, 51–71. https://doi.org/10.1016/j.enbuild.2018.09.026
Liu, W.H., Alwi, S.R.W., Hashim, H., Muis, Z.A., Klemeš, J.J., Rozali, N.E.M., Lim, J.S., Ho, W.S., 2017. Optimal design and sizing of integrated centralized and decentralized energy systems. Energy Procedia 105, 3733–3740.
Liu, W.H., Ho, W.S., Lee, M.Y., Hashim, H., Lim, J.S., Klemeš, J.J., Mah, A.X.Y., 2019. Development and optimization of an integrated energy network with centralized and decentralized energy systems using mathematical modelling approach. Energy 183, 617–629.
Llc, T., 2003. Matching the Sensible Heat Ratio of Air Conditioning Equipment with the Building Load SHR. Analysis.

Lopes, J.A.P., Hatziargyriou, N., Mutale, J., Djapic, P., Jenkins, N., 2007. Integrating distributed generation into electric power systems: A review of drivers, challenges and opportunities. Electr. power Syst. Res. 77, 1189–1203.
M. Raugei, M.S.. F.R.I.P.S.M. de W.-S.J.Z.V.F.H.C.K., 2015. Life Cycle Inventories and Life Cycle Assessments of Photovoltaic Systems Life Cycle Inventories and Life Cycle Assessments of Photovoltaic Systems.
Macknick, J., Newmark, R., Heath, G., Hallett, K.C., 2011. A Review of Operational Water Consumption and Withdrawal Factors for Electricity Generating Technologies. Natl. Renew. Energy Lab. 7, 275–3000. https://doi.org/10.1088/1748-9326/7/4/045802
Manwell, J.F., McGowan, J.G., 1993. Lead acid battery storage model for hybrid energy systems. Sol. Energy 50, 399–405.
Maps, G., 2020. 17 Pinckney St, Google Maps/Google Earth [WWW Document]. URL https://www.google.com/maps/place/17+Pinckney+St,+Boston,+MA+02114/@42.3588378,-71.0658112,3a,75y,26.89h,90t/data=!3m6!1e1!3m4!1sO1SyfECguQHcrmrbt058nA!2e0!7i16384!8i8192!4m5!3m4!1s0x89e3709b91ffc6fd:0x486d85e4e77c5aa6!8m2!3d42.3589645!4d-71.0657247
Mariaud, A., Acha, S., Ekins-Daukes, N., Shah, N., Markides, C.N., 2017. Integrated optimisation of photovoltaic and battery storage systems for UK commercial buildings. Appl. Energy 199, 466–478. https://doi.org/10.1016/j.apenergy.2017.04.067
Martins, R., Hesse, H.C., Jungbauer, J., Vorbuchner, T., Musilek, P., 2018. Optimal component sizing for peak shaving in battery energy storage system for industrial applications. Energies 11. https://doi.org/10.3390/en11082048
Mason, J.E., Fthenakis, V.M., Hansen, T., Kim, H.C., 2006. Energy payback and life-cycle CO2 emissions of the BOS in an optimized 3.5MW PV installation. Prog. Photovoltaics Res. Appl. 14, 179–190. https://doi.org/10.1002/pip.652
Mass.gov, 2021. Mass.gov, Program Summaries, Summaries of all the Renewable and Alternative Energy Portfolio Standard programs [WWW Document]. URL https://www.mass.gov/service-details/program-summaries
Mass.gov, 2020a. 2020 Commonwealth of Massachusetts, Energy Storage Initiative [WWW Document]. URL https://www.mass.gov/energy-storage-initiative
Mass.gov, 2020b. Commonwealth of Massachusetts, Net Metering Guide [WWW Document]. URL https://www.mass.gov/guides/net-metering-guide
Mass.gov, 2018. Mass.gov, How Massachusetts Households Heat Their Homes [WWW Document]. URL https://www.mass.gov/service-details/how-massachusetts-households-heat-their-homes
MassCEC, 2020. Massachusetts Clean Energy Center, Solar Electricity, Incentives and Programs [WWW Document]. URL https://www.masscec.com/solar-incentives-and-programs
McAvoy, S., Grant, T., Smith, C., Bontinck, P., 2021. Combining Life Cycle Assessment and System Dynamics to improve impact assessment: A systematic review. J. Clean. Prod. 315, 128060. https://doi.org/10.1016/j.jclepro.2021.128060
McFarland, E.W., 2014. Solar energy: setting the economic bar from the top-down. Energy Environ. Sci. 7, 846–854.
McHenry, M.P., Johnson, J., Hightower, M., 2016. Why Do Electricity Policy and Competitive Markets Fail to Use Advanced PV Systems to Improve Distribution Power Quality? J. Sol. Energy 2016, 1–10. https://doi.org/10.1155/2016/5187317

Meier, P.J., 2002. Life-cycle assessment of electricity generation systems and applications for climate change policy analysis.
Meldrum, J., Nettles-Anderson, S., Heath, G., Macknick, J., 2013. Life cycle water use for electricity generation: a review and harmonization of literature estimates. Environ. Res. Lett. 8, 15031.
Melius, J., Margolis, R., Ong, S., 2013. Estimating Rooftop Suitability for PV : A Review of Methods , Patents , and Validation Techniques. NREL Tech. Rep. 35.
Muhammad-Sukki, F., Abu-Bakar, S.H., Munir, A.B., Mohd Yasin, S.H., Ramirez-Iniguez, R., McMeekin, S.G., Stewart, B.G., Sarmah, N., Mallick, T.K., Abdul Rahim, R., Karim, M.E., Ahmad, S., Mat Tahar, R., 2014. Feed-in tariff for solar photovoltaic: The rise of Japan. Renew. Energy 68, 636–643. https://doi.org/10.1016/J.RENENE.2014.03.012
Mukwekwe, L., Venugopal, C., Davidson, I.E., 2017. A review of the impacts and mitigation strategies of high PV penetration in low voltage networks. Proc. - 2017 IEEE PES-IAS PowerAfrica Conf. Harnessing Energy, Inf. Commun. Technol. Afford. Electrif. Africa, PowerAfrica 2017 274–279. https://doi.org/10.1109/PowerAfrica.2017.7991236
Muñoz-García, M.A., Marin, O., Alonso-García, M.C., Chenlo, F., 2012. Characterization of thin film PV modules under standard test conditions: Results of indoor and outdoor measurements and the effects of sunlight exposure. Sol. Energy 86, 3049–3056.
Muratori, M., 2018. Impact of uncoordinated plug-in electric vehicle charging on residential power demand. Nat. Energy 3, 193–201.
Muratori, M., Marano, V., Sioshansi, R., Rizzoni, G., 2012. Energy consumption of residential HVAC systems: A simple physically-based model. IEEE Power Energy Soc. Gen. Meet. 1–8. https://doi.org/10.1109/PESGM.2012.6344950
Muratori, M., Roberts, M.C., Sioshansi, R., Marano, V., Rizzoni, G., 2013. A highly resolved modeling technique to simulate residential power demand. Appl. Energy 107, 465–473. https://doi.org/10.1016/j.apenergy.2013.02.057
Nawaz, I., Tiwari, G.N., 2006. Embodied energy analysis of photovoltaic (PV) system based on macro- and micro-level. Energy Policy 34, 3144–3152. https://doi.org/10.1016/j.enpol.2005.06.018
Nelson, D.B., Nehrir, M.H., Wang, C., 2006. Unit sizing and cost analysis of stand-alone hybrid wind/PV/fuel cell power generation systems. Renew. Energy 31, 1641–1656. https://doi.org/https://doi.org/10.1016/j.renene.2005.08.031
Newsham, G.R., Bowker, B.G., 2010. The effect of utility time-varying pricing and load control strategies on residential summer peak electricity use: A review. Energy Policy 38, 3289–3296. https://doi.org/10.1016/j.enpol.2010.01.027
NHMA, 2015. New Hampshire Municipal Association, C&I Solar Rebate Program [WWW Document]. URL https://www.nhmunicipal.org/Resources/ViewDocument/419
Nieuwlaar, E., Alsema, E., van Engelenburg, B., 1996. Using life-cycle assessments for the environmental evaluation of greenhouse gas mitigation options. Energy Convers. Manag. 37, 831–836. https://doi.org/10.1016/0196-8904(95)00264-2
Nikolakakis, T., Fthenakis, V., 2013. Modeling the environmental impact of PV and wind large scale penetration in regional grids. Conf. Rec. IEEE Photovolt. Spec. Conf. 2326–2330. https://doi.org/10.1109/PVSC.2013.6744942
NOAA, 2021. National Oceanic and Atmospheric Administration, Global Monitoring Laboratory, Sunrise Table for 2021, Sunset Table for 2021 [WWW Document]. URL https://gml.noaa.gov/grad/solcalc/table.php?lat=42.35&lon=-71.05&year=2021

Nojavan, S., Majidi, M., Najafi-Ghalelou, A., Ghahramani, M., Zare, K., 2017. A cost-emission model for fuel cell/PV/battery hybrid energy system in the presence of demand response program: ε-constraint method and fuzzy satisfying approach. Energy Convers. Manag. 138, 383–392. https://doi.org/10.1016/j.enconman.2017.02.003

Nottrott, A., Kleissl, J., Washom, B., 2012. Storage dispatch optimization for grid-connected combined photovoltaic-battery storage systems. IEEE Power Energy Soc. Gen. Meet. 1–7. https://doi.org/10.1109/PESGM.2012.6344979

NREL, 2017. National Renewable Energy Laboratory, Sustainable Energy, PVWatts® Calculator [WWW Document]. URL https://pvwatts.nrel.gov/index.php

NREL, 2015. National Renewable Energy Laboratory, National Solar Radiation Database [WWW Document]. URL https://rredc.nrel.gov/solar/old_data/nsrdb/

NREL, 2014. National Renewable Energy Laboratory, U.S. Department of Energy, Commercial and Residential Hourly Load Profiles for all TMY3 Locations in the United States [WWW Document]. URL https://openei.org/datasets/files/961/pub/

O'Neal, D.L., Hirst, E., 1980. An energy use model of the residential sector. IEEE Trans. Syst. Man Cybern. 10, 749–755. https://doi.org/10.1109/TSMC.1980.4308396

O'Shaughnessy, E., Cutler, D., Ardani, K., Margolis, R., 2018. Solar plus: A review of the end-user economics of solar PV integration with storage and load control in residential buildings. Appl. Energy 228, 2165–2175. https://doi.org/10.1016/j.apenergy.2018.07.048

Oconnell, N., Pinson, P., Madsen, H., Omalley, M., 2014. Benefits and challenges of electrical demand response: A critical review. Renew. Sustain. Energy Rev. 39, 686–699. https://doi.org/10.1016/j.rser.2014.07.098

Pacca, S., Sivaraman, D., Keoleian, G.A., 2007. Parameters affecting the life cycle performance of PV technologies and systems. Energy Policy 35, 3316–3326. https://doi.org/10.1016/j.enpol.2006.10.003

Parida, B., Iniyan, S., Goic, R., 2011. A review of solar photovoltaic technologies. Renew. Sustain. energy Rev. 15, 1625–1636. https://doi.org/10.1016/j.rser.2010.11.032

Parra, D., Patel, M.K., 2016. Effect of tariffs on the performance and economic benefits of PV-coupled battery systems. Appl. Energy 164, 175–187. https://doi.org/10.1016/j.apenergy.2015.11.037

Parrish, T., 2016. PUC Approves Cap on Home-Produced Energy Sold to Grid [WWW Document]. URL https://www.mcall.com/mc-pa-resale-electricity-20160214-story.html

Peng, J., Lu, L., Yang, H., 2013. Review on life cycle assessment of energy payback and greenhouse gas emission of solar photovoltaic systems. Renew. Sustain. Energy Rev. 19, 255–274. https://doi.org/10.1016/j.rser.2012.11.035

Peng, W., Sokolowski, P., Patel, R., Yu, X., Alahakoon, D., 2017. A multi-agent simulation framework for distributed generation with battery storage, in: 2017 IEEE 26th International Symposium on Industrial Electronics (ISIE). IEEE, pp. 37–42.

Perez, M.J.R., Fthenakis, V., Kim, H., Pereira, A.O., 2012. Façade–integrated photovoltaics: a life cycle and performance assessment case study. Prog. Photovoltaics Res. Appl. 20, 975–990.

Poullikkas, A., 2013. A comparative assessment of net metering and feed in tariff schemes for residential PV systems. Sustain. Energy Technol. Assessments 3, 1–8. https://doi.org/https://doi.org/10.1016/j.seta.2013.04.001

PP-MASS, 2021. Provider Power, MASS, Average Electric Bill, Rates and Consumption in Massachusetts [WWW Document]. URL https://providerpower.com/power-to-help/average-

electric-bill-rates-consumption-massachusetts/#:~:text=Average Residential Electricity Consumption in Massachusetts&text=So much so%2C the average,in the U.S. per capita.
Price, S., Margolis, R., Barbose, G., Bartlett, J., Cory, K., Couture, T., DeCesaro, J., Denholm, P., Drury, E., Frickel, M., 2010. 2008 solar technologies market report. Lawrence Berkeley National Lab.(LBNL), Berkeley, CA (United States).
Prüggler, N., 2013. Economic potential of demand response at household level—Are Central-European market conditions sufficient? Energy Policy 60, 487–498. https://doi.org/https://doi.org/10.1016/j.enpol.2013.04.044
Quezada, V.H.M., Abbad, J.R., Roman, T.G.S., 2006. Assessment of energy distribution losses for increasing penetration of distributed generation. IEEE Trans. power Syst. 21, 533–540.
Raugei, M., Bargigli, S., Ulgiati, S., 2007. Life cycle assessment and energy pay-back time of advanced photovoltaic modules: CdTe and CIS compared to poly-Si. Energy 32, 1310–1318. https://doi.org/10.1016/j.energy.2006.10.003
Rawat, B.S., Negi, P., Pant, P.C., Joshi, G.C., 2018. Evaluation of energy yield ratio (EYR), energy payback period (EPBP) and GHG-emission mitigation of solar home lighting PV-systems of 37Wp modules in India. Int. J. Renew. Energy Res. 8.
Rebitzer, G., Ekvall, T., Frischknecht, R., Hunkeler, D., Norris, G., Rydberg, T., Schmidt, W.-P., Suh, S., Weidema, B.P., Pennington, D.W., 2004. Life cycle assessment: Part 1: Framework, goal and scope definition, inventory analysis, and applications. Environ. Int. 30, 701–720.
Reddi, K.R., Li, W., Wang, B., Moon, Y., 2013. System dynamics modelling of hybrid renewable energy systems and combined heating and power generator. Int. J. Sustain. Eng. 6, 31–47.
Rehman, S., Bader, M.A., Al-Moallem, S.A., 2007. Cost of solar energy generated using PV panels. Renew. Sustain. Energy Rev. 11, 1843–1857. https://doi.org/https://doi.org/10.1016/j.rser.2006.03.005
Reichelstein, S., Yorston, M., 2013. The prospects for cost competitive solar PV power. Energy Policy 55, 117–127.
Ren, M., Mitchell, C.R., Mo, W., 2021. Managing residential solar photovoltaic-battery systems for grid and life cycle economic and environmental co-benefits under time-of-use rate design. Resour. Conserv. Recycl. 169, 105527. https://doi.org/10.1016/j.resconrec.2021.105527
Ren, M., Mitchell, C.R., Mo, W., 2020. Dynamic life cycle economic and environmental assessment of residential solar photovoltaic systems. Sci. Total Environ. 722. https://doi.org/10.1016/j.scitotenv.2020.137932
Robinson, S.A., Stringer, M., Rai, V., Tondon, A., 2013. GIS-Integrated Agent-Based Model of Residential Solar PV Diffusion. 32nd USAEE/IAEE North Am. Conf. July 28-31, 2013 1–19.
Saha, G.P., Stephenson, J., 1980. A model of residential energy use in New Zealand. Energy 5, 167–175. https://doi.org/10.1016/0360-5442(80)90005-5
Satchwell, A., Mills, A., Barbose, G., 2015. Quantifying the financial impacts of net-metered PV on utilities and ratepayers. Energy Policy 80, 133–144. https://doi.org/10.1016/j.enpol.2015.01.043
Schaefer, H., Hagedorn, G., 1992. Hidden energy and correlated environmental characteristics of P.V. power generation. Renew. Energy 2, 159–166. https://doi.org/10.1016/0960-1481(92)90101-8

Schibuola, L., Scarpa, M., Tambani, C., 2017. Influence of charge control strategies on electricity import/export in battery-supported photovoltaic systems. Renew. Energy 113, 312–328. https://doi.org/10.1016/j.renene.2017.05.089
SEIA, 2021. Solar Energy Industries Association, Solar Photovoltaic Technology [WWW Document]. URL https://www.seia.org/research-resources/solar-photovoltaic-technology
SEIA, 2020a. Solar Energy Industries Association, U.S. Solar Market Insight [WWW Document]. URL https://www.seia.org/us-solar-market-insight
SEIA, 2020b. Solar Energy Industries Association, Solar Industry Research Data [WWW Document]. URL https://www.seia.org/solar-industry-research-data
SEIA, 2019a. Solar Energy Industries Association, U.S. Solar Market Insight [WWW Document]. URL https://www.seia.org/us-solar-market-insight
SEIA, 2019b. Solar Energy Industries Association, Solar Investment Tax Credit (ITC) [WWW Document]. URL https://www.seia.org/initiatives/solar-investment-tax-credit-itc
SEIA, 2012. Solar Energy Industries Association, Potential Impact of Solar PV on Electricity Markets in Texas [WWW Document]. URL https://www.seia.org/research-resources/potential-impact-solar-pv-electricity-markets-texas
Sharma, S., Jain, K.K., Sharma, A., 2015. Solar Cells: In Research and Applications—A Review. Mater. Sci. Appl. 06, 1145–1155. https://doi.org/10.4236/msa.2015.612113
Shea, R.P., Worsham, M.O., Chiasson, A.D., Kelly Kissock, J., McCall, B.J., 2020. A lifecycle cost analysis of transitioning to a fully-electrified, renewably powered, and carbon-neutral campus at the University of Dayton. Sustain. Energy Technol. Assessments 37, 100576. https://doi.org/10.1016/J.SETA.2019.100576
Sherwani, A.F., Usmani, J.A., Varun, 2010a. Life cycle assessment of solar PV based electricity generation systems: A review. Renew. Sustain. Energy Rev. 14, 540–544. https://doi.org/10.1016/j.rser.2009.08.003
Sherwani, A.F., Usmani, J.A., Varun, 2010b. Life cycle assessment of solar PV based electricity generation systems: A review. Renew. Sustain. Energy Rev. 14, 540–544. https://doi.org/10.1016/j.rser.2009.08.003
Shimoda, Y., Yamaguchi, Y., Iwafune, Y., Hidaka, K., Meier, A., Yagita, Y., Kawamoto, H., Nishikiori, S., 2020. Energy demand science for a decarbonized society in the context of the residential sector. Renew. Sustain. Energy Rev. 132, 110051. https://doi.org/10.1016/j.rser.2020.110051
Singh, G.K., 2013. Solar power generation by PV (photovoltaic) technology: A review. Energy 53, 1–13. https://doi.org/10.1016/j.energy.2013.02.057
SNL, 2018. Sandia National Laboratories, National Technology and Engineering Solutions of Sandia, Sandia Module Temperature Model [WWW Document]. URL https://pvpmc.sandia.gov/modeling-steps/2-dc-module-iv/module-temperature/sandia-module-temperature-model/
Solangi, K.H., Aman, M.M., Badarudin, A., Mokhlis, H., Bakar, A.H.A., Hossain, M.S., Jasmon, G.B., Kazi, S.., 2014. A review of Safety, Health and Environmental (SHE) issues of solar energy system. Renew. Sustain. Energy Rev. 41, 1190–1204. https://doi.org/10.1016/j.rser.2014.08.086
SolarBuzz, 2011. Solar photovoltaic electricity price index [WWW Document]. URL http://register.solarbuzz.com/Solarindices.htm
Song, C., Omalley, A., Roy, S.G., Barber, B.L., Zydlewski, J., Mo, W., 2019a. Managing dams for energy and fish tradeoffs: What does a win-win solution take? Sci. Total Environ. 669,

833–843. https://doi.org/10.1016/j.scitotenv.2019.03.042
Song, C., Omalley, A., Roy, S.G., Barber, B.L., Zydlewski, J., Mo, W., 2019b. Managing dams for energy and fish tradeoffs: What does a win-win solution take? Sci. Total Environ. 669, 833–843. https://doi.org/https://doi.org/10.1016/j.scitotenv.2019.03.042
Spanos, C., Turney, D.E., Fthenakis, V., 2015. Life-cycle analysis of flow-assisted nickel zinc-, manganese dioxide-, and valve-regulated lead-acid batteries designed for demand-charge reduction. Renew. Sustain. Energy Rev. 43, 478–494.
Stamford, L., Azapagic, A., 2018. Environmental impacts of photovoltaics: the effects of technological improvements and transfer of manufacturing from Europe to China. Energy Technol. 6, 1148–1160.
Stein, J.S., 2012. The photovoltaic Performance Modeling Collaborative (PVPMC). Conf. Rec. IEEE Photovolt. Spec. Conf. 3048–3052. https://doi.org/10.1109/PVSC.2012.6318225
Sterman, J.D., 2000. Business dynamics: systems thinking and modeling for a complex world.
Stolz, P., 2017. Water Footprint of European Rooftop Photovoltaic Electricity based on Regionalised Life Cycle Inventories Water Footprint of European Rooftop Photovoltaic.
Stoppato, A., 2008. Life cycle assessment of photovoltaic electricity generation. Energy 33, 224–232. https://doi.org/10.1016/j.energy.2007.11.012
Strbac, G., 2008. Demand side management: Benefits and challenges. Energy Policy 36, 4419–4426. https://doi.org/https://doi.org/10.1016/j.enpol.2008.09.030
Sukumar, S., Marsadek, M., Agileswari, K.R., Mokhlis, H., 2018. Ramp-rate control smoothing methods to control output power fluctuations from solar photovoltaic (PV) sources—A review. J. Energy Storage 20, 218–229. https://doi.org/10.1016/j.est.2018.09.013
Sun, S.I., Crossland, A.F., Chipperfield, A.J., Wills, R.G.A., 2019. An emissions arbitrage algorithm to improve the environmental performance of domestic PV-battery systems. Energies 12. https://doi.org/10.3390/en12030560
Sutula, R.A., 2006. Solar Energy Technologies Program: Multi Year Program Plan 2007-2011. Energy Effic. Renew. Energy, US Dep. Energy, Washingt. DC USA.
Swan, L.G., Ugursal, V.I., 2009. Modeling of end-use energy consumption in the residential sector: A review of modeling techniques. Renew. Sustain. Energy Rev. 13, 1819–1835. https://doi.org/10.1016/j.rser.2008.09.033
Systems, G.S.P. V, 2019. A Comparative Study into Enhancing the PV Penetration Limit of a LV CIGRE Residential Network.
Tebbetts, H., 2018. Liberty Utilities (Granite State Electric) Corp. TOU Rate Calculation.
The White House, 2021. The White House, FACT SHEET: President Biden Takes Executive Actions to Tackle the Climate Crisis at Home and Abroad, Create Jobs, and Restore Scientific Integrity Across Federal Government [WWW Document]. URL https://www.whitehouse.gov/briefing-room/statements-releases/2021/01/27/fact-sheet-president-biden-takes-executive-actions-to-tackle-the-climate-crisis-at-home-and-abroad-create-jobs-and-restore-scientific-integrity-across-federal-government/
Thomson, M., Infield, D.G., 2007. Impact of widespread photovoltaics generation on distribution systems. IET Renew. Power Gener. 1, 33–40. https://doi.org/10.1049/iet-rpg:20060009
Thoy, E.J.W., Go, Y.I., 2021. Enhancement and validation of building integrated PV system: 3D modelling, techno-economics and environmental assessment. Energy Built Environ. https://doi.org/10.1016/j.enbenv.2021.05.001
Tierney, S., 2019. Clean Energy in New York State: The Role and Economic Impacts of a Carbon Price in NYISO's Wholesale Electricity Markets.

Tonkoski, R., Turcotte, D., El-Fouly, T.H.M., 2012. Impact of high PV penetration on voltage profiles in residential neighborhoods. IEEE Trans. Sustain. Energy 3, 518–527.
Tripanagnostopoulos, Y., Souliotis, M., Battisti, R., Corrado, A., 2005. Energy, cost and LCA results of PV and hybrid PV/T solar systems. Prog. Photovoltaics Res. Appl. 13, 235–250. https://doi.org/10.1002/pip.590
Tsang, M.P., Sonnemann, G.W., Bassani, D.M., 2016. Life-cycle assessment of cradle-to-grave opportunities and environmental impacts of organic photovoltaic solar panels compared to conventional technologies. Sol. Energy Mater. Sol. Cells 156, 37–48. https://doi.org/10.1016/j.solmat.2016.04.024
Tsoutsos, T., Frantzeskaki, N., Gekas, V., 2005. Environmental impacts from the solar energy technologies. Energy Policy 33, 289–296. https://doi.org/https://doi.org/10.1016/S0301-4215(03)00241-6
Turconi, R., Boldrin, A., Astrup, T., 2013. Life cycle assessment (LCA) of electricity generation technologies: Overview, comparability and limitations. Renew. Sustain. Energy Rev. 28, 555–565. https://doi.org/10.1016/j.rser.2013.08.013
U.S. Census Bureau, 2005. U.S. Census Bureau, American housing survey for the United States: 2005, H 150/05 edition [WWW Document]. URL https://www.census.gov/prod/2006pubs/h150-05.pdf
Uddin, K., Gough, R., Radcliffe, J., Marco, J., Jennings, P., 2017. Techno-economic analysis of the viability of residential photovoltaic systems using lithium-ion batteries for energy storage in the United Kingdom. Appl. Energy 206, 12–21. https://doi.org/10.1016/j.apenergy.2017.08.170
Uddin, M., Romlie, M.F., Abdullah, M.F., Abd Halim, S., Abu Bakar, A.H., Chia Kwang, T., 2018. A review on peak load shaving strategies. Renew. Sustain. Energy Rev. 82, 3323–3332. https://doi.org/10.1016/j.rser.2017.10.056
UJ, 2016. Unit Juggler V.40, Convert kg of oil equivalent to megajoules [WWW Document]. URL https://www.unitjuggler.com/convert-energy-from-koe-to-MJ.html
USC, 1986. The United States Congress, Electric Consumers Protection Act of 1986, United States [WWW Document]. URL https://www.usbr.gov/power/legislation/ecpa.pdf
van der Stelt, S., AlSkaif, T., van Sark, W., 2018. Techno-economic analysis of household and community energy storage for residential prosumers with smart appliances. Appl. Energy 209, 266–276. https://doi.org/10.1016/j.apenergy.2017.10.096
Venkatesan, N., Solanki, J., Solanki, S.K., 2012. Residential demand response model and impact on voltage profile and losses of an electric distribution network. Appl. Energy 96, 84–91.
Ventana Systems, I., 2015. Vensim Software [WWW Document]. URL http://vensim.com/vensim-software/
Verlinden, P., Yingbin, Z., Zhiqiang, F., 2013. Cost analysis of current PV production and strategy for future silicon PV modules, in: 28th European Photovoltaic Conference and Exhibition, Paris.
Villavicencio Gastelu, J., Melo Trujillo, J.D., Padilha-Feltrin, A., 2018. Hierarchical Bayesian Model for Estimating Spatial-Temporal Photovoltaic Potential in Residential Areas. IEEE Trans. Sustain. Energy 9, 971–979. https://doi.org/10.1109/TSTE.2017.2768824
Walker, I.S., Mingee, M.D., Brenner, D.E., 2003. Improving Air Handler Efficiency in Residential HVAC Applications.
Wang, H., Wang, J., Piao, Z., Meng, X., Sun, C., Yuan, G., Zhu, S., 2020. The optimal allocation and operation of an energy storage system with high penetration grid-connected

photovoltaic systems. Sustain. 12. https://doi.org/10.3390/su12156154
Watson, J.D., Watson, N.R., Santos-Martin, D., Wood, A.R., Lemon, S., Miller, A.J.V., 2016. Impact of solar photovoltaics on the low-voltage distribution network in New Zealand. IET Gener. Transm. Distrib. 10, 1–9. https://doi.org/10.1049/iet-gtd.2014.1076
Weisstein, E.W., 2002. Bernoulli distribution.
Westacott, P., Candelise, C., 2016. Assessing the impacts of photovoltaic penetration across an entire low-voltage distribution network containing 1.5 million customers. IET Renew. Power Gener. 10, 460–466. https://doi.org/10.1049/iet-rpg.2015.0535
Wikipedia, 2021. List of tallest buildings in Boston [WWW Document]. URL https://en.wikipedia.org/wiki/List_of_tallest_buildings_in_Boston
Wilson, E., Engebrecht Metzger, C.., Horowitz, S., Hendron, R., 2014. 2014 Building America House Simulation Protocols (NREL/TP-5500-60988).
Wu, P., Ma, X., Ji, J., Ma, Y., 2017a. Review on Life Cycle Assessment of Energy Payback of Solar Photovoltaic Systems and a Case Study. Energy Procedia 105, 68–74. https://doi.org/https://doi.org/10.1016/j.egypro.2017.03.281
Wu, P., Ma, X., Ji, J., Ma, Y., 2017b. Review on Life Cycle Assessment of Greenhouse Gas Emission Profit of Solar Photovoltaic Systems. Energy Procedia 105, 1289–1294. https://doi.org/10.1016/j.egypro.2017.03.460
Xu, L., Zhang, S., Yang, M., Li, W., Xu, J., 2018. Environmental effects of China's solar photovoltaic industry during 2011–2016: A life cycle assessment approach. J. Clean. Prod. 170, 310–329. https://doi.org/10.1016/j.jclepro.2017.09.129
Yang, D., Latchman, H., Tingling, D., Amarsingh, A.A., 2015. Design and return on investment analysis of residential solar photovoltaic systems. IEEE Potentials 34, 11–17.
Yang, F., Xia, X., 2017. Techno-economic and environmental optimization of a household photovoltaic-battery hybrid power system within demand side management. Renew. Energy 108, 132–143. https://doi.org/10.1016/j.renene.2017.02.054
Zamuda, C.D., Larsen, P.H., Collins, M.T., Bieler, S., Schellenberg, J., Hees, S., 2019. Monetization methods for evaluating investments in electricity system resilience to extreme weather and climate change. Electr. J. 32, 106641. https://doi.org/10.1016/j.tej.2019.106641
Zhang, H., Cai, J., Fang, K., Zhao, F., Sutherland, J.W., 2017. Operational optimization of a grid-connected factory with onsite photovoltaic and battery storage systems. Appl. Energy 205, 1538–1547. https://doi.org/10.1016/j.apenergy.2017.08.140
Zhang, S., Tang, Y., 2019. Optimal schedule of grid-connected residential PV generation systems with battery storages under time-of-use and step tariffs. J. Energy Storage 23, 175–182. https://doi.org/10.1016/j.est.2019.01.030
Zhang, X., Li, M., Ge, Y., Li, G., 2016. Techno-economic feasibility analysis of solar photovoltaic power generation for buildings. Appl. Therm. Eng. 108, 1362–1371. https://doi.org/10.1016/j.applthermaleng.2016.07.199
Zhang, Y., Gatsis, N., Giannakis, G.B., 2013. Robust energy management for microgrids with high-penetration renewables. IEEE Trans. Sustain. Energy 4, 944–953.
Zhao, J., Kucuksari, S., Mazhari, E., Son, Y.-J., 2013. Integrated analysis of high-penetration PV and PHEV with energy storage and demand response. Appl. Energy 112, 35–51.
Zheng, M., Meinrenken, C.J., Lackner, K.S., 2015. Smart households: Dispatch strategies and economic analysis of distributed energy storage for residential peak shaving. Appl. Energy 147, 246–257. https://doi.org/https://doi.org/10.1016/j.apenergy.2015.02.039